

UNCLASSIFIED

AD NUMBER	
AD110591	
CLASSIFICATION CHANGES	
TO:	UNCLASSIFIED
FROM:	CONFIDENTIAL
LIMITATION CHANGES	
TO: Approved for public release; distribution is unlimited.	
FROM: Distribution authorized to U.S. Gov't. agencies and their contractors; Administrative/Operational Use; DEC 1955. Other requests shall be referred to Aeronautical Systems Div., Wright-Patterson AFB, OH 45433.	
AUTHORITY	
ASD ltr 19 Feb 1962 ; ASD ltr 12 Oct 1966	

THIS PAGE IS UNCLASSIFIED

UNCLASSIFIED

AD 110 591

CLASSIFICATION CHANGED

TO: UNCLASSIFIED

FROM: CONFIDENTIAL

AUTHORITY:

ASD Ltr 19 Feb. 62;
Public release Sec Ltr 12 Oct 66



UNCLASSIFIED

**Best
Available
Copy**

NOTICE: When government or other drawings, specifications or other data are used for any purpose other than in connection with a definitely related government procurement operation, the U. S. Government thereby incurs no responsibility, nor any obligation whatsoever; and the fact that the Government may have formulated, furnished, or in any way supplied the said drawings, specifications, or other data is not to be regarded by implication or otherwise as in any manner licensing the holder or any other person or corporation, or conveying any rights or permission to manufacture, use or sell any patented invention that may in any way be related thereto.

CONFIDENTIAL

110591
WADC TECHNICAL REPORT 56-97
PART I
ASTIA DOCUMENT NO. AD 110591

FC

(UNCLASSIFIED - Title)

**THEORETICAL STUDIES ON THE PREDICTION
OF UNSTEADY SUPERSONIC AIRLOADS ON ELASTIC WINGS**

**Part I. Investigations on the Use of
Oscillatory Supersonic Aerodynamic Influence Coefficients**

Garabed Zartarian

Dr. Pao-Tan Hsu

MASSACHUSETTS INSTITUTE OF TECHNOLOGY

December 1955

WRIGHT AIR DEVELOPMENT CENTER

MAR 8 1957

56WCLS-5098

CONFIDENTIAL

**NOTICE: THIS DOCUMENT CONTAINS INFORMATION AFFECTING THE
NATIONAL DEFENSE OF THE UNITED STATES WITHIN THE MEANING
OF THE ESPIONAGE LAWS, TITLE 18, U.S.C., SECTIONS 793 and 794.
THE TRANSMISSION OR THE REVELATION OF ITS CONTENTS IN
ANY MANNER TO AN UNAUTHORIZED PERSON IS PROHIBITED BY LAW.**

CONFIDENTIAL

WADC TECHNICAL REPORT 56-97
PART I
ASTIA DOCUMENT NO. AD 110591

(UNCLASSIFIED - Title)
THEORETICAL STUDIES ON THE PREDICTION
OF UNSTEADY SUPERSONIC AIRLOADS ON ELASTIC WINGS
Part 1. Investigations on the Use of
Oscillatory Supersonic Aerodynamic Influence Coefficients

Garabed Zartarian

Dr. Pao-Tan Hsu

MASSACHUSETTS INSTITUTE OF TECHNOLOGY

December 1955

Aircraft Laboratory
Contract AF33(616)-2482
Project 1370

Wright Air Development Center
Air Research and Development Command
United States Air Force
Wright-Patterson Air Force Base, Ohio

56WCLS-5098

CONFIDENTIAL

CONFIDENTIAL

FOREWORD

This report, which presents the studies on the use of the aerodynamic influence coefficient method, was prepared by the Aeroelastic and Structures Research Laboratory, Massachusetts Institute of Technology, Cambridge 39, Massachusetts for the Aircraft Laboratory, Wright Air Development Center, Wright-Patterson Air Force Base, Ohio. The work was performed at the MIT under the direction of Professor H. Ashley, and the project was supervised by Mr. G. Zartarian. The research and development work was accomplished under Air Force Contract, No. AF 33(616)-2482, Project No. 1370 (Unclassified Title) "Aeroelasticity, Vibration and Noise," and Task No. 13478 (Unclassified Title) "Theoretical Supersonic Flutter Studies." Mr. Walter J. Mykytow of the Dynamics Branch, Aircraft Laboratory, is task engineer. Research was started on 1 July 1954. This report is part of a continuing effort in the flutter of aircraft structures at supersonic speeds. This is Part I of a report which will be published in two parts.

The coauthor, Dr. Pao-Tan Hsu, has contributed substantially to the unclassified portions of this report. Since he has no security clearance, he has not had access to classified information. He has not read the report in its final form, nor has he seen the complete manuscript of the report. The first author, Mr. G. Zartarian, integrated Dr. Hsu's contributions into the final document form without divulging security information to him.

The authors are indebted to Professor H. Ashley, Mr. A. Heller, and Mr. W. Weatherill for their contributions to the research. In addition, acknowledgements are due to Mr. G. Anitole for preparing the figures and to Mrs. B. Marks for typing the final manuscript.

This document, including the illustrations, is classified **CONFIDENTIAL** (excepting the title) because it contains the development of improved methods for conducting supersonic flutter analysis; hence more accurate flutter analyses for modern aircraft can be made.

CONFIDENTIAL

CONFIDENTIAL


ABSTRACT

An extensive investigation is presented into the applicability and accuracy of the method of aerodynamic influence coefficients for calculating the airload distribution on thin wings of arbitrary planform, executing small steady or simple harmonic motions in a supersonic flow of perfect gas. Several representative examples, involving wings with various combinations of subsonic and supersonic edges, are worked out. Where possible, comparisons are made with results of more exact linearized theory. The relative advantages of three types of elementary area for subdividing the wing planform are studied. The type which appears most satisfactory from considerations of versatility, accuracy and simplicity is the "Mach box," a rectangular area element with diagonals parallel to the Mach lines. On the basis of all available evidence, the method is concluded to be satisfactory for use in flutter prediction or similar applications, and recommendations are put forth regarding preparation of tables of aerodynamic influence coefficients. A set of working rules to assist the engineer in using these coefficients is published in a subsequent report (Ref. 31).

PUBLICATION REVIEW

This report has been reviewed and is approved.

FOR THE COMMANDER:

for 
DANIEL D. McKEE
Colonel, USAF
Chief, Aircraft Laboratory

CONFIDENTIAL

CONFIDENTIAL

TABLE OF CONTENTS

SECTION	PAGE
I. INTRODUCTION	1
II. Aerodynamic Influence Coefficient Expressions for the Three Basic Types of Grid System	5
II.1 Aerodynamic Theory	5
II.2 Expressions for the Aerodynamic Influence Coefficients of the Square Grid System	6
II.3 Expressions for the Aerodynamic Influence Coefficients of the Mach Box Grid System	11
II.4 Expressions for the Aerodynamic Influence Coefficients of the Characteristic Grid System	19
III. Application to Two-Dimensional Problems	26
III.1 Representation of Swept Leading Edges by Broken Lines	26
III.2 Adequacy of the Assumption of Average Constant Downwash over Each Elementary Area: Steady Motion	36
III.3 Adequacy of the Assumption of Average Constant Downwash over Each Elementary Area: Unsteady Motion	43
III.4 Comments on the Accuracy of the Approximate Formulas for the Aerodynamic Influence Coefficients	56
IV. Loading of Planforms With Subsonic Edges	60
IV.1 The Side-Edge Problem in Steady Flow	61
IV.2 The Side-Edge Problem in Unsteady Flow	73
IV.3 The Subsonic Leading and Trailing Edge Problems	85
V. Supplementary Numerical Examples	97
V.1 Purely Supersonic Planforms	97
V.2 Planforms with Subsonic Edges	100

CONFIDENTIAL

TABLE OF CONTENTS

VI. Alternative Numerical Approaches	108
VI.1 The Inverse Pressure Influence Coefficient	103
VI.2 The Lift Influence Coefficient	115
BIBLIOGRAPHY	117
APPENDIX A - Evaluation of the Functions \bar{I}_n and \bar{P}_n	121

CONFIDENTIAL

LIST OF ILLUSTRATIONS

	<u>Page</u>
Fig. II.1 The Square Box Grid System	8
Fig. II.2 Subdivision of Near Boxes	10
Fig. II.3 The Mach Box Grid System	13
Fig. II.4 Characteristic Coordinate System	20
Fig. II.5 Basic Regions Under Consideration for the Characteristic System	22
Fig. II.6 Numbering System for Characteristic Boxes	24
Fig. III.1 Pressure Distribution on a Two-Dimensional Swept Wing Using Mach (or Square) Boxes. ($k=0$, $\tan \Lambda = 1/2$, $M = \sqrt{2}$)	27
Fig. III.2 Pressure Distribution on a Two-Dimensional Swept Wing Using Mach (or Square) Boxes. ($k=0$, $\tan \Lambda = 2/3$, $M = \sqrt{2}$)	31
Fig. III.3 Pressure Distribution on a Two-Dimensional Swept Wing Using Square Boxes. ($k=0$, $\tan \Lambda = 1/3$, $M = 1.2$)	33
Fig. III.4 Pressure Distribution on a Two-Dimensional Swept Wing Using Characteristic Boxes. ($k=0$, $\tan \Lambda = 1/2$, $M = \sqrt{2}$)	34
Fig. III.5 Proper Representation of the Leading Edge when Characteristic Grid System is Employed	35
Fig. III.6 A Two-Dimensional, Unswept Wing in Steady Flow. (Mach Box System)	37
Fig. III.7 A Two-Dimensional Wing in Steady Flow. Downwash Varying Linearly Along the Chord. (Characteristic Box System)	38
Fig. III.8 A Two-Dimensional Wing in Steady Flow. Downwash Varying Linearly Along the Chord. (Characteristic System with Control Points at Centers of Boxes)	39
Fig. III.9 A Two-Dimensional Wing in Steady Flow. (Modified Characteristic System)	40
Fig. III.10 Notations for a Finite Rectangular Wing in Steady Flow with Spanwise Variation in Downwash	41

CONFIDENTIAL

LIST OF ILLUSTRATIONS (Cont'd.)

	<u>Page</u>
Fig. III.11 Illustrative Example: the Use of the Mach Grid System for a Two-Dimensional Wing with Variation of Downwash Across the Chord	45
Fig. III.12 Real Part of Chordwise Pressure Distribution for a Two-Dimensional Unswept Wing. (Motion: $z = 2bx e^{i\omega t}$, $k = 0.3$, $M = 1.2$)	47
Fig. III.13 Imaginary Part of Chordwise Pressure Distribution for a Two-Dimensional Unswept Wing. (Motion: $z = 2bx e^{i\omega t}$, $k = 0.3$, $M = 1.2$)	48
Fig. III.14 Real Part of Chordwise Pressure Distribution for a Two-Dimensional Unswept Wing. (Motion: $z = 2bx^2 e^{i\omega t}$, $k = 0.3$, $M = 1.2$)	49
Fig. III.15 Imaginary Part of Chordwise Pressure Distribution for a Two-Dimensional Unswept Wing. (Motion: $z = 2bx^2 e^{i\omega t}$, $k = 0.3$, $M = 1.2$)	50
Fig. III.16 Chordwise Pressure Distribution for a Two-Dimensional Unswept Wing. (Motion: $z = 2bx e^{i\omega t}$, $k = 0.99$, $M = 1.2$)	51
Fig. III.17 Chordwise Pressure Distribution for a Two-Dimensional Unswept Wing. (Motion: $z = 2bx^2 e^{i\omega t}$, $k = 0.99$, $M = 1.2$)	52
Fig. IV.1 Illustrative Example for the Treatment of a Side Edge	61
Fig. IV.2 Characteristic Grid System for a Rectangular Wing in Steady Motion at a Constant Angle of Attack	62
Fig. IV.3 Characteristic Coordinate System for the Treatment of the Side-Edge Downwash Singularity	66
Fig. IV.4 Singular Downwash Distribution Near a Side Edge	67
Fig. IV.5 Mach Grid System for a Rectangular Wing in Steady Motion at Constant Angle of Attack	69
Fig. IV.6 Spanwise Lift Distribution on a Rectangular Wing in Steady Supersonic Flight at Constant Angle of Attack, as Calculated by the Methods Indicated on the Various Curves	74

CONFIDENTIAL

LIST OF ILLUSTRATIONS (Cont'd.)

	<u>Page</u>
Fig. IV.7 Spanwise Moment Distribution on a Rectangular Wing in Steady Supersonic Flight at Constant Angle of Attack, as Calculated by the Methods Indicated on the Various Curves	75
Fig. IV.8 Square Grid System for a Rectangular Wing in Steady Motion at Constant Angle of Attack. ($M = 1.2$)	76
Fig. IV.9 Dimensionless Spanwise Lift Distribution on a Rectangular Wing in Translational Oscillation, as Calculated by the Methods Indicated on the Curves. ($k = 0.3$, $M = 1.2$)	82
Fig. IV.10 Dimensionless Spanwise Moment Distribution on a Rectangular Wing in Translational Oscillation, as Calculated by the Methods Indicated on the Curves. ($k = 0.3$, $M = 1.2$)	83
Fig. IV.11 Dimensionless Spanwise Lift Distribution on a Rectangular Wing in Pitching Oscillation About its Mid-Chord Axis, as Calculated by the Indicated Methods. ($k = 0.6$, $M = 1.5$)	86
Fig. IV.12 Dimensionless Spanwise Distribution of Pitching Moment About the Mid-Chord of a Rectangular Wing in Pitching Oscillation About its Mid-Chord Axis, as Calculated by the Indicated Methods. ($k = 0.6$, $M = 1.5$)	87
Fig. IV.13 Dimensionless Pressure Distribution on a Triangular Wing at Constant Angle of Attack. ($k = 0$, $\cot \Lambda = 0.64$, $M = \sqrt{2}$)	90
Fig. IV.14 Spanwise Lift Distribution on a Triangular Wing at Constant Angle of Attack as Calculated by the Methods Indicated on the Curves. ($k = 0$, $\cot \Lambda = 0.64$, $M = \sqrt{2}$)	92
Fig. IV.15 Spanwise Pitching Moment Distribution on a Triangular Wing at Constant Angle of Attack as Calculated by the Methods Indicated on the Curves. ($k = 0$, $\cot \Lambda = 0.64$, $M = \sqrt{2}$)	93
Fig. V.1 Spanwise Lift Distribution for a Triangular Wing at Constant Angle of Attack in Steady Flow. ($\Lambda = 45^\circ$, $M = 1.5$)	98
Fig. V.2 Spanwise Distribution of Pitching Moment About an Axis Through the Apex of a Triangular Wing at Constant Angle of Attack in Steady Flow. ($\Lambda = 45^\circ$, $M = 1.5$)	99

CONFIDENTIAL

LIST OF ILLUSTRATIONS (Cont'd.)

		<u>Page</u>
Fig. V.3	Spanwise Lift Distribution for a Triangular Wing in Uniform Translational Motion. ($k=0.2$, $\Lambda=60^\circ$, $M=1.5$)	101
Fig. V.4	Spanwise Distribution of Pitching Moment About an Axis Through the Root Mid-Chord of a Triangular Wing in Uniform Translational Motion. ($k=0.2$, $\Lambda=60^\circ$, $M=1.5$)	102
Fig. V.5	Spanwise Lift Distribution for a Triangular Wing in Uniform Pitching Motion About an Axis Through the Root Mid-Chord. ($k=0.2$, $\Lambda=60^\circ$, $M=1.5$)	103
Fig. V.6	Spanwise Pitching Moment Distribution for a Triangular Wing in Uniform Pitching Motion About an Axis Through the Root Mid-Chord. ($k=0.2$, $\Lambda=60^\circ$, $M=1.5$)	104
Fig. V.7	Spanwise Lift Distribution for a Triangular Wing in Parabolic Translational Motion. ($k=0.1$, $\Lambda=45^\circ$, $M=1.2$)	106
Fig. V.8	Spanwise Distribution of Pitching Moment About an Axis Through the Apex of a Triangular Wing in Parabolic Translational Motion. ($k=0.1$, $\Lambda=45^\circ$, $M=1.2$)	107
Fig. VI.1	Dimensionless Pressures on the Mixed Region of a Rectangular Wing in Steady Supersonic Motion at a Constant Angle of Attack. Comparison Between Exact Results and Three Forms of the Mach Box Method	113
Fig. VI.2	Pressure Distribution on a Triangular Wing in Steady Supersonic Motion at a Constant Angle of Attack with the Inverse Pressure Coefficient Method. ($\cot \Lambda=0.64$, $M=\sqrt{2}$)	114
Fig. VI.3	The Use of Mach System in Connection with the Lift Influence Coefficient	116

LIST OF TABLES

Table III.1	Comparison of Lift by Numerical Methods with Exact Lift for a Two-Dimensional Swept Wing. ($k=0$, $\tan \Lambda=1/2$, $M=\sqrt{2}$)	29
Table III.2	Comparison of Lift by Numerical Methods with Exact Lift for a Two-Dimensional Swept Wing. ($k=0$, $\tan \Lambda=2/3$, $M=\sqrt{2}$)	32

CONFIDENTIAL

LIST OF TABLES (Cont'd.)

	<u>Page</u>
Table III.3 Comparison of Lift by the Square Grid System with Exact Lift for a Two-Dimensional Swept Wing. ($\beta=0$, $\tan \Lambda = 1/3$, $M=1.2$)	34
Table III.4 Comparison of Lift Distribution According to the Mach Box Scheme with the Exact for the Purely Supersonic Region of a Rectangular Wing in Steady Motion (Downwash Varying Parabolically Across the Span)	42
Table III.5 Comparison of Lift and Moment About the Leading Edge per Unit Span, Computed Using Mach Boxes, with the Exact Values for a Two-Dimensional Unswept Wing Oscillating in the Motion $z = 2b e^{i\omega t}$	53
Table III.6 Comparison of Lift and Moment About the Leading Edge per Unit Span, Computed Using Mach Boxes, with the Exact Values for a Two-Dimensional Unswept Wing Oscillating in the Motion $z = 2bx e^{i\omega t}$	54
Table III.7 Comparison of Lift and Moment About the Leading Edge per Unit Span, Computed Using Mach Boxes, with the Exact Values for a Two-Dimensional Unswept Wing Oscillating in the Motion $z = 2bx^2 e^{i\omega t}$	54
Table III.8 Aerodynamic Influence Coefficients in Row $\bar{v}=2$ Calculated with and without Subdivision. ($\beta_1 = 0.4$, $M=1.2$)	57
Table III.9 The Sum of the Aerodynamic Influence Coefficients $p_{\bar{v}}$ in Rows $\bar{v}=0, \dots, 4$ for $\beta_1 = 0.4$, $M=1.2$, Calculated by Various Methods	58
Table IV.1 Dimensionless Pressures on the Mixed Region of a Rectangular Wing in Steady Supersonic Motion at a Constant Angle of Attack. Comparison Between Exact Results and Two Forms of the Characteristic Box Method	64
Table IV.2 Dimensionless Pressures on the Mixed Region of a Rectangular Wing in Steady Supersonic Flow at a Constant Angle of Attack. Comparison Between Exact Results and Calculations by Two Forms of the Mach Box Method	70
Table IV.3 Pressures on the Mixed Region of a Rectangular Wing in Steady Motion at a Constant Angle of Attack. (Square Boxes, $M=1.2$)	78

CONFIDENTIAL

LIST OF TABLES (Con't.d)

	<u>Page</u>
Table IV.4 Total Lifts and Moments on a Triangular Wing at Constant Angle of Attack in Steady Flow, Calculated by the AIC Method with an Increasing Number of Chordwise Boxes. ($\cot \Lambda = 0.64$, $M = \sqrt{2}$)	94
Table VI.1 A Short Table for Inverse Pressure Influence Coefficients in the Mach Grid System. Steady State. ($k = 0$)	111

CONFIDENTIAL

LIST OF SYMBOLS

B	Reference semi-chord
b	Streamwise dimension of a box
d	Reference length
\bar{h}, \bar{h}_0	Amplitude of translational oscillation
i	$\sqrt{-1}$
k	Reduced frequency based on reference semi-chord ($k = \omega b / U$)
k_i	Reduced frequency based on streamwise dimension of a box ($k_i = \omega b_i / U$)
\bar{k}_i	Modified reduced frequency based on b_i ($\bar{k}_i = k_i M^2 / \beta^2$)
l	Dimensionless lift per unit span
m, n	Indices designating location of receiving box
m	Dimensionless moment per unit span
$\bar{p}, \Delta \bar{p}$	Complex amplitude of pressure difference ($\bar{p} = \Delta \bar{p} = \overline{p_u - p_l}$)
p'	Dimensionless amplitude of pressure difference
p'_v	Pressure contribution from row v
r, s	Characteristic coordinates [Eqs. (2.33) and Eqs. (4.5a-b)]
t	Time
\bar{w}	Complex amplitude of downwash (positive down)
\bar{w}_s	Amplitude (strength) of singular downwash distribution
x, y	Cartesian coordinates
z	Deflection of the mean surface of a wing (positive down)
$A, A(x, y)$	Entire or elementary area influencing (x, y) within the forward Mach lines emanating from (x, y)
$A_{v, \mu}^+, A_{v, \mu}^-, B_{v, \mu}$	Necessary functions for tabulating AIC's for square boxes [Eqs. (2.9)]
$\mathcal{A}_{v, \mu}^+, \mathcal{A}_{v, \mu}^-, \mathcal{B}_{v, \mu}$	Necessary functions for tabulating AIC's for Mach boxes [Eqs. (2.16)]

CONFIDENTIAL

LIST OF SYMBOLS (Con't.d)

AIC	Aerodynamic influence coefficient (Abbreviation)
$C^{(s)}, C_a^{(s)}, C_b^{(s)}$	Pressure influence coefficients associated with singular downwash distribution [Eqs. (4.8) and Eqs. (4.15)]
$C_{\mu, \nu}^{()}$	Aerodynamic influence coefficients for characteristic boxes [Steady state, Eqs. (2.48)]
$E(x, \pi/2)$	Complete elliptic integral of the second kind
$\mathcal{F}(x), C(x), S(x)$	Fresnel integrals [Eq. (2.43)]
$F(x-\xi, y-\eta)$	Kernel representing the pressure at (x, y) due to unit downwash at (ξ, η) [Eq. (6.1)]
$\bar{I}_0, \bar{I}_1, \bar{P}_0, \bar{P}_1$	Functions defined by Eqs. (4.16)
J_p	Bessel function of the first kind of order p
$K(x-\xi, y-\eta)$	Inverse kernel representing the downwash at (x, y) due to unit pressure at (ξ, η) [Eq. (6.2)]
L, M	Dimensionless total lift and total moment respectively
$L_1, L'_2, M'_1, \dots, L_q, \dots$	Aerodynamic derivatives (Customary notations from Ref. 36)
M	Mach number
$P_{\bar{v}, \bar{\mu}}$	Inverse pressure influence coefficient [Eq. (6.5)]
$\bar{R} + i\bar{I}$	Aerodynamic influence coefficient for square boxes [Eq. (2.5)]
$\mathcal{Q} + i\mathcal{J}$	Aerodynamic influence coefficient for Mach boxes [Eq. (2.14)]
S	Surface of planform
U	Speed of flight (Supersonic)
\bar{U}	Step function [Eq. (6.4)]
α	Angle of attack
$\bar{\alpha}, \bar{\alpha}_0$	Amplitude of pitching oscillation
β	$\sqrt{M^2 - 1}$
θ	Modified reduced frequency based on the side length of a rhombus [Eq. (2.35)]

CONFIDENTIAL

LIST OF SYMBOLS (Cont.d)

μ, ν	Indices designating location of sending box
$\bar{\mu}, \bar{\nu}$	Indices designating location of sending box relative to receiving box
ξ, η	Running variables in the Cartesian coordinate system
ρ	Density of the undisturbed medium
$\bar{\varphi}$	Complex amplitude of velocity potential
ω	Circular frequency of oscillation
$\bar{\omega}$	Modified reduced frequency based on b ($\bar{\omega} = 2k M^2 / \beta^2$)
Λ	Sweep angle of leading edge

CONFIDENTIAL

SECTION I

INTRODUCTION

The problem of determining the aerodynamic forces on a harmonically oscillating, thin, almost-plane lifting surface in supersonic flow has received considerable attention since the original work of von Borbely (Ref. 1) in the early 1940's. Two distinct approaches have been followed in developing solutions for various wing planforms.

The first is the analytic approach of finding exact solutions for the linearized differential equation. The two-dimensional case may be considered completely solved; an extensive list of references on it appears in Refs. 2-5.* For finite wings, several authors have presented solutions limited to specific planforms. Miles (Refs. 3,4) treated the quarter-infinite wing and extended his formulation to planforms with oblique straight leading edges, (Ref. 5). Although the prescribed motions are arbitrary, the results obtained for the velocity potential are in integral form, and the application of this theory is limited by practical considerations to cases where the mode of oscillation is independent of the spanwise coordinate. Other contributors, e.g., Goodman (Ref. 6), Stewartson (Ref. 7) and Rott (Ref. 8), arrived at similar solutions for deformations which are variable in the stream direction only. Evvard's equivalent-area concept was used by Stewart and Li for the oscillating rectangular wing (Ref. 9) and by Chang for an oscillating swept finite wing with supersonic leading and trailing edges (Ref. 10). It was subsequently found that this concept is valid only for low frequencies. An extension (Ref. 11) was proposed by Stewart and Li, which would validate the method for higher frequencies. Concurrently Watkins treated the rectangular wing, oscillating in rigid-body motions, by a series expansion of the kernel function of the governing integral equation in terms of the frequency (up to the third power in Ref. 12 and up to the seventh power in Ref. 13).

The simpler problem of the triangular or delta wing with supersonic edges performing rigid-body motions was studied by Miles (Ref. 14), Froehlich (Ref. 15) and Nelson (Ref. 16). Using a suitable form of the reverse-flow theorem, Walsh, Zartarian and Voss (Ref. 17) were able to obtain direct generalized-force expressions for this "wide" delta associated

* — — — — —
A recent publication by J. W. Miles summarizes the existing aerodynamic theories for unsteady supersonic flow. (Ref. 44)

Manuscript released by the author December 1955 for publication as a WADC Technical Report.

CONFIDENTIAL

with rather general elastic modes. The case of the "narrow" delta, i.e., the triangular wing with subsonic leading edges, was formulated by Haskind and Falkovich (Ref. 18) and by Watkins and Berman (Refs. 19, 20). The former solution is considered impractical in view of the tediousness of the numerical computations. One may conveniently use Ref. 19 for rigid body motions and Ref. 20 for harmonic deformations representable by a quadratic form. However, the limitation to low frequency and the inadequacy of the quadratic form for representing many types of deformation restrict the usefulness of the results of Ref. 20.

In view of the variety of shapes and aspect ratios adopted for modern aircraft wing and tail surfaces, it is desirable to devise a unified theory which is free from the limitations inherent in nearly all of the analytical methods mentioned above. A promising avenue in this direction, entirely numerical in character, was first suggested by Pines and collaborators (Refs. 21, 22)* for any planform with all supersonic edges (and later extended to planforms with subsonic edges) oscillating in an arbitrary deformation mode. Their scheme is based on the use of the "aerodynamic influence coefficient," defined as the pressure developed at a point on the wing by constant normal velocity of the fluid (downwash) on an elementary area of the wing, while the downwash is assumed zero over the rest of the planform. This influence coefficient method can readily be adapted to loading computation or flutter analysis by overlaying a grid of boxes on the wing and relating the pressure on any box to the known motions of all the boxes. Numerical applications yield quite satisfactory accuracy for the planforms considered in Refs. 21, 22. This method was extended for planforms with subsonic edges by introducing the diaphragm concept of Evvard (Ref. 23)* and placing boxes over the disturbed flow region off the planform.

The elementary areas employed in these references are squares, and this can be shown to limit the applicability for wings with subsonic edges to the range of $M \geq \sqrt{2}$. Extensive tabulations for the aerodynamic influence coefficients associated with square boxes are now available (Ref. 25). Following a suggestion by Pines, Li (Refs. 26, 27) carried out similar analysis using as elementary areas the so-called Mach boxes, whose diagonals are parallel to the Mach lines. Although the Mach box appears to be the most useful and versatile of the

*Reference 24 summarizes the essential features of Refs. 21-23.

CONFIDENTIAL

elementary-area shapes proposed to date, some of the approximations adopted by Li when computing influence coefficients are inadequate. His work is discussed in a subsequent section. In a recent report (Ref. 28) the present authors suggested another alternative grid system, made up of so-called characteristic boxes. These elementary areas are rhombuses with sides parallel to the Mach lines.

Another numerical scheme has been suggested by Brandstatter and Mortzschky (Refs. 29,30) for tapered planforms with supersonic leading and trailing edges, performing arbitrary simple harmonic motions. They employ Miles' solution for the quarter-infinite wing, replacing the tapered wing with a rectangular one (the foremost points of the two wings being the same) and setting the downwash equal to zero on the region of the rectangular wing between the leading edges of the two planforms. This step is permissible since the leading edge is supersonic. The downwash is represented as a power series in the coordinates, and if such a representation is to be satisfactory, one must take a large number of terms to account for the discontinuous downwash at the leading edge of the tapered planform. The method of Ref. 29 will undoubtedly be useful for particular types of wing performing certain oscillations, but it is organized in such a way as not to appear as efficient as the box methods from the computational standpoint. Seven distinct types of region must be treated on the most general planform considered.

An attractive feature of all these numerical methods is that they are highly systematized and therefore well suited to high-speed machine computations. The aerodynamic theory can be reduced to a large aggregate of repetitive, elementary operations, which involve the use of universally applicable tables. However, preparing such tables for the first time is likely to be an expensive project and requires careful and efficient planning.

The motivation for the present research is to furnish recommendations for influence coefficient tables and to present a set of working rules for the proper use of the box method in practical flutter analyses. The basic problem is to study the proposed grid systems and their applications to various types of wings of current and future interest. Associated with each of these systems there are certain difficulties which must be clearly recognized, so that appropriate steps can be derived to alleviate them. Possible modified procedures for particular cases, such as the special treatment of subsonic edges, must also be taken into consideration. For

CONFIDENTIAL

CONFIDENTIAL

these purposes many aspects of the problem have been isolated and investigated separately. The accuracy of the method has been studied by comparing the results for specific examples according to the present numerical techniques with those according to other unsteady aerodynamic theories of known validity.

The present paper describes all the detailed investigations and illustrative cases, along with complete statements of the conclusions reached therefrom. A summary report (Ref. 31) summarizes these conclusions, for the reader who desires to apply the method, in the form of working rules for the computation of airload distributions and aerodynamic terms in flutter equations.

When trying to formulate a set of rules for the application of aerodynamic influence coefficients, one is faced with the question of what degree of accuracy is needed in the determination of the airloads. This is particularly hard to answer when the problem being analyzed involves the interaction of several types of forces, such as in flutter prediction. It is known that in some cases a given percentage error in the aerodynamic forces can give rise to a larger error in the estimated flutter speed, whereas at other times this speed may be very insensitive. It is important to minimize each of the sources of error in any flutter calculation, and to this end the ideal would be to have the percentage error of the airloads (compared to their exact theoretical values) smaller by at least one order of magnitude than the largest uncertainty known to be present in other terms of the flutter equations. Such precision can rarely be attained, so that the analyst must normally be satisfied with an accuracy no worse than that of other terms. As a general rule, it is believed that this sort of accuracy or better will be obtained if the procedures suggested in the present work are followed.

The conclusions reached herein regarding evaluation of the airloads are based on the following underlying principles:

- (1) Computations should be organized and limited so that generally available high-speed computing facilities can handle any practical problem within a reasonable period of time.
- (2) Maximum accuracy should be obtained, up to a point where any further significant improvement is associated with excessive additional labor.
- (3) Refined techniques which produce marked improvements in accuracy should be sought and recommended, but only when they yield greater computational efficiency and do not interfere seriously with the conceptual simplicity and degree of organization of the basic method.

CONFIDENTIAL

SECTION II

AERODYNAMIC INFLUENCE COEFFICIENT EXPRESSIONS FOR THE THREE BASIC TYPES OF GRID SYSTEM

II.1 Aerodynamic Theory

According to linearized potential flow theory for simple harmonic motion of an almost-plane lifting surface (Ref. 12), the complex amplitude of the velocity potential $\bar{\varphi}(x, y)$ at a point (x, y) on the upper side of the surface is*

$$\bar{\varphi}(x, y) = -\frac{1}{\pi} \int_A \frac{\bar{w}(\xi, \eta) e^{-i \frac{\omega M^2}{U \beta^2} (x - \xi)} \cos \left(\frac{\omega M}{U \beta^2} \sqrt{(x - \xi)^2 - \beta^2 (y - \eta)^2} \right)}{\sqrt{(x - \xi)^2 - \beta^2 (y - \eta)^2}} d\xi d\eta$$

Eq. (2.1)

where $\bar{w}(\xi, \eta)$ is the complex amplitude of the normal component of fluid velocity (downwash) produced by the wing's motion,

$$\bar{w}(\xi, \eta) = (i\omega + U \frac{\partial}{\partial \xi}) \bar{z}(\xi, \eta)$$

Eq. (2.2)

and

$x, y; \xi, \eta$
 $\bar{z}(\xi, \eta)$

are rectangular coordinates (cf. Fig. II.1),
is the deflection amplitude of the mean surface of the wing at (ξ, η) (positive down),
 A is the entire disturbed region bounded by the forward Mach lines emanating from (x, y) ,

and the various constants are defined in the list of symbols.

*In accordance with the standard procedure for representing simple harmonic motion, the actual numerical values of the velocity potential, downwash, etc., are the real parts of the complex expressions $\bar{\varphi} e^{i\omega t}$, $\bar{w} e^{i\omega t}$ etc., where ω is the circular frequency.

CONFIDENTIAL

The expression for the complex amplitude of pressure difference between the upper and lower surfaces ($\bar{p}_u - \bar{p}_l$) is:

$$\begin{aligned}\bar{p} \equiv \bar{p}_u - \bar{p}_l &= 2\rho \left[i\omega + U \frac{\partial}{\partial x} \right] \bar{\varphi}(x, y) \\ &= -\frac{2\rho}{\pi} \left[i\omega + U \frac{\partial}{\partial x} \right] \iint_A \frac{\bar{w}(\xi, \eta) e^{-i \frac{\omega M^2}{U \beta^2} (x-\xi)} \cos \left(\frac{\omega M}{U \beta^2} \sqrt{(x-\xi)^2 - \beta^2(y-\eta)^2} \right)}{\sqrt{(x-\xi)^2 - \beta^2(y-\eta)^2}} d\xi d\eta\end{aligned}$$

Eq. (2.3)

Except for some special cases, such as algebraic-polynomial deformation shapes in steady flow, the double integral cannot be evaluated in terms of tabulated functions, with the result that a numerical method must be resorted to. Following Pines' idea (Refs. 21-24), one may split the area A into sufficiently small elementary areas to allow certain approximations in the evaluation of the double integral. If one assumes that the downwash is constant over each area, for example, one obtains the approximate expression

$$\bar{p}(x, y) = 2\rho U \sum_j \bar{w}_j \left[-\frac{1}{\pi} \left(\frac{i\omega}{U} + \frac{\partial}{\partial x} \right) \right] \iint_{A_j} \frac{e^{-i \frac{\omega M^2}{U \beta^2} (x-\xi)} \cos \left(\frac{\omega M}{U \beta^2} \sqrt{(x-\xi)^2 - \beta^2(y-\eta)^2} \right)}{\sqrt{(x-\xi)^2 - \beta^2(y-\eta)^2}} d\xi d\eta$$

Eq. (2.4)

where \bar{w}_j is a suitable average downwash over area A_j . The quantity in the square brackets of Eq. (2.4) is the aerodynamic influence coefficient (abbreviated AIC from here on), i.e., the pressure at point (x, y) due to a unit downwash over A_j . The AIC will depend on the location of A_j relative to (x, y) and the shape of A_j . Three basic shapes have been proposed for the elementary areas (boxes): square boxes, rectangles with diagonals parallel to the Mach lines (Mach boxes) and rhombuses with sides parallel to Mach lines (characteristic boxes). For grid systems constructed of each of these box shapes, the expressions for the AIC are now derived.

II.2 Expressions for the Aerodynamic Influence Coefficients of the Square Grid System

a. Approximate Formulas of Pines and Harvard Computation Laboratory (Refs. 24, 25).

The only complete table of supersonic aerodynamic influence coefficients now in existence (Ref. 25) has been

CONFIDENTIAL

calculated on the basis of certain approximate integrations of Eq. (2.4), which are now described.

Equation (2.4) may be put into the form

$$\begin{aligned} \bar{p}(x, y) &= 2\beta U \sum_j \bar{w}_j \left[-\frac{1}{\pi} \left(i \bar{k}_j \frac{\beta^2}{M^2} + \frac{\partial}{\partial x_1} \right) \iint_{(A_j)_1} \frac{e^{-i \bar{k}_j (x - \xi)} \cos\left(\frac{\bar{k}_j R}{M}\right)}{R} d\xi, d\eta \right] \\ &\equiv 2\beta U \sum_j \bar{w}_j (\bar{R} + i \bar{I}) \end{aligned} \quad \text{Eq. (2.5)}$$

where

$$x_1 = \frac{x}{b_1}, \quad y_1 = \frac{y}{b_1}, \quad \xi_1 = \frac{\xi}{b_1}, \quad \eta_1 = \frac{\eta}{b_1}$$

are the dimensionless coordinates, b_1 is the side of the square box,

$$\bar{k}_1 = \frac{\omega b_1}{U} \frac{M^2}{\beta^2},$$

$$R = \sqrt{(x_1 - \xi_1)^2 - \beta^2 (y_1 - \eta_1)^2}$$

and $(A_j)_1$ is the dimensionless area of integration corresponding to A_j . In subsequent derivations, the subscript 1 will be dropped from the quantities $x_1, y_1, \xi_1, \eta_1, (A_j)_1$. As shown in Fig. II.1, the pressure at the center of the receiving box (n, m) due to a constant unit downwash at the sending box (v, μ) is dependent on the distances

$$x_n - x_v = n - v \equiv \bar{v}$$

$$y_m - y_\mu = m - \mu \equiv \bar{\mu}$$

Eqs. (2.6a-b)

where $n, m, v, \mu, \bar{v}, \bar{\mu}$ are all integers. The box (n, m) is the n^{th} box downstream, and the m^{th} box to the right of an arbitrarily chosen origin box $(0, 0)$. Since the parameters \bar{k}_1 and M appear within the brackets of Eq. (2.5) along with \bar{v} and $\bar{\mu}$, the aerodynamic influence coefficient is fixed by four independent quantities. A complete tabulation of these coefficients therefore involves "four-dimensional" tables.

CONFIDENTIAL

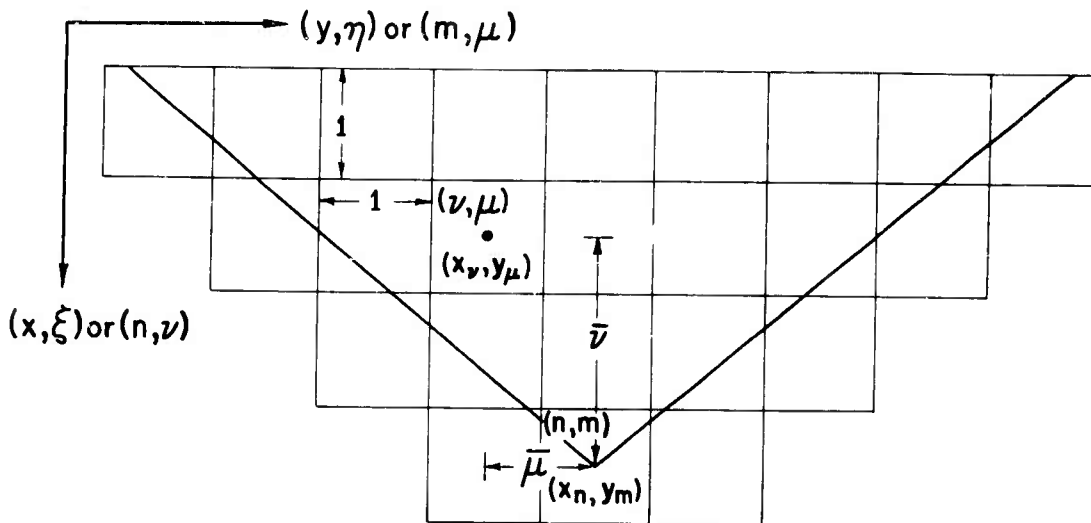


Fig. II.1 The Square Box Grid System

For "far boxes" (i.e., $\bar{v} \geq 2$), the following types of approximations are used:

$$e^{-i\bar{k}_1(x-\xi)} \cong e^{-i\bar{k}_1(x-\xi_c)},$$

$$\cos\left(\frac{\bar{k}_1}{M}R\right) \cong \cos\left(\frac{\bar{k}_1}{M}R_c\right) = \cos\left(\frac{\bar{k}_1}{M}\sqrt{(x-\xi_c)^2 - \beta^2(y-\eta_c)^2}\right), \quad \text{Eqs. (2.7a-b)}$$

where (ξ_c, η_c) denotes the center of the sending box. For sending boxes which lie completely inside the forward Mach lines from (x, y) , the areas of integration are squares. Then one obtains for the AIC the expression

$$\begin{aligned} \bar{R}_{\bar{v}, \bar{\mu}} + i\bar{I}_{\bar{v}, \bar{\mu}} = \frac{1}{\pi\beta} & \left[-\cos(\bar{v} + \frac{1}{2})\bar{k}_1 \cdot \cos\left(\frac{\bar{k}_1}{M}\sqrt{(\bar{v} + \frac{1}{2})^2 - \beta^2\bar{\mu}^2}\right) A_{\bar{v}, \bar{\mu}}^+ \right. \\ & + \cos(\bar{v} - \frac{1}{2})\bar{k}_1 \cdot \cos\left(\frac{\bar{k}_1}{M}\sqrt{(\bar{v} - \frac{1}{2})^2 - \beta^2\bar{\mu}^2}\right) A_{\bar{v}, \bar{\mu}}^- \\ & - \bar{k}_1 \frac{\beta^2}{M^2} \sin \bar{v} \bar{k}_1 \cdot \cos\left(\frac{\bar{k}_1}{M}\sqrt{\bar{v}^2 - \beta^2\bar{\mu}^2}\right) B_{\bar{v}, \bar{\mu}} \Big] \\ & + \frac{i}{\pi\beta} \left[\sin(\bar{v} + \frac{1}{2})\bar{k}_1 \cdot \cos\left(\frac{\bar{k}_1}{M}\sqrt{(\bar{v} + \frac{1}{2})^2 - \beta^2\bar{\mu}^2}\right) A_{\bar{v}, \bar{\mu}}^+ \right. \\ & - \sin(\bar{v} - \frac{1}{2})\bar{k}_1 \cdot \cos\left(\frac{\bar{k}_1}{M}\sqrt{(\bar{v} - \frac{1}{2})^2 - \beta^2\bar{\mu}^2}\right) A_{\bar{v}, \bar{\mu}}^- \\ & - \bar{k}_1 \frac{\beta^2}{M^2} \cos \bar{v} \bar{k}_1 \cdot \cos\left(\frac{\bar{k}_1}{M}\sqrt{\bar{v}^2 - \beta^2\bar{\mu}^2}\right) B_{\bar{v}, \bar{\mu}} \Big] \quad (\bar{v} \geq 2) \end{aligned}$$

Eq. (2.8)

CONFIDENTIAL

CONFIDENTIAL

where

$$A_{\bar{v}, \bar{\mu}}^+ = \cos^{-1} \frac{\beta(\bar{\mu} - \frac{1}{2})}{\bar{v} + \frac{1}{2}} - \cos^{-1} \frac{\beta(\bar{\mu} + \frac{1}{2})}{\bar{v} + \frac{1}{2}},$$

$$A_{\bar{v}, \bar{\mu}}^- = \cos^{-1} \frac{\beta(\bar{\mu} - \frac{1}{2})}{\bar{v} - \frac{1}{2}} - \cos^{-1} \frac{\beta(\bar{\mu} + \frac{1}{2})}{\bar{v} - \frac{1}{2}} = A_{\bar{v}-1, \bar{\mu}}^+,$$

$$B_{\bar{v}, \bar{\mu}} = (\bar{v} + \frac{1}{2}) A_{\bar{v}, \bar{\mu}}^+ - (\bar{v} - \frac{1}{2}) A_{\bar{v}, \bar{\mu}}^- + \beta(\bar{\mu} - \frac{1}{2}) \left[\frac{\cosh^{-1} \bar{v} - \frac{1}{2}}{\beta(\bar{\mu} - \frac{1}{2})} - \frac{\cosh^{-1} \bar{v} + \frac{1}{2}}{\beta(\bar{\mu} - \frac{1}{2})} \right] \\ - \beta(\bar{\mu} + \frac{1}{2}) \left[\frac{\cosh^{-1} \bar{v} - \frac{1}{2}}{\beta(\bar{\mu} + \frac{1}{2})} - \frac{\cosh^{-1} \bar{v} + \frac{1}{2}}{\beta(\bar{\mu} + \frac{1}{2})} \right]. \quad \text{Eqs. (2.9a-c)}$$

If the sending box is cut by a Mach line, the above expressions are still valid provided the following interpretations are adopted:

$$\begin{aligned} \cos^{-1} x &= 0 & \text{for } 1 \leq x \\ \cos^{-1} x &= 0 \text{ to } \pi/2 & \text{for } 0 \leq x \leq 1 \\ \cos^{-1} x &= \pi - \cos^{-1}(-x) & \text{for } -1 \leq x \leq 0 \\ \cos^{-1} x &= \pi & \text{for } x \leq -1 \\ \sqrt{x} &= 0 & \text{for } x \leq 0 \\ \cosh^{-1} x &= 0 \text{ to } \infty & \text{for } 1 \leq x \\ \cosh^{-1} x &= 0 & \text{for } -1 \leq x \leq 1 \\ \cosh^{-1} x &= \cosh^{-1}(-x) & \text{for } x \leq -1 \end{aligned}$$

Eqs. (2.10a-h)

It should be noted that only positive values of $\bar{\mu}$ need be considered since by symmetry

$$\bar{R}_{\bar{v}, -\bar{\mu}} + i \bar{I}_{\bar{v}, -\bar{\mu}} = \bar{R}_{\bar{v}, \bar{\mu}} + i \bar{I}_{\bar{v}, \bar{\mu}} \quad \text{Eq. (2.11)}$$

CONFIDENTIAL

Equation (2.8) is identical with Eqs. (3a-b) of Ref. 25. For near boxes ($\bar{\nu}=0, 1$) a different numerical method is followed in Ref. 25 to insure sufficient accuracy at high values of \bar{k} . As illustrated in Fig. II.2, each near box is subdivided by a 5x5 grid. For this finer grid system, the reference length is $b_1/5$ and the reduced frequency is $\bar{k}_1/5$;

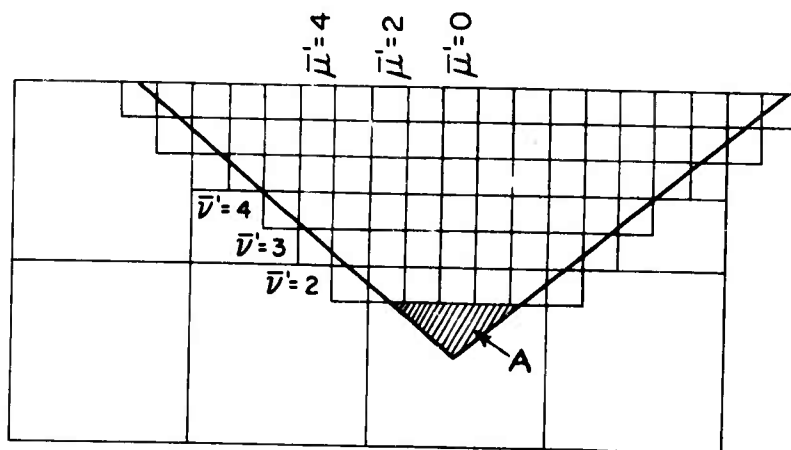


Fig. II.2 Subdivision of Near Boxes

associated with the small boxes, there is a new set of indices $\bar{\nu}', \bar{\mu}'$. The contributions due to each box in rows $\bar{\nu}'=2$ to $\bar{\nu}'=7$ may then be calculated using Eq. (2.8), employing $\bar{k}_1' = \bar{k}_1/5$ instead of \bar{k}_1 . The AIC of a large box in row $\bar{\nu}=1$ is obtained by summing the contributions due to the corresponding small boxes. For example, one has for box $\bar{\nu}=1, \bar{\mu}=0$,

$$\bar{R}_{1,0} + i \bar{I}_{1,0} = \sum_{\bar{\nu}'=3}^7 \sum_{\bar{\mu}'=-2}^2 (\bar{R}_{\bar{\nu}', \bar{\mu}'} + i \bar{I}_{\bar{\nu}', \bar{\mu}'})_{\bar{k}_1'} \quad \text{Eq. (2.12)}$$

It remains to show how one may compute the contributions of the small boxes in rows $\bar{\nu}' = 0, 1$. If $M \geq \sqrt{1.36}$, which is an estimate of the practical range of applicability of this theory, these rows are confined to the large box (0, 0)

CONFIDENTIAL

and they form a triangular region A as shown in Fig. II.2. The contribution of the whole region A is given by the first few terms of the exact infinite series:

$$\begin{aligned} \bar{R}_A + i\bar{I}_A = & \frac{1}{\beta} \left[-1 + \frac{27}{400} \left(\frac{\bar{K}_1}{M} \right)^2 - \frac{9(9+12M^2)}{128,000} \left(\frac{\bar{K}_1}{M} \right)^4 \right] \\ & + \frac{i}{M\beta} \left[\frac{3}{10} \left(\frac{\bar{K}_1}{M} \right) - \frac{9(4M^2+1)}{4,000} \left(\frac{\bar{K}_1}{M} \right)^3 \right] \end{aligned} \quad \text{Eq. (2.13)}$$

The third term in the real part of Eq. (2.13) is different from the corresponding term of Eq. (7) of Ref. 25. This discrepancy has introduced a small inaccuracy into the tabulations of $\bar{R}_{c,o}$ in the above reference. This error is not regarded as significant, since it is at most five units in the third place for the highest \bar{K}_1 and lowest Mach number, whereas the accuracy of the tabulations for rows $\bar{v} \geq 2$ from Eqs. (2.8) is much poorer, as will be shown in Section III.4.

b. Exact Formulas

Making use of well-known relations in the theory of Bessel functions, Watkins (private communication; no formal reference yet available) was able to reduce the double integral of the potential function [Eq. (2.1)] into a single integral with an integrand expressed in terms of an infinite series. Following this idea, similar reduction is possible for the double integral of Eq. (2.4). Inasmuch as the AIC's are extensively tabulated in Ref. 25 using the approximate formulas of Section II.2a, the exact expressions for the square grid system will not be presented here. The same mathematical technique will be fully discussed in connection with the Mach grid system in Section II.3.

II.3 Expressions for the Aerodynamic Influence Coefficients of the Mach Box Grid System

For the Mach box grid system, Eq. (2.4) may be put in the form

$$\begin{aligned} \bar{p}(x,y) = & \frac{2\rho U}{\beta} \sum_j \bar{w}_j \left[-\frac{1}{\pi} \left(i\bar{K}_1 \frac{\partial^2}{\partial x_1^2} + \frac{\partial}{\partial x_1} \right) \iint_{(A_j)} \frac{e^{-i\bar{K}_1(x_1-\xi_1)} \cos\left(\frac{\bar{K}_1}{M} R\right)}{R} d\xi_1 d\eta_1 \right] \\ = & \frac{2\rho U}{\beta} \sum_j \bar{w}_j (\mathcal{R} + i\mathcal{I}) \end{aligned} \quad \text{Eq. (2.14)}$$

CONFIDENTIAL

where

$$x_1 = \frac{x}{b_1}, \quad y_1 = \frac{\beta y}{b_1}, \quad \xi_1 = \frac{\xi}{b_1}, \quad \eta_1 = \frac{\beta \eta}{b_1}$$

are the dimensionless coordinates and b_1 is the streamwise dimension of a box (the spanwise dimension is b_1/β).

$$\bar{k}_1 = \frac{\omega b_1}{U} \frac{M^2}{\beta^2},$$

$$R = \sqrt{(x_1 - \xi_1)^2 + (y_1 - \eta_1)^2}$$

and (A_1) is the dimensionless area of a Mach box. Here, $R + iJ$ is defined differently from $\bar{R} + i\bar{I}$ (by a factor of β). This new definition is more convenient, since for steady flow, the AIC becomes independent of Mach number.

a. Approximate Formulas

The procedure in obtaining the approximate expressions is similar to that for the square box and need not be repeated here. It is worth noting that, in Fig. II.3, the dimensions of Mach boxes are so proportioned that the forward Mach lines from (x, y) always cut the boxes along the diagonal. Consequently, for complete boxes $\bar{v} > |\bar{\mu}|$, and for partial boxes (half boxes) on the Mach line $\bar{v} = |\bar{\mu}|$. Again, because of the symmetry

$$R_{\bar{v}, -\bar{\mu}} + iJ_{\bar{v}, -\bar{\mu}} = R_{\bar{v}, \bar{\mu}} + iJ_{\bar{v}, \bar{\mu}}$$

The approximate influence coefficient formulas read:

$$\begin{aligned} R_{\bar{v}, \bar{\mu}} + iJ_{\bar{v}, \bar{\mu}} = & \frac{1}{\pi} \left[-\cos(\bar{v} + \frac{1}{2})\bar{k}_1 \cdot \cos(\frac{\bar{k}_1}{M} \sqrt{(\bar{v} + \frac{1}{2})^2 - \bar{\mu}^2}) \mathcal{A}_{\bar{v}, \bar{\mu}}^+ \right. \\ & + \cos(\bar{v} - \frac{1}{2})\bar{k}_1 \cdot \cos(\frac{\bar{k}_1}{M} \sqrt{(\bar{v} - \frac{1}{2})^2 - \bar{\mu}^2}) \mathcal{A}_{\bar{v}, \bar{\mu}}^- \\ & \left. - \bar{k}_1 \frac{\beta^2}{M^2} \sin \bar{v} \bar{k}_1 \cdot \cos(\frac{\bar{k}_1}{M} \sqrt{\bar{v}^2 - \bar{\mu}^2}) \mathcal{B}_{\bar{v}, \bar{\mu}} \right] \\ & + \frac{i}{\pi} \left[\sin(\bar{v} + \frac{1}{2})\bar{k}_1 \cdot \cos(\frac{\bar{k}_1}{M} \sqrt{(\bar{v} + \frac{1}{2})^2 - \bar{\mu}^2}) \mathcal{A}_{\bar{v}, \bar{\mu}}^+ \right. \\ & - \sin(\bar{v} - \frac{1}{2})\bar{k}_1 \cdot \cos(\frac{\bar{k}_1}{M} \sqrt{(\bar{v} - \frac{1}{2})^2 - \bar{\mu}^2}) \mathcal{A}_{\bar{v}, \bar{\mu}}^- \\ & \left. - \bar{k}_1 \frac{\beta^2}{M^2} \cos \bar{v} \bar{k}_1 \cdot \cos(\frac{\bar{k}_1}{M} \sqrt{\bar{v}^2 - \bar{\mu}^2}) \mathcal{B}_{\bar{v}, \bar{\mu}} \right] \quad (\bar{v} \geq \bar{\mu} \geq 2) \end{aligned}$$

Eq. (2.15)

CONFIDENTIAL

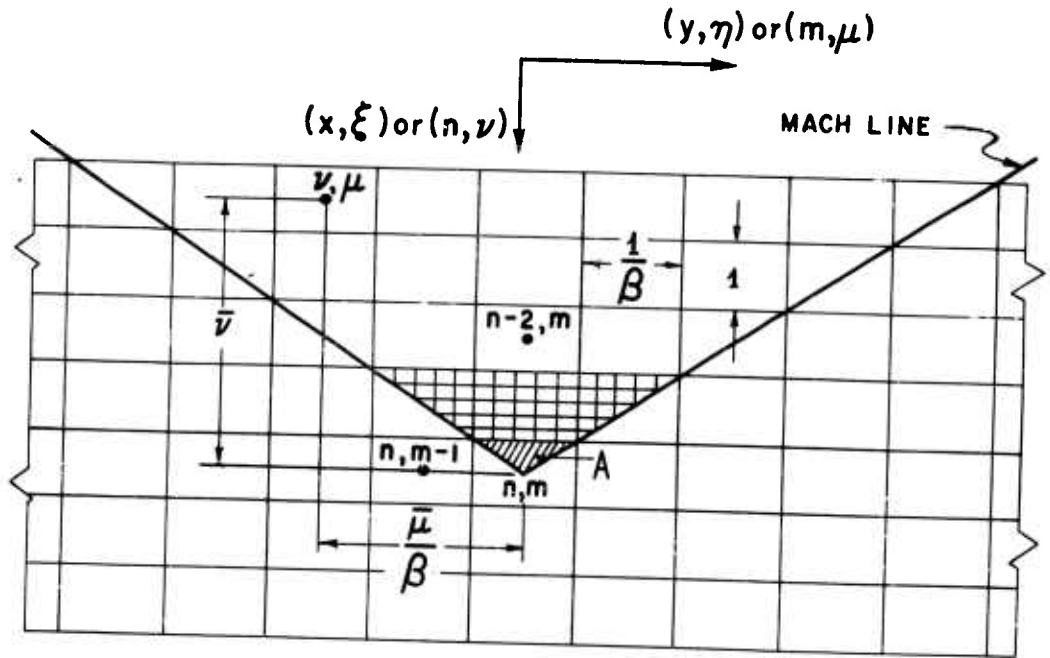


Fig. II.3 The Mach Box Grid System

where

$$A_{\bar{\nu}, \bar{\mu}}^+ = \cos^{-1} \frac{\bar{\mu} - \frac{1}{2}}{\bar{\nu} + \frac{1}{2}} - \cos^{-1} \frac{\bar{\mu} + \frac{1}{2}}{\bar{\nu} + \frac{1}{2}},$$

$$A_{\bar{\nu}, \bar{\mu}}^- = \cos^{-1} \frac{\bar{\mu} - \frac{1}{2}}{\bar{\nu} - \frac{1}{2}} - \cos^{-1} \frac{\bar{\mu} + \frac{1}{2}}{\bar{\nu} - \frac{1}{2}} = A_{\bar{\nu}-1, \bar{\mu}}^+,$$

$$B_{\bar{\nu}, \bar{\mu}} = (\bar{\nu} + \frac{1}{2}) A_{\bar{\nu}, \bar{\mu}}^+ - (\bar{\nu} - \frac{1}{2}) A_{\bar{\nu}, \bar{\mu}}^- + (\bar{\mu} - \frac{1}{2}) \left[\cosh^{-1} \frac{\bar{\nu} - \frac{1}{2}}{\bar{\mu} - \frac{1}{2}} - \cosh^{-1} \frac{\bar{\nu} + \frac{1}{2}}{\bar{\mu} - \frac{1}{2}} \right] \\ - (\bar{\mu} + \frac{1}{2}) \left[\cosh^{-1} \frac{\bar{\nu} - \frac{1}{2}}{\bar{\mu} + \frac{1}{2}} - \cosh^{-1} \frac{\bar{\nu} + \frac{1}{2}}{\bar{\mu} + \frac{1}{2}} \right], \quad (\bar{\nu} \geq \bar{\mu} \geq 2)$$

Eqs. (2.16a-c)

CONFIDENTIAL

CONFIDENTIAL

and the interpretations given in Eqs. (2.10a-h) apply. The quantities $\mathcal{A}_{\bar{v}, \bar{\mu}}^+$, $\mathcal{A}_{\bar{v}, \bar{\mu}}^-$ and $\mathcal{B}_{\bar{v}, \bar{\mu}}$ are independent of Mach number and reduced frequency. They are tabulated in Ref. 31 for $\bar{v}=2$ to 25 and $\bar{\mu}=0$ to 25. For the boxes in row $\bar{v}=1$, the subdivision technique of Section II.2 may be employed, as shown in Fig. II.3, to yield

$$\begin{aligned} \mathcal{R}_{1,0} + i\mathcal{J}_{1,0} &= \sum_{\bar{v}'=3}^7 (\mathcal{R}_{\bar{v}',0} + i\mathcal{J}_{\bar{v}',0})_{\bar{k}'=\bar{k}_1/5} + 2 \sum_{\bar{v}'=3}^7 \sum_{\bar{\mu}'=1}^2 (\mathcal{R}_{\bar{v}',\bar{\mu}'} + i\mathcal{J}_{\bar{v}',\bar{\mu}'})_{\bar{k}'=\bar{k}_1/5} \\ \mathcal{R}_{1,1} + i\mathcal{J}_{1,1} &= \sum_{\bar{v}'=3}^7 \sum_{\bar{\mu}'=3}^{\bar{v}'} (\mathcal{R}_{\bar{v}',\bar{\mu}'} + i\mathcal{J}_{\bar{v}',\bar{\mu}'})_{\bar{k}'=\bar{k}_1/5} \end{aligned} \quad \text{Eqs. (2.17a-b)}$$

For the only box (0,0) in row $\bar{v}=0$, no subdivision is necessary and the contribution of this box (Region A) is

$$\begin{aligned} \mathcal{R}_{0,0} + i\mathcal{J}_{0,0} &= \left\{ -1 + \frac{3}{16} \left(\frac{\bar{k}_1}{M} \right)^2 - \frac{5(4M^2+3)}{3072} \left(\frac{\bar{k}_1}{M} \right)^4 \right. \\ &\quad \left. + \frac{i}{M} \left\{ \frac{1}{2} \left(\frac{\bar{k}_1}{M} \right) - \frac{(4M^2+1)}{96} \left(\frac{\bar{k}_1}{M} \right)^3 \right\} \right\} \quad (\bar{\mu}=\bar{v}=0) \end{aligned} \quad \text{Eq. (2.18)}$$

Equation (2.18) is obtained from the infinite series expansion of the exact expression for $\mathcal{R}_{0,0} + i\mathcal{J}_{0,0}$, which is given below in Eq. (2.29a).

It should be noted here that, although the exact expressions given by Li for the AIC are correct (cf. Eq. 20, page 18, Ref. 26), certain approximations for the integrals, necessitated by the type of computing equipment available, are inadequate. For example, Li approximates his Eq. (23b) by Eq. (33). Consider the exact expression for the steady-state case with constant downwash equal to unity:

$$\begin{aligned} K_{\mu, s-(g-\mu)} &= \frac{V}{\beta} \int_{\mu-\frac{1}{2}}^{\mu+\frac{1}{2}} \left\{ -(g-\mu-\frac{1}{2})(g-\xi)^{-1} [(g-\xi)^2 - (g-\mu-\frac{1}{2})^2]^{-1/2} \right\} d\xi \\ &= -\frac{V}{\beta} \cos^{-1} \frac{g-\mu-\frac{1}{2}}{g-\mu+\frac{1}{2}} \end{aligned}$$

Eq. (2.19a)

Li's approximate formula (Eq. 33) for $K_{\mu, s-(g-\mu)}$ reads

CONFIDENTIAL

$$k_{\mu, s-(g-\mu)} \approx -\frac{V}{\beta} (g-\mu-\frac{1}{2})(g-\mu)^{-1}(g-\mu-\frac{1}{4})^{-\frac{1}{2}}$$

Eq. (2.19b)

The integrand of Eq. (23) is singular at the upper limit and therefore the finite power series expansion used by Li for the singular term leads to large inaccuracies. This fact is confirmed by the brief table below, which compares Eqs. (2.19a) and (2.19b):

$(g-\mu)$	Exact $(-\frac{\beta K}{V})$ Eq. (2.19a)	Approximate $(-\frac{\beta K}{V})$ Eq. (2.19b)
1	1.231	0.577
2	0.927	0.567
3	0.775	0.503
4	0.680	0.452

b. Exact Formulas

Following Watkin's idea mentioned above, it is possible to reduce the dimensionless expression for the AIC, i.e.,

$$R+iJ = -\frac{1}{\pi} (i\bar{k}_1 \frac{\beta^2}{M^2} + \frac{\partial}{\partial x}) \iint_{(A_j)} \frac{e^{-i\bar{k}_1(x-\xi)} \cos(\frac{\bar{k}_1}{M} \sqrt{(x-\xi)^2 - (y-\eta)^2})}{\sqrt{(x-\xi)^2 - (y-\eta)^2}} d\xi d\eta$$

Eq. (2.20)

in the following manner. Consider an area A_j in the influencing region, bounded by the lines $(\xi = \xi_a \text{ and } \xi_b, \eta = \eta_a \text{ and } \eta_b)$. Using a relation which can be derived from Eq. (1) on page 415, Ref. 32

$$\int_0^\infty J_0(x\sqrt{\tau^2 + b^2}) \cos a\tau d\tau = \frac{\cos b\sqrt{x^2 - a^2}}{\sqrt{x^2 - a^2}} \quad \text{for } x > a$$

$$= 0$$

for $x < a$

Eq. (2.21)

CONFIDENTIAL

Equation (2.20) may be put in the form

$$R+iJ = -\frac{1}{\pi} \left(i\bar{k}_1 \frac{\beta^2}{M^2} + \frac{\partial}{\partial x} \right) \int_{\xi_a}^{\xi_b} \int_{\eta_a}^{\eta_b} e^{-i\bar{k}_1(x-\xi)} \int_0^\infty \frac{1}{\tau} J_0 \left[(x-\xi) \sqrt{\tau^2 + \left(\frac{\bar{k}_1}{M} \right)^2} \right] \cos(y-\eta) \tau d\tau d\xi d\eta$$

Eq. (2.22)

Changing the order of integration, and carrying out the η -part, one has

$$R+iJ = -\frac{1}{\pi} \left(i\bar{k}_1 \frac{\beta^2}{M^2} + \frac{\partial}{\partial x} \right) \int_{\xi_a}^{\xi_b} e^{-i\bar{k}_1(x-\xi)} \int_0^\infty \frac{1}{\tau} J_0 \left[(x-\xi) \sqrt{\tau^2 + \left(\frac{\bar{k}_1}{M} \right)^2} \right] \left\{ \sin \tau(y-\eta_a) - \sin \tau(y-\eta_b) \right\} d\tau d\xi$$

Eq. (2.23)

With the additional relations, Eq. (1), page 358 and Eq. (2), page 405 of Ref. 32

$$J_0(\sqrt{a^2+b^2}) = J_0(a)J_0(b) + 2 \sum_{r=1}^{\infty} (-1)^r J_{2r}(a)J_{2r}(b)$$

$$\int_0^\infty J_{2r}(a\tau) \frac{\sin b\tau}{\tau} d\tau = \frac{1}{2r} \sin(2r \sin^{-1} \frac{b}{a}) \quad \text{for } a > b$$

Eqs. (2.24a-b)

and since $|y-\eta| \leq (x-\xi)$ for this region, there results

$$R+iJ = -\frac{1}{\pi} \left(i\bar{k}_1 \frac{\beta^2}{M^2} + \frac{\partial}{\partial x} \right) \int_{\xi_a}^{\xi_b} e^{-i\bar{k}_1(x-\xi)} \left\{ J_0 \left(\frac{\bar{k}_1}{M} [x-\xi] \right) \left[\sin^{-1} \frac{y-\eta_a}{x-\xi} - \sin^{-1} \frac{y-\eta_b}{x-\xi} \right] \right. \\ \left. + \sum_{r=1}^{\infty} \frac{(-1)^r}{r} J_{2r} \left(\frac{\bar{k}_1}{M} [x-\xi] \right) \left\{ \sin(2r \sin^{-1} \frac{y-\eta_a}{x-\xi}) - \sin(2r \sin^{-1} \frac{y-\eta_b}{x-\xi}) \right\} \right\} d\xi.$$

Eq. (2.25)

Furthermore, since the limits are constant and the integrand I of Eq. (2.25) is a function of $(x-\xi)$

$$\frac{\partial}{\partial x} \int_{\xi_a}^{\xi_b} (I) d\xi = \int_{\xi_a}^{\xi_b} \frac{\partial}{\partial x} (I) d\xi = - \int_{\xi_a}^{\xi_b} \frac{\partial}{\partial \xi} (I) d\xi \\ = I(\xi_a) - I(\xi_b).$$

Eq. (2.26)

Equation (2.25) becomes

CONFIDENTIAL

$$R_{+i} J = -\frac{1}{\pi} i \bar{k}_1 \frac{\beta^2}{M^2} \int_{\xi_a}^{\xi_b} I d\xi - \frac{1}{\pi} (I(\xi_a) - I(\xi_b)).$$

Eq. (2.27)

It can be proved that Eq. (2.27) holds true even for the partial boxes (boxes cut by Mach lines) provided the following definitions are observed:

$$\begin{aligned} \sin^{-1} \chi &= \frac{\pi}{2}, & 1 \leq \chi \\ \sin^{-1} \chi &= -\frac{\pi}{2} \text{ to } \frac{\pi}{2}, & -1 \leq \chi \leq 1 \\ \sin^{-1} \chi &= -\frac{\pi}{2}, & \chi \leq -1 \end{aligned}$$

Eqs. (2.28a-c)

In the Mach box grid system, for a box with its center \bar{v} and $\bar{\mu}$ units away from the point (x, y) , ξ_a , ξ_b , η_a and η_b can be written as $x - (\bar{v} + \frac{1}{2})$, $x - (\bar{v} - \frac{1}{2})$, $y - (\bar{\mu} + \frac{1}{2})$, and $y - (\bar{\mu} - \frac{1}{2})$. An exception is box $(0, 0)$, where $x - \xi_a$ is zero instead of $-\frac{1}{2}$. The following expressions are therefore obtained:

$$R_{0,0} + i J_{0,0} = -e^{-i \frac{\bar{k}_1}{2}} J_0\left(\frac{\bar{k}_1}{2M}\right) - \frac{i \bar{k}_1}{2} \frac{\beta^2}{M^2} f_0\left(M, \frac{\bar{k}_1}{2}\right) \quad (\bar{v} = \bar{\mu} = 0)$$

$$\begin{aligned} R_{\bar{v}, \bar{v}} + i J_{\bar{v}, \bar{v}} &= \frac{1}{\pi} e^{-i \bar{k}_1 (\bar{v} + \frac{1}{2})} \left[J_0\left(\frac{\bar{k}_1}{M} [\bar{v} + \frac{1}{2}]\right) \left(\sin^{-1} \frac{\bar{v} - \frac{1}{2}}{\bar{v} + \frac{1}{2}} - \frac{\pi}{2} \right) + \sum_{r=1}^{\infty} \frac{(-1)^r}{r} J_{2r}\left(\frac{\bar{k}_1}{M} [\bar{v} + \frac{1}{2}]\right) \sin\left(2r \sin^{-1} \frac{\bar{v} - \frac{1}{2}}{\bar{v} + \frac{1}{2}}\right) \right] \\ &\quad + \frac{i \bar{k}_1}{\pi} \frac{\beta^2}{M^2} \int_{\bar{v} - \frac{1}{2}}^{\bar{v} + \frac{1}{2}} e^{-i \bar{k}_1 X} \left[-\frac{\pi}{2} J_0\left(\frac{\bar{k}_1}{M} X\right) + J_0\left(\frac{\bar{k}_1}{M} X\right) \sin^{-1} \frac{\bar{v} - \frac{1}{2}}{X} \right. \\ &\quad \left. + \sum_{r=1}^{\infty} \frac{(-1)^r}{r} J_{2r}\left(\frac{\bar{k}_1}{M} X\right) \sin\left(2r \sin^{-1} \frac{\bar{v} - \frac{1}{2}}{X}\right) \right] dX \end{aligned}$$

($\bar{v} = \bar{\mu} \geq 1$)

Eqs. (2.29a-b)

CONFIDENTIAL

$$\begin{aligned}
 R_{\bar{\nu}, \bar{\mu}} + i J_{\bar{\nu}, \bar{\mu}} = & \frac{1}{\pi} e^{-i \bar{k}_1 (\bar{\nu} + \frac{1}{2})} \left[J_0 \left(\frac{\bar{k}_1}{M} [\bar{\nu} + \frac{1}{2}] \right) \left\{ \sin^{-1} \frac{\bar{\mu} - \frac{1}{2}}{\bar{\nu} + \frac{1}{2}} - \sin^{-1} \frac{\bar{\mu} + \frac{1}{2}}{\bar{\nu} + \frac{1}{2}} \right\} \right. \\
 & + \sum_{r=1}^{\infty} \frac{(-1)^r}{r} J_{2r} \left(\frac{\bar{k}_1}{M} [\bar{\nu} + \frac{1}{2}] \right) \left\{ \sin(2r \sin^{-1} \frac{\bar{\mu} - \frac{1}{2}}{\bar{\nu} + \frac{1}{2}}) - \sin(2r \sin^{-1} \frac{\bar{\mu} + \frac{1}{2}}{\bar{\nu} + \frac{1}{2}}) \right\} \Big] \\
 & - \frac{1}{\pi} e^{-i \bar{k}_1 (\bar{\nu} - \frac{1}{2})} \left[J_0 \left(\frac{\bar{k}_1}{M} [\bar{\nu} - \frac{1}{2}] \right) \left\{ \sin^{-1} \frac{\bar{\mu} - \frac{1}{2}}{\bar{\nu} - \frac{1}{2}} - \sin^{-1} \frac{\bar{\mu} + \frac{1}{2}}{\bar{\nu} - \frac{1}{2}} \right\} \right. \\
 & + \sum_{r=1}^{\infty} \frac{(-1)^r}{r} J_{2r} \left(\frac{\bar{k}_1}{M} [\bar{\nu} - \frac{1}{2}] \right) \left\{ \sin(2r \sin^{-1} \frac{\bar{\mu} - \frac{1}{2}}{\bar{\nu} - \frac{1}{2}}) - \sin(2r \sin^{-1} \frac{\bar{\mu} + \frac{1}{2}}{\bar{\nu} - \frac{1}{2}}) \right\} \Big] \\
 & + \frac{i \bar{k}_1 \beta^2}{\pi M^2} \int_{\bar{\nu} - \frac{1}{2}}^{\bar{\nu} + \frac{1}{2}} e^{-i \bar{k}_1 X} \left[J_0 \left(\frac{\bar{k}_1}{M} X \right) \left\{ \sin^{-1} \frac{\bar{\mu} - \frac{1}{2}}{X} - \sin^{-1} \frac{\bar{\mu} + \frac{1}{2}}{X} \right\} \right. \\
 & + \sum_{r=1}^{\infty} \frac{(-1)^r}{r} J_{2r} \left(\frac{\bar{k}_1}{M} X \right) \left\{ \sin(2r \sin^{-1} \frac{\bar{\mu} - \frac{1}{2}}{X}) - \sin(2r \sin^{-1} \frac{\bar{\mu} + \frac{1}{2}}{X}) \right\} \Big] dX \quad (\bar{\nu} > \bar{\mu} \geq 0)
 \end{aligned}$$

Eq. (2.29c)

where f_0 is the familiar function of linearized unsteady supersonic flow theory (cf. Ref. 36 or Section III) and J_{2r} is the Bessel function of the first kind of order $2r$. Although, at first glance, these expressions seem rather complicated, the evaluations are not difficult because of the rapid convergence of the infinite series. For the ranges of Mach number and reduced frequency of interest, only the first three or four terms need be retained. Furthermore, the sine functions can be reduced to Chebyshev polynomials $S_n(x)$ (Ref. 33) when $|x| \leq 1$:

$$\begin{aligned}
 \sin(2r \sin^{-1} X) &= (-1)^{r+1} \sqrt{1-X^2} S_{2r-1}(2X) & |X| \leq 1 \\
 &= 0 & |X| \geq 1
 \end{aligned}$$

Eq. (2.30)

where $S_{2r-1}(2X)$ are represented by the simple expressions

$$\begin{aligned}
 S_1(2X) &= 2X \\
 S_3(2X) &= (2X)^3 - 2(2X) \\
 S_5(2X) &= (2X)^5 - 4(2X)^3 + 3(2X) \\
 &\vdots
 \end{aligned}$$

Eq. (2.31)

CONFIDENTIAL

c. Steady-State Formulas

Since frequent use will be made of the Mach box scheme for steady-flow problems, it is useful to have the corresponding formulas and a tabulation for the AIC. For $\bar{K}_1 = 0$, from Eqs. (2.29a-b), one finds all the imaginary parts equal to zero and

$$R_{0,0} = -1$$

$$R_{1,0} = \frac{1}{\pi} \left\{ -2 \sin^{-1} \frac{1}{3} + \pi \right\}$$

$$R_{1,1} = \frac{1}{\pi} \left\{ \sin^{-1} \frac{1}{3} - \frac{\pi}{2} \right\} = -\frac{1}{2} R_{1,0}$$

$$R_{\bar{\nu}, \bar{\mu}} = \frac{1}{\pi} \left\{ -A_{\bar{\nu}, \bar{\mu}}^+ + A_{\bar{\nu}, \bar{\mu}}^- \right\}$$

Eqs. (2.32a-d)

The values of $R_{\bar{\nu}, \bar{\mu}}$ are given in Table A.2 of Ref. 31 for $\bar{\nu}, \bar{\mu}$ from 0 to 12. It should be emphasized that these coefficients are independent of Mach number, unlike the corresponding ones for the square box.

II.4 Expressions for the Aerodynamic Influence Coefficients of the Characteristic Grid System

In supersonic flow, the most natural coordinate system for many purposes is one with axes parallel to Mach lines. Consider such a dimensionless system with origin at (ξ, η) , as in Fig. II.4. The characteristic coordinates (r, s) are defined by the transformation

$$r = \frac{M}{2\beta d} [(x - \xi) - \beta(y - \eta)]$$

$$s = \frac{M}{2\beta d} [(x - \xi) + \beta(y - \eta)]$$

or

Eqs. (2.33a-b)

$$x - \xi = \frac{d\beta}{M}(r + s)$$

$$y - \eta = -\frac{d}{M}(r - s)$$

Eqs. (2.33c-d)

CONFIDENTIAL

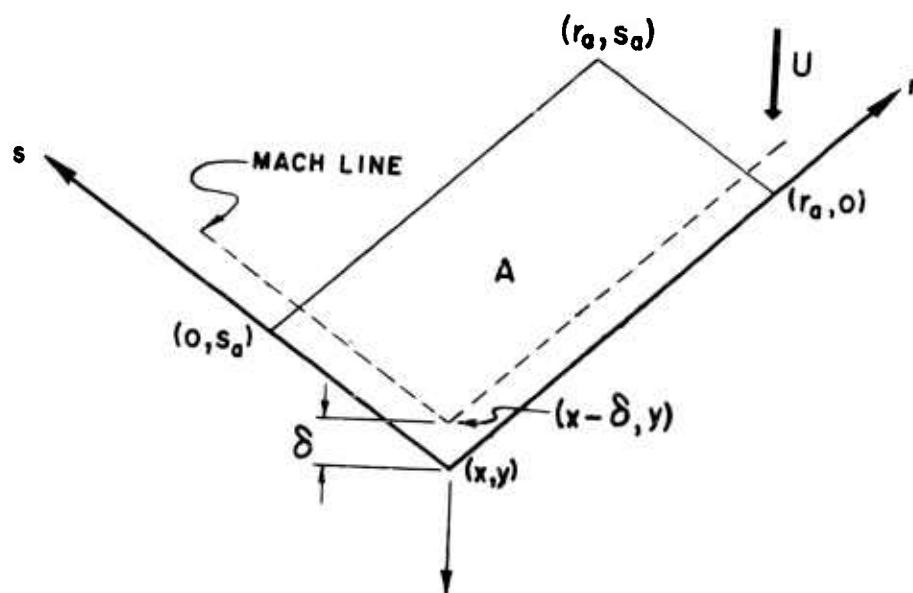


Fig. II.4 Characteristic Coordinate System

where d is a reference length. From Eq. (2.1), the potential at point (x, y) due to a unit constant downwash over a parallelogram (such as Region A) is

$$\varphi(x, y) = -\frac{d}{\pi M} \int_0^{s_a} \int_0^{r_a} \frac{e^{-i\theta(r+s)} \cos\left(\frac{2\theta}{M} \sqrt{rs}\right)}{\sqrt{rs}} dr ds$$

Eq. (2.34)

where

$$\theta = \frac{\omega M d}{U \beta}$$

Eq. (2.35)

Similarly at point $(x-\delta, y)$, the potential is

$$\varphi(x-\delta, y) = -\frac{d}{\pi M} \int_0^{s_a - \frac{SM}{2\beta d}} \int_0^{r_a - \frac{SM}{2\beta d}} \frac{e^{-i\theta(r+s)} \cos\left(\frac{2\theta}{M} \sqrt{rs}\right)}{\sqrt{rs}} dr ds$$

Eq. (2.36)

CONFIDENTIAL

CONFIDENTIAL

The x -derivative of φ is conveniently obtained from the operation

$$\begin{aligned} \frac{\partial \varphi}{\partial x} \Big|_{x,y} &= \lim_{\delta \rightarrow 0} \frac{\varphi(x,y) - \varphi(x-\delta,y)}{\delta} = - \frac{\partial \varphi(x-\delta,y)}{\partial \delta} \Big|_{\delta=0} \\ &= \frac{-1}{2\pi\beta} \left[\int_0^{r_a} \frac{e^{-i\theta(r+s)} \cos\left(\frac{2\theta}{M} \sqrt{rs_a}\right)}{\sqrt{rs_a}} dr + \int_0^{s_a} \frac{e^{-i\theta(r+s)} \cos\left(\frac{2\theta}{M} \sqrt{r_a s}\right)}{\sqrt{r_a s}} ds \right] \end{aligned} \quad \text{Eq. (2.37)}$$

The pressure at (x,y) due to region A, according to Eq. (2.3) in dimensionless form is

$$\begin{aligned} \bar{p}_A(x,y) &= 2\beta U \left[-\frac{i\theta\beta}{\pi M^2} \int_0^{s_a} \int_0^{r_a} \frac{e^{-i\theta(r+s)} \cos\left(\frac{2\theta}{M} \sqrt{rs}\right)}{\sqrt{rs}} dr ds \right. \\ &\quad \left. - \frac{1}{2\pi\beta} \left\{ \frac{e^{-i\theta s_a}}{\sqrt{s_a}} \int_0^{r_a} \frac{e^{-i\theta r}}{\sqrt{r}} \cos\left(\frac{2\theta}{M} \sqrt{rs_a}\right) dr + \frac{e^{-i\theta r_a}}{\sqrt{r_a}} \int_0^{s_a} \frac{e^{-i\theta s}}{\sqrt{s}} \cos\left(\frac{2\theta}{M} \sqrt{r_a s}\right) ds \right\} \right] \\ &\equiv \bar{p}_A(r_a, s_a) \end{aligned} \quad \text{Eq. (2.38)}$$

Similarly, for regions B and C of Fig. II.5, one obtains

$$\begin{aligned} \bar{p}_B(r_b, s_b) &= 2\beta U \left[-\frac{i\theta\beta}{\pi M^2} \int_0^{s_b} \int_0^{r_b+s_b-s} \frac{e^{-i\theta(r+s)} \cos\left(\frac{2\theta}{M} \sqrt{rs}\right)}{\sqrt{rs}} dr ds \right. \\ &\quad \left. - \frac{1}{\pi\beta} e^{-i\theta(r_b+s_b)} \int_0^{s_b} \frac{\cos\left(\frac{2\theta}{M} \sqrt{(r_b+s_b-s)s}\right)}{\sqrt{(r_b+s_b-s)s}} ds \right. \\ &\quad \left. - \frac{1}{2\pi\beta} \frac{e^{-i\theta s_b}}{\sqrt{s_b}} \int_0^{r_b} \frac{e^{-i\theta r} \cos\left(\frac{2\theta}{M} \sqrt{rs_b}\right)}{\sqrt{r}} dr \right] \end{aligned} \quad \text{Eq. (2.39)}$$

$$\begin{aligned} \bar{p}_C(r_c, s_c) &= 2\beta U \left[-\frac{i\theta\beta}{\pi M^2} \int_0^{s_c} \int_0^{r_c-s_c+s} \frac{e^{-i\theta(r+s)} \cos\left(\frac{2\theta}{M} \sqrt{rs}\right)}{\sqrt{rs}} dr ds \right. \\ &\quad \left. - \frac{1}{2\pi\beta} \frac{e^{-i\theta s_c}}{\sqrt{s_c}} \int_0^{r_c} \frac{e^{-i\theta r} \cos\left(\frac{2\theta}{M} \sqrt{rs_c}\right)}{\sqrt{r}} dr \right] \end{aligned} \quad \text{Eq. (2.40)}$$

CONFIDENTIAL

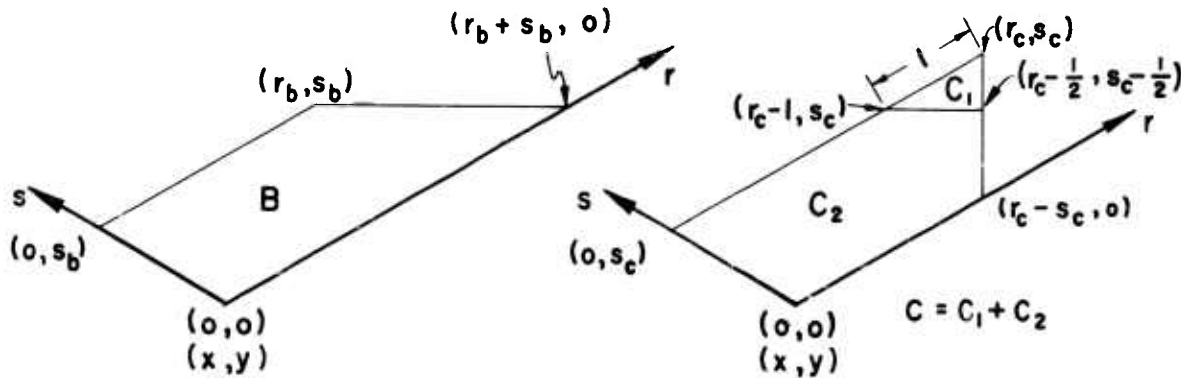


Fig. II.5 Basic Regions Under Consideration for the Characteristic System

The expressions for the three basic regions A , B , C may be combined appropriately to yield the contribution of complete, half or quarter-rhombic boxes. For instance, the contribution of the subregion C , (Fig. II.5) is

$$\bar{P}_C = \bar{P}_C(r_c, s_c) - \bar{P}_C(r_c - \frac{1}{2}, s_c - \frac{1}{2}) - \bar{P}_B(r_c - 1, s_c) + \bar{P}_B(r_c - \frac{1}{2}, s_c - \frac{1}{2}) \quad \text{Eq. (2.41)}$$

The single integrals and the inner portions of the double integrals in Eqs. (2.38)-(2.40) can be expressed explicitly in terms of Fresnel integrals or Bessel functions. For instance,

CONFIDENTIAL

CONFIDENTIAL

$$\int_0^{r_a} e^{-i\theta r} \frac{\cos(\frac{2\theta}{M} \sqrt{r s_a})}{\sqrt{r}} dr = e^{i\theta \frac{s_a}{M^2}} \left[\int_{\frac{\sqrt{s_a}}{M}}^{\frac{\sqrt{r_a} + \frac{\sqrt{s_a}}{M}}{M}} e^{-i\theta z^2} dz + \int_{-\frac{\sqrt{s_a}}{M}}^{\frac{\sqrt{r_a} - \frac{\sqrt{s_a}}{M}}{M}} e^{-i\theta z^2} dz \right]$$

Eq. (2.42)

From the definition of the Fresnel integrals which have been tabulated in Ref. 34,

$$\mathcal{F}(x) = C(x) - i S(x) = \frac{1}{\sqrt{2\pi}} \int_0^x \frac{e^{-it}}{\sqrt{t}} dt$$

Eq. (2.43)

one may deduce the following identity

$$\int_0^x e^{-i\theta z^2} dz = \frac{x}{|x|} \sqrt{\frac{\pi}{2\theta}} \mathcal{F}(\theta x^2)$$

Eq. (2.44)

Therefore, Eq. (2.42) becomes

$$\int_0^{r_a} e^{-i\theta r} \frac{\cos(\frac{2\theta}{M} \sqrt{r s_a})}{\sqrt{r}} dr = e^{i\theta \frac{s_a}{M^2}} \sqrt{\frac{\pi}{2\theta}} \left[\frac{\sqrt{r_a} - \frac{\sqrt{s_a}}{M}}{|\sqrt{r_a} - \frac{\sqrt{s_a}}{M}|} \mathcal{F}\left(\theta \left[\sqrt{r_a} - \frac{\sqrt{s_a}}{M}\right]^2\right) + \mathcal{F}\left(\theta \left[\sqrt{r_a} + \frac{\sqrt{s_a}}{M}\right]^2\right) \right]$$

Eq. (2.45)

Also, using relations similar to Eqs. (2.21) and (2.24a-b), one obtains

$$\int_0^{s_b} \frac{\cos(\frac{2\theta}{M} \sqrt{(r_b + s_b - s)s})}{\sqrt{(r_b + s_b - s)s}} ds = J_0\left(\frac{\theta}{M} [r_b + s_b]\right) \left[\frac{\pi}{2} + \sin^{-1} \frac{s_b - r_b}{s_b + r_b} \right] + \sum_{n=1}^{\infty} \frac{(-1)^n}{n} J_{2n}\left(\frac{\theta}{M} [r_b + s_b]\right) \sin\left(2n \sin^{-1} \frac{s_b - r_b}{s_b + r_b}\right)$$

Eq. (2.46)

Formulas of various types obtainable from Eqs. (2.38)-(2.40) and (2.45)-(2.46) are given in Ref. 28.

a. Steady-State Formulas

Since frequent use will be made of the characteristic grid system for steady-flow problems, the corresponding formulas are

CONFIDENTIAL

CONFIDENTIAL

now presented. For $\theta = 0$, Eqs. (2.38-2.40) reduce to the simple expressions

$$\begin{aligned}\bar{p}_A(r_a, s_a) &= \frac{2\beta U}{\beta} \left[-\frac{1}{\pi} \left\{ \sqrt{\frac{r_a}{s_a}} + \sqrt{\frac{s_a}{r_a}} \right\} \right] \\ \bar{p}_B(r_b, s_b) &= \frac{2\beta U}{\beta} \left[-\frac{1}{\pi} \left(\frac{\pi}{2} + \sin^{-1} \frac{s_b - r_b}{s_b + r_b} \right) - \frac{1}{\pi} \sqrt{\frac{r_b}{s_b}} \right] \\ \bar{p}_C(r_c, s_c) &= \frac{2\beta U}{\beta} \left[-\frac{1}{\pi} \sqrt{\frac{r_c}{s_c}} \right]\end{aligned}$$

Eqs. (2.47a-c)

If the grid numbering system is that of Fig. II.6, the above expressions yield, respectively, the following formulas for the complete rhombus, the inverted triangle and the right-half rhombus:

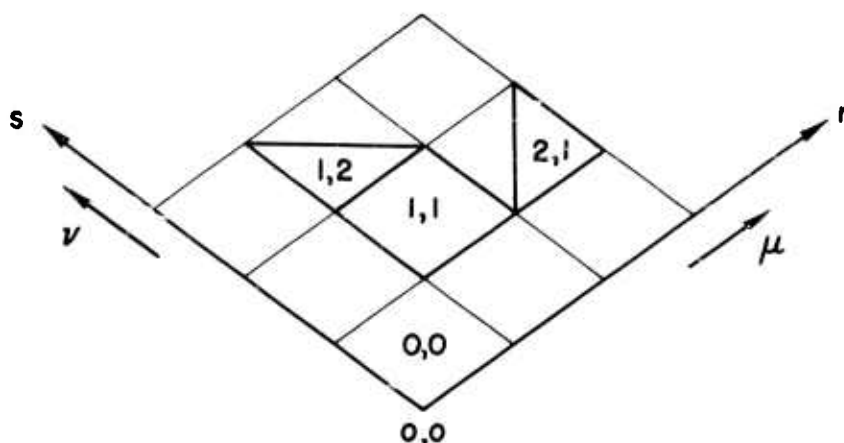


Fig. II.6 Numbering System for Characteristic Boxes

CONFIDENTIAL

$$\begin{aligned}\bar{p} &\equiv \frac{2\beta U}{\beta} C_{\mu, \nu}^{(1)} = \frac{2\beta U}{\beta} \left[-\frac{2}{\pi} \right] & \mu = \nu = 0 \\ &= \frac{2\beta U}{\beta} \left[-\frac{1}{\pi} \left\{ \frac{\nu+2}{\sqrt{\nu+1}} - \frac{\nu+1}{\sqrt{\nu}} \right\} \right] & \mu = 0, \nu > 0 \\ &= \frac{2\beta U}{\beta} \left[-\frac{1}{\pi} \left\{ \frac{\mu+\nu+2}{\sqrt{(\mu+1)(\nu+1)}} + \frac{\mu+\nu}{\sqrt{\mu\nu}} - \frac{\mu+\nu+1}{\sqrt{\mu(\nu+1)}} - \frac{\mu+\nu+1}{\sqrt{(\mu+1)\nu}} \right\} \right] & \mu, \nu > 0\end{aligned}$$

$$C_{\mu, \nu}^{(1)} = C_{\nu, \mu}^{(1)}$$

$$\begin{aligned}\bar{p} &\equiv \frac{2\beta U}{\beta} C_{\mu, \nu}^{(2)} = \frac{2\beta U}{\beta} [-1] & \mu = \nu = 0 \\ &= \frac{2\beta U}{\beta} \left[-\frac{1}{\pi} \left\{ -\sqrt{\frac{1}{\nu}} + \frac{\pi}{2} - \sin^{-1} \frac{\nu-1}{\nu+1} \right\} \right] & \mu = 0, \nu > 0 \\ &= \frac{2\beta U}{\beta} \left[-\frac{1}{\pi} \left\{ -\sqrt{\frac{\mu+1}{\nu}} + \frac{\mu+\nu}{\sqrt{\mu\nu}} - \sqrt{\frac{\nu+1}{\mu}} \right. \right. \\ &\quad \left. \left. - \sin^{-1} \frac{\mu-\nu-1}{\mu+\nu+1} - \sin^{-1} \frac{\nu-\mu-1}{\mu+\nu+1} \right\} \right] & \mu, \nu > 0\end{aligned}$$

$$C_{\mu, \nu}^{(2)} = C_{\nu, \mu}^{(2)}$$

$$\begin{aligned}\bar{p} &\equiv \frac{2\beta U}{\beta} C_{\mu, \nu}^{(3)} = \frac{2\beta U}{\beta} \left[-\frac{1}{\pi} \left\{ \sqrt{\frac{1}{\mu+1}} \right\} \right] & \nu = 0 \\ &= \frac{2\beta U}{\beta} \left[-\frac{1}{\pi} \left\{ \sqrt{\frac{\nu+1}{\mu+1}} + \sqrt{\frac{\mu}{\nu}} - \sqrt{\frac{\mu+1}{\nu}} - \sqrt{\frac{\nu}{\mu+1}} \right\} \right] & \nu > 0\end{aligned}$$

$$C_{\mu, \nu}^{(3)} + C_{\nu, \mu}^{(3)} = C_{\mu, \nu}^{(1)}$$

Eqs. (2.48a-f)

The quantities inside the square brackets of Eqs. (2.48a-f), i.e., $C_{\mu, \nu}^{(i)}$, represent the aerodynamic influence coefficients.

CONFIDENTIAL

CONFIDENTIAL

SECTION III

APPLICATION TO TWO-DIMENSIONAL PROBLEMS

Before attempting to apply the aerodynamic-influence-coefficient methods to finite wings, it is advantageous to study various aspects of their application to two-dimensional flow problems. In so doing, the following are three of the important questions which can be partially answered with relative simplicity:

- (1) Is it acceptable to represent a swept leading edge by a broken line, an approximation which is necessitated by practical considerations if numerical approaches are to be followed?
- (2) Is the assumption of an average constant downwash over each elementary area adequate?
- (3) How many boxes must be distributed along the chord of a wing before an acceptable degree of accuracy is achieved?

While carrying out simple examples for these purposes, one can also study the accuracy of the tabulations for the aerodynamic influence coefficients.

III.1 Representation of Swept Leading Edges by Broken Lines

Consider a two-dimensional swept wing in steady flow with sweep angle Λ ; assume that the Mach number is large enough so that the parallel leading and trailing edges are supersonic. If the wing produces constant downwash everywhere (constant angle of attack), the dimensionless pressure difference at each point is constant and is given by the exact formula of linearized theory (cf. Ref. 2)

$$p' = \frac{\bar{p}}{\left(\frac{2\beta U^2}{\beta}\right)} = - \frac{\beta \cot \Lambda}{\sqrt{\beta^2 \cot^2 \Lambda - 1}}$$

Eq. (3.1)

As a first example, let $M = \sqrt{2}$ and $\Lambda = \tan^{-1}(1/2)$. Since $\beta = 1$, the square and the Mach grid systems are identical. A grid system is placed on the wing as shown in Fig. III.1. The

CONFIDENTIAL

CONFIDENTIAL

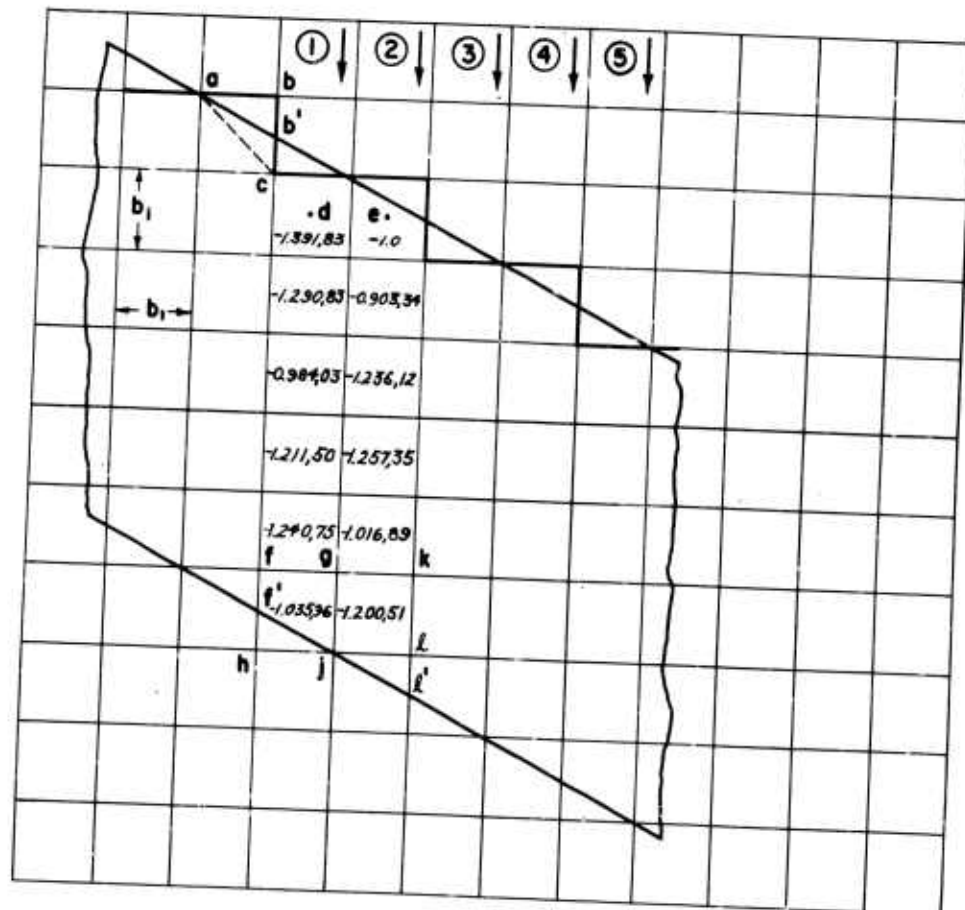


Fig. IX.1 Pressure Distribution on a Two-Dimensional Swept Wing Using Mach (or Square) Boxes.
($k=0$, $\tan \Lambda = 1/2$, $M = \sqrt{2}$)

leading edge region is replaced by complete boxes having centers on the wing, with the result that the leading edge is approximated by the broken line composed of the sides of the foremost boxes. (It will be shown shortly that one must resort to this representation.) The positioning of the grid system is such that the sum of the areas off the wing taken in by the resultant

CONFIDENTIAL

CONFIDENTIAL

jagged edge is equal to the sum of the areas omitted on the wing. Experience has shown that this way of positioning yields the best accuracy for the determination of airloads. Since $\tan \Lambda = (1/2)$, the sequence of types of chordwise columns of boxes repeats with every second column, i.e., the results for columns (3) and (5) will be identical with those for (1), etc. Therefore only rows (1) and (2) need be considered. Using Eq. (2.14) and tabulations of the AICs (Table A.2, Ref. 31), one can calculate the approximate dimensionless pressure p' at the center of each box. The results for p' are shown in Fig. III.1. According to Eq. (3.1), the exact value of the pressure p' at all points is

$$p' = - \frac{2}{\sqrt{3}} = -1.154,70$$

and the dimensionless lift per unit distance perpendicular to the flow is

$$l(y) = \frac{\text{Lift/unit span}}{\left(\frac{\rho U^2 c}{8}\right) 2b} = -1.154,70$$

where $2b$ is the chord of the wing in the stream direction. Although the comparison of the individual pressures on the boxes of Fig. III.1 with their exact value reveals appreciable discrepancies, the average lift per unit span proves surprisingly close to the exact.

Since the trailing edge is supersonic, the pressures on the wing are not influenced by the representation of the trailing edge, and therefore one need not insist on complete boxes near the trailing edge. Therefore, if the pressures are assumed constant over each trailing edge box, one may write, for instance, for the contribution of the partial box $fghf'$ to the lift of column (1)

$$(-1.035,96 b_1^2) \left(\frac{\text{Area of } fghf'}{\text{Area of } fghh} \right)$$

Similarly, for the contribution of the partial boxes $ghklj'$ to the lift of column (2),

$$(-1.200,51 b_1^2) \left(\frac{\text{Area of } ghklj'}{\text{Area of } ghklj} \right)$$

Here b_1^2 is the area of a complete box. If this way of dealing with trailing edge lift is adopted in the evaluation of the lifts over columns (1) and (2), one obtains the numbers

CONFIDENTIAL

No. of Chordwise Boxes	$l(y)$ Col.(1)	$l(y)$ Col.(2)	$l(y)$ Average Cols. (1) and (2)
3	-1.140,23	-1.149,50	-1.144,87
4	-1.143,83	-1.177,79	-1.160,81
5	-1.161,75	-1.133,58	-1.147,67
6	-1.149,32	-1.152,39	-1.150,85
Exact	-1.154,70	-1.154,70	-1.154,70

Table III.1 Comparison of Lift by Numerical Methods with Exact Lift for a Two-Dimensional Swept Wing.
($\dot{\epsilon}=0$, $\tan \Lambda = 1/2$, $M = \sqrt{2}$)

shown in Table III.1. The table includes cases where three, four, five and six boxes are successively assumed to fill up the chordwise dimension $2b$ of the wing.

Several conclusions can be drawn from these results:

- (1) The deviations in pressure from the exact value become less pronounced for boxes farther downstream, indicating that, if more and more chordwise boxes are taken, the estimates of the generalized forces (which are weighted integrals of the pressure over the planform) will improve. Therefore, it is desirable to have as many chordwise boxes as practical.

CONFIDENTIAL

- (2) For calculating the lift, which is the lowest-order generalized force, relatively few boxes suffice. However, for the higher order generalized forces, such as the "first moment" and the "second moment," the results are not expected in general to be as accurate with few chordwise boxes.
- (3) Since the pressures fluctuate appreciably from the exact, the only logical and justifiable chordwise integration technique is the rectangular rule. This rule assumes that the pressure times the weighting factor associated with each generalized mode is constant over each box and is taken to have its value at the center of the box.

The pressure fluctuations across the chord are due to the representation of the leading edge. The question that arises at this point is whether it is possible to improve upon this representation. If one had the tabulations for the AICs for partial boxes, no such step would be necessary. However, such tabulations would involve not only the sweep angle as a parameter, but also would have to account for various types of cuts of the boxes by the leading edge. The scope of such an extensive tabulation is prohibitive. Another alternative, which at first glance might seem reasonable, is to take the AIC for a partial box to be that of the corresponding complete box times an area factor which is the ratio of the area of the partial box to that of the complete box. Upon closer study, this procedure proves inadequate. For instance, the contribution to the pressure p' at point d from area $ab'c$ of Fig. III.1 is $(-1/\sqrt{3}) = -0.577$ whereas the corresponding contribution for the large area abc is $[-(1/\pi) \cos^{-1}(1/3)] = -0.392$. Now, if the proposed correction had been used, one would have for the contribution of $ab'c$, the value

$$(-0.392) \left(\frac{\text{Area of } ab'c}{\text{Area of } abc} \right) = -0.196$$

as compared to the exact value of -0.577 . This shows that a simple "area correction" for the determination of the AIC for partial boxes is not satisfactory. Incidentally, this type of adjustment is suggested by Li (pages 33-37, Ref. 26). If this correction had been used for the determination of the pressures at d and e in the figure one would obtain the poorer results

$$p'_d = -1 \quad , \quad p'_e = -0.333,33.$$

CONFIDENTIAL

CONFIDENTIAL

The exact p' and $l(y)$ in the foregoing example will retain the value of -1.15470 as long as $\beta \cot \Lambda = 2$. Also, the results of Fig. III.1 will not change if Mach boxes are used for other two-dimensional wings in steady flow with constant downwash U_α and $\beta \cot \Lambda = 2$. Accordingly, if one uses Mach boxes, the accuracy of the numerical method is dependent on the factor $\beta \cot \Lambda$. To investigate this dependency, consider a wing at the same Mach number $M = \sqrt{2}$, with sweep $\Lambda = \tan^{-1}(2/3)$. Here $\beta \cot \Lambda = 1.5$. The results for p' are shown in Fig. III.2, and the corresponding values of $l(y)$ are given in Table III.2.

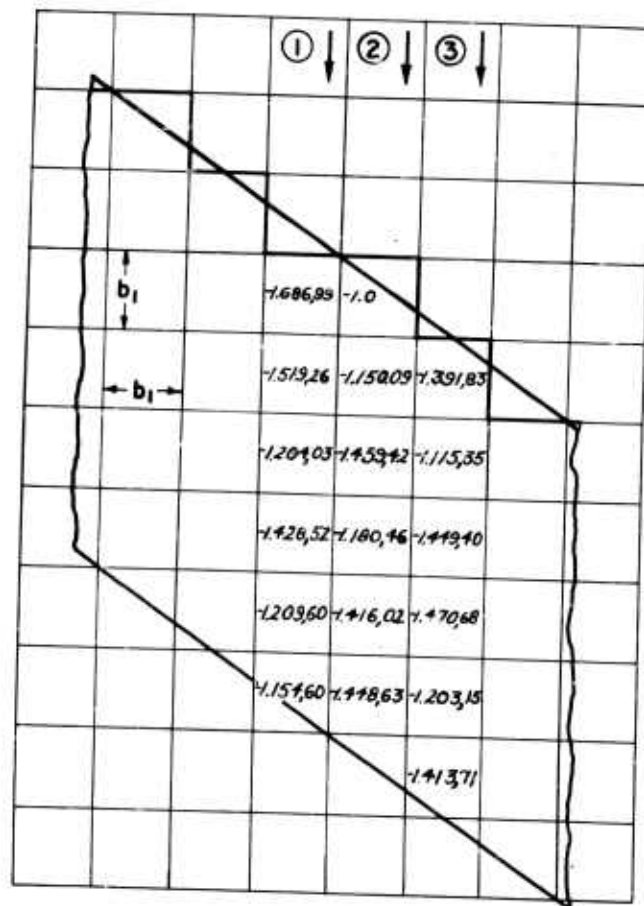


Fig. III.2 Pressure Distribution on a Two-Dimensional Swept Wing Using Mach (or Square) Boxes.

($k=0$, $\tan \Lambda = 2/3$, $M = \sqrt{2}$)

CONFIDENTIAL

No. of Chordwise Boxes	$l(y)$ Col.(1)	$l(y)$ Col.(2)	$l(y)$ Col.(3)	$l(y)$ Average Cols. (1), (2) and (3)
4	-1.340,65	-1.295,86	-1.356,82	-1.331,11
5	-1.329,04	-1.335,60	-1.331,58	-1.332,07
6	-1.303,02	-1.356,25	-1.345,27	-1.334,85
Exact	-1.341,64	-1.341,64	-1.341,64	-1.341,64

Table III.2 Comparison of Lift by Numerical Methods with Exact Lift for a Two-Dimensional Swept Wing.
($k=0$, $\tan \Lambda = 2/3$, $M = \sqrt{2}$)

It is seen that the accuracies of the lifts for individual columns are slightly poorer than in the case $\beta \cot \Lambda = 2$, but the average lift per unit span over the three columns is still quite close, being within 1 per cent. Therefore, when $\beta \cot \Lambda$ is changed from 2 to 1.5, no significant change in accuracy for the total lift is observed. Of course, when one approaches the sonic condition, ($\beta \cot \Lambda \rightarrow 1$), the accuracy is not expected to be as good, but is probably still tolerable for wings of finite span. (The sonic case cannot be checked with a two-dimensional wing.) The above and other examples related to two-dimensional swept wings in steady flow suggest the conclusion that the accuracy is essentially uniform for all sweeps and Mach number combinations yielding $\beta \cot \Lambda > 1$. Since at $M = \sqrt{2}$, the Mach and square grid systems are the same, the results of Figs. III.1 and III.2 also bear on the case of the square grid. At the lower Mach number, $M = 1.2$, for a wing with sweep $\Lambda = \tan^{-1}(1/3)$ ($\beta \cot \Lambda \approx 1.99$), the results for the square grid are shown in Fig. III.3 and in Table III.3. Evidently the accuracy is poorer at lower Mach number when square boxes are used than that which would have been obtained with Mach boxes.

CONFIDENTIAL

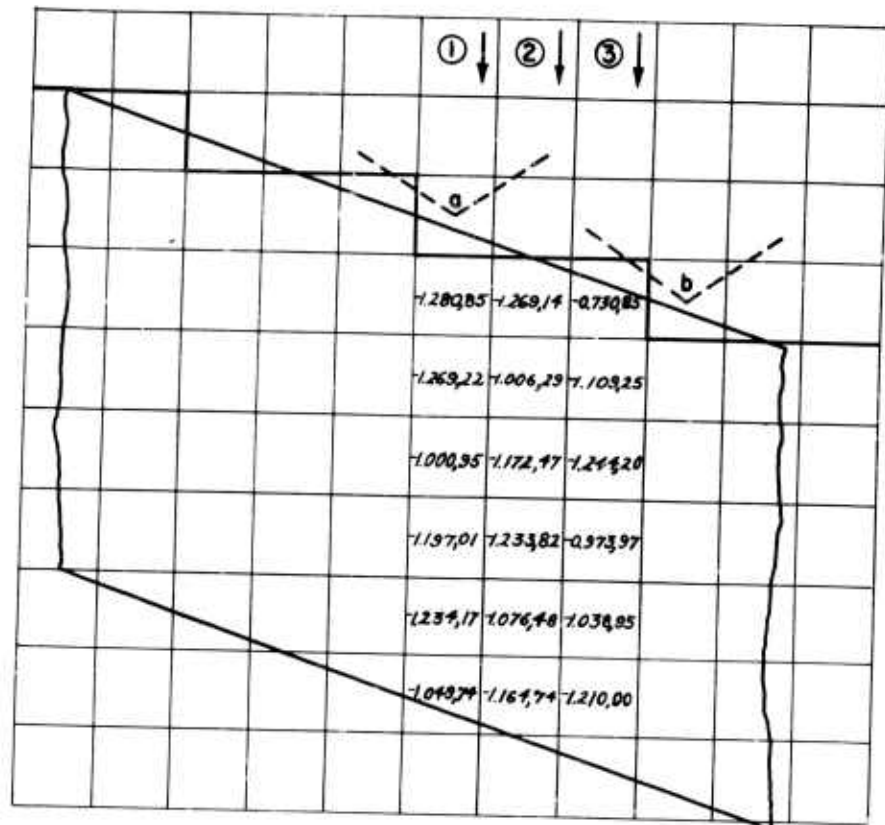


Fig. III.3 Pressure Distribution on a Two-Dimensional Swept Wing Using Square Boxes.

($k = 0$, $\tan \Lambda = 1/3$, $M = 1.2$)

For the purpose of examining the same factors as above for the characteristic box system, consider again the two-dimensional wing for which $M = \sqrt{2}$ and $\Lambda = \tan^{-1}(1/2)$. The Mach lines bounding the boxes are arranged so that the broken line representing the leading edge is as shown in Fig. III.4. In this case a serious difficulty arises: the resultant pressures are always low compared to the exact value of $\beta' = -1.154, 70$. Furthermore, the convergence toward this value is very slow as more and more boxes are taken along the chord. This failure may be explained as follows.

CONFIDENTIAL

CONFIDENTIAL

No. of Chordwise Boxes	$l(y)$ Col.(1)	$l(y)$ Col.(2)	$l(y)$ Col.(3)	$l(y)$ Average Cols. (1)(2) and (3)
4	-1.087,26	-1.170,43	-1.095,73	-1.117,81
6	-1.113,67	-1.153,82	-1.118,43	-1.128,64
Exact	-1.156,65	-1.156,65	-1.156,65	-1.156,65

Table III.3 Comparison of Lift by the Square Grid System with Exact Lift for a Two-Dimensional Swept-Wing.
($k=0$, $\tan \Lambda = 1/3$, $M=1.2$)

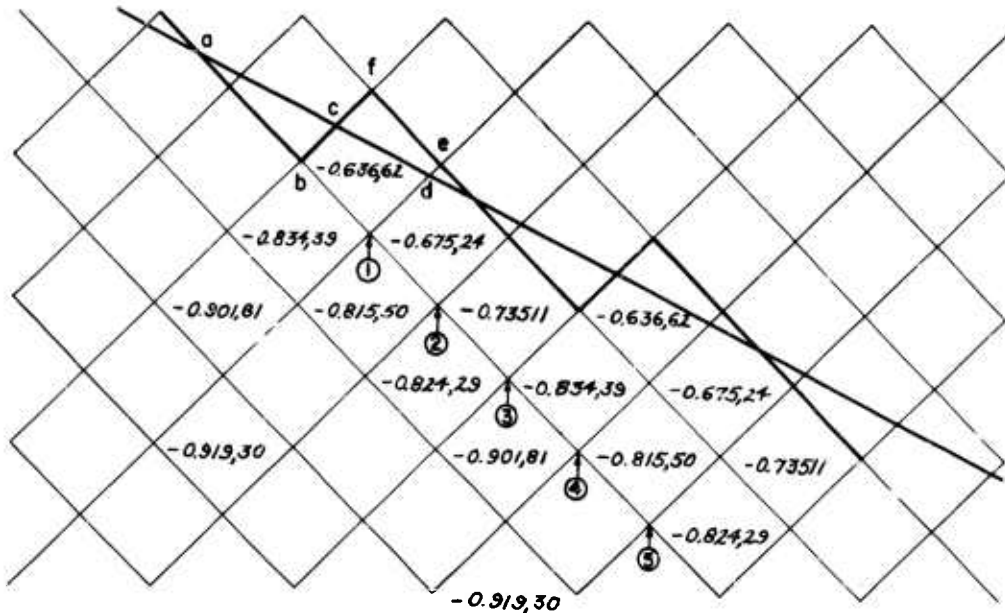


Fig. III.4 Pressure Distribution on a Two-Dimensional Swept Wing Using Characteristic Boxes.
($k=0$, $\tan \Lambda = 1/2$, $M = \sqrt{2}$)

CONFIDENTIAL

CONFIDENTIAL

In the evaluation of ρ' at point (1), the actual contributing area abc is effectively replaced by the area $cdef$. Even though the two areas are approximately equal, the contribution of abc to ρ' is a large negative quantity (as may be easily proven for the steady-state case), whereas $cdef$ contributes a small positive quantity. Similar considerations for points (2), (3) etc. explain why one obtains such low values of ρ' . This error is consistently in one direction, for the characteristic grid system, in contrast with the Mach box system where it can be in either direction and produces compensating inaccuracies.

If use is to be made of the characteristic system, one must apparently represent the leading edge by lines parallel and perpendicular to the flow, as in the Mach box system (see Fig. III.5). In so doing, one is forced to tabulate the AICs for half-rhombic boxes. It will be shown below that even these half boxes are insufficient when there is a variation of downwash along the chord, so that in the final analysis one must tabulate the coefficients for quarter-rhombic boxes.

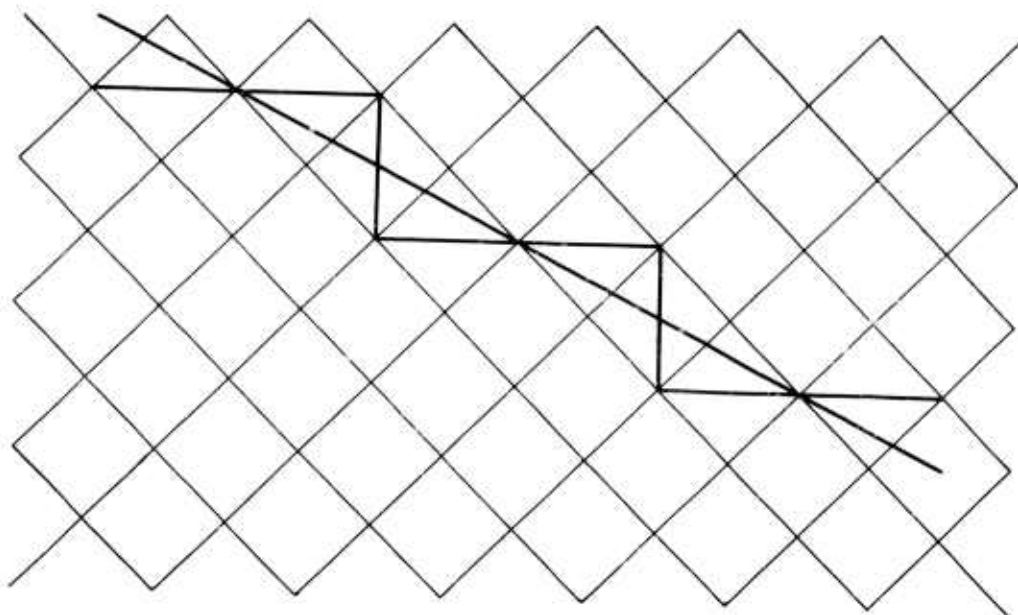


Fig. III.5 Proper Representation of the Leading Edge when Characteristic Grid System is Employed

CONFIDENTIAL

III.2 Adequacy of the Assumption of Average Constant Downwash over Each Elementary Area: Steady Motion

In any of the numerical methods, with the planforms split into elementary areas, a basic assumption is that the downwash distribution over the wing can be adequately approximated by a set of suitably average constant downwashes over these areas. Although it is possible to represent the downwash in each elementary area by some simple function other than a constant (such as the case of the singular downwash associated with a side edge, which will be discussed below), the arbitrariness of these functions would require an undesirably large amount of tabulation. The degree of precision obtainable using the constant-downwash assumption is closely related to the reduced frequency of oscillation and to the rapidity of variation of local angle of attack along the chord, as will now be shown.

In order to separate the effects of frequency and downwash variation on the accuracy of the results for pressure distribution and generalized forces, the study is carried out in two steps. First, a straight two-dimensional wing in steady flow is considered for which there is a chordwise variation in downwash. In connection with this point, some remarks are also included for the case when there is variation of downwash across the span. Secondly, the results of going to unsteady flow and increasing the reduced frequency are examined.

For a two-dimensional, unswept wing in steady motion, the pressure is a point-function of the downwash, i.e.,

$$p' = \frac{\bar{p}}{\left(\frac{\rho U^2}{2\beta}\right)} = -\frac{w}{U}$$

Eq. (3.2)

The pressure calculated by AIC's at the center (x, y) of any Mach box (n, m) in Fig. III.6 will also be equal to the quantity $(-w/U)$, because all rows $\bar{v}=1, 2, \dots$ contribute zero to the pressure p' at (x, y) . This can be proved easily. All spanwise boxes in any particular row \bar{v} ($\bar{v} \geq 1$) have the same downwash; hence, according to Eq. (2.32d), the total contribution of this row to the pressure at (x, y) is

$$p'_{\bar{v}} = \frac{1}{U} w_{\bar{v}} \sum_{\bar{\mu}=-\bar{v}}^{\bar{v}} R_{\bar{v}, \bar{\mu}} = \frac{w_{\bar{v}}}{U w} \sum_{\bar{\mu}=-\bar{v}}^{\bar{v}} \left\{ -A_{\bar{v}, \bar{\mu}}^+ + A_{\bar{v}, \bar{\mu}}^- \right\} \quad \bar{v} \geq 1$$

Eq. (3.3)

CONFIDENTIAL

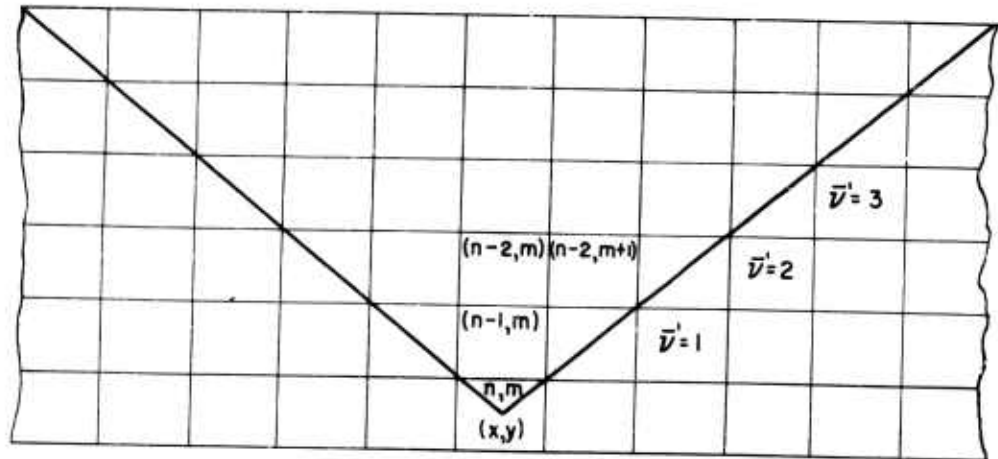


Fig. III.6 A Two-Dimensional, Unswept Wing in Steady Flow.
(Mach Box System)

which is identically zero in view of Eqs. (2.17a-b). The pressure at (x, y) is therefore

$$p' = \frac{1}{U} w(x) R_{0,0} = - \frac{w(x)}{U}$$

Eq. (3.4)

A similar proof holds true also for the square grid system. Equation (3.4) implies that, for the two-dimensional steady-state case, the pressures calculated at the centers of Mach (or square) boxes by numerical methods are exact, regardless of the type of motion in the chordwise direction (provided the constant downwash over each box is set equal to the value of the downwash at its center). Specifically, if the downwash variation is linear in x , say $(Ux/2b)$, the pressure p' will be given by the relation $p' = -(x/2b)$.

If two chordwise boxes are taken, the pressures at the centers of the two boxes will be exactly

$$p'_1 = -0.25 \quad , \quad p'_2 = -0.75$$

where $2b$ is the chord. Using the rectangular rule (shown in Sec. III.1 to be the numerical integration formula which one

CONFIDENTIAL

CONFIDENTIAL

should adopt in general), one obtains for the lift

$$l(y) = \frac{\text{Lift/unit span}}{\left(\frac{2\rho U^2}{\beta}\right)(2b)} = -0.5$$

This happens to be the exact value. However, one obtains for the moment about the leading edge

$$m(y) = \frac{\text{Moment/unit span}}{\left(\frac{2\rho U^2}{\beta}\right)(2b^2)} = -0.625$$

as compared to the exact value of $(-2/3)$. If, say, six boxes had been used, one would have found

$$l(y) = -0.5, \quad m(y) = -0.662, 0.$$

This result suggests that, to insure adequate chordwise integrations for the generalized forces, one must have a sufficient number of integration points along the chord, even if the pressures are obtainable exactly with few chordwise boxes.

For the same wing, consider the use of the characteristic grid system. If the downwash is constant along the chord (i.e., if the wing has no camber), the results for the pressures p' will again be exact. If the downwash varies linearly with x , $w = U(x/2b)$, the pressure varies linearly along the chord according to exact theory, whereas the pressures yielded by the characteristic-grid calculation deviate. (See Fig. III.7).

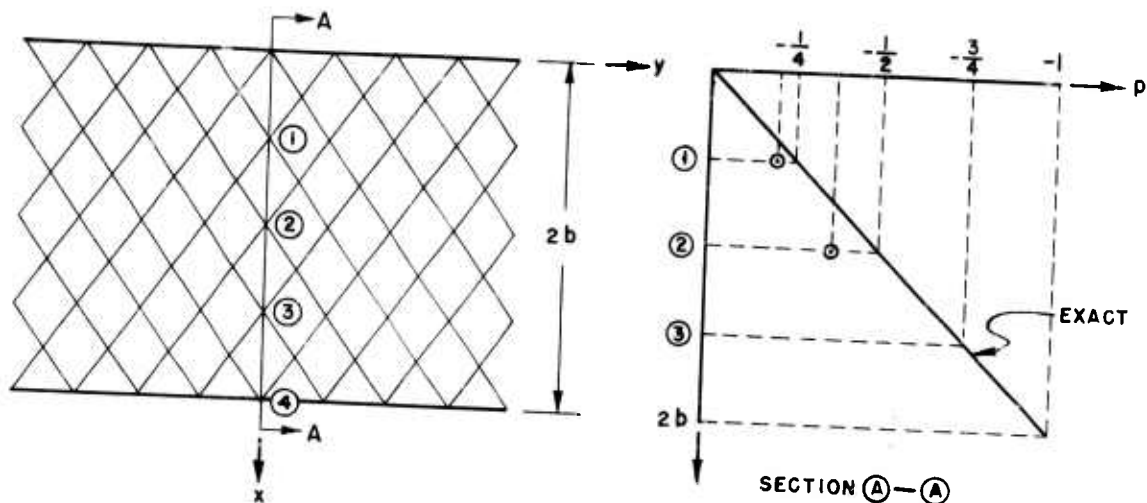


Fig. III.7 A Two-Dimensional Wing in Steady Flow. Downwash Varying Linearly Along the Chord. (Characteristic Box System).

CONFIDENTIAL

Taking as one possible alternative, the constant downwash over each box to be equal to its value at the lowest corner of the box, one has for the pressures at points (1) and (2) in the figure

$$p'_{(1)} = -0.204,58 \quad , \quad p'_{(2)} = -0.388,36$$

These should be compared to the exact results of -0.25 and -0.5 , respectively. This deviation of the value of p' is always present and will be even worse for points farther along the chord. The representation of Fig. III.7 is therefore unsatisfactory when the downwash varies along the chord.

Another possible approach is to make the downwash over each box equal to its value at the mid-chord of the box and find the pressure at this central point. For example, if the constant downwashes over boxes A,..... F (Fig. III.8) are taken from the linearly varying case as

$$\frac{w_A}{U} = \frac{1}{8} \quad , \quad \frac{w_B}{U} = \frac{1}{16} \quad , \quad \frac{w_C}{U} = \frac{3}{8} \quad , \quad \frac{w_D}{U} = \frac{1}{4} \quad , \quad \frac{w_E}{U} = \frac{1}{8} \quad , \quad \frac{w_F}{U} = \frac{1}{16} \quad ,$$

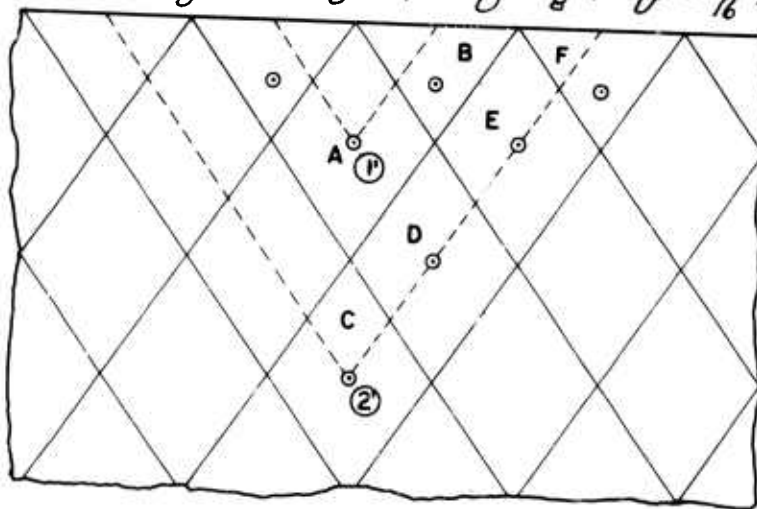


Fig. III.8 A Two-Dimensional Wing in Steady Flow. Downwash Varying Linearly Along the Chord. (Characteristic System with Control Points at Centers of Boxes)

one obtains the results for points (1') and (2')

$$p'_{(1')} = -0.102,29 \quad , \quad \text{and} \quad p'_{(2')} = -0.300,94$$

These contrast with the corresponding exact values of -0.125

CONFIDENTIAL

and -0.375 , respectively. Again, the error is not tolerable.

A final alternative is to divide the full rhombic boxes into half rhombuses such that the cuts are perpendicular to the flow, as shown in Fig. III.9.

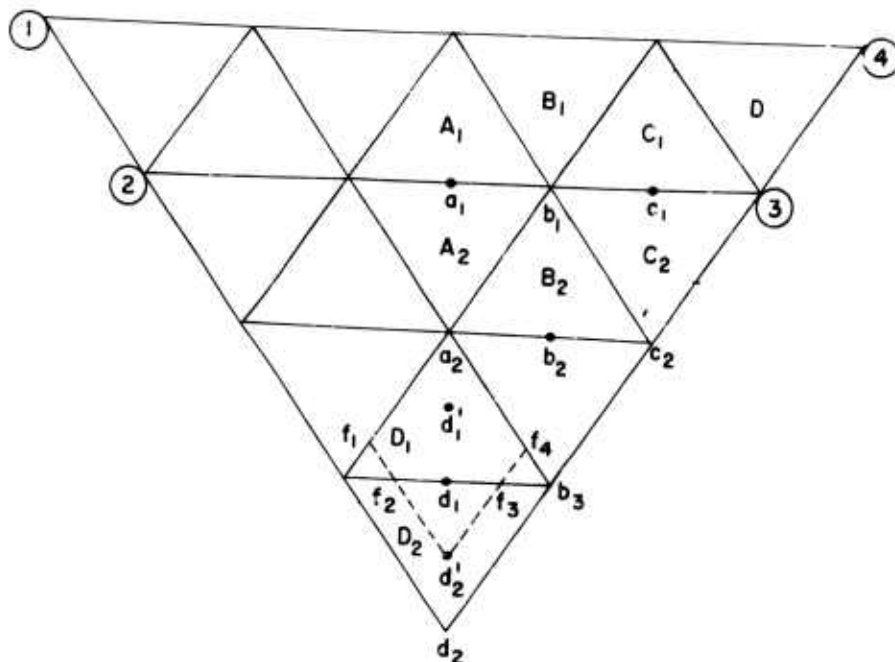


Fig. III.9 A Two-Dimensional Wing in Steady Flow. (Modified Characteristic System)

Assuming that the downwashes over boxes A_1, A_2, B_1 are assigned the values at the points a_1, a_2, b_1 , the pressures thus obtained prove to be exact for all types of chordwise variations when the motion is steady. If the motion is unsteady, chordwise strips (such as (1)(2)(3)(4) in Fig. III.9) will make contributions to the pressure at point d_2 . Then, it can be shown that a consistent error is introduced for the pressure at d_2 , since the downwashes over the strips are taken to be those at the downstream edges (such as (2)(3)) rather than average values at the centers of these strips. If central control points were employed, i.e., if one took the downwash at the mid-chord points of boxes d_2', d_1' , etc.,..., the results could be improved, but one would then have to tabulate the AIC for an odd-shaped area such as $a_2 f_1 f_2 f_3 f_4$. If the reduced frequency based on box size is sufficiently small, however, the

CONFIDENTIAL

error associated with taking lower points rather than central points as control stations is not serious.

When a three-dimensional wing has swept leading edges or side edges, there will exist half-rhombic boxes with one edge parallel to the flow. Since the foregoing analysis has shown that it is desirable to divide the rhombic boxes by cuts perpendicular to the flow, quarter rhombuses will appear at such edges. Hence the AIC must be tabulated for quarter rhombic boxes. This is a serious disadvantage, since the number of entries in the tables will be four times that for a Mach grid system.

With this fact in view, the characteristic grid system is not recommended for general applications. Some small further use will be made of the system, however, in special cases where no chordwise variation of downwash exist.

As a next instructive example, consider linear and parabolic variations in downwash across the span of a finite wing (Fig. III.10). For the sake of simplicity at this stage,

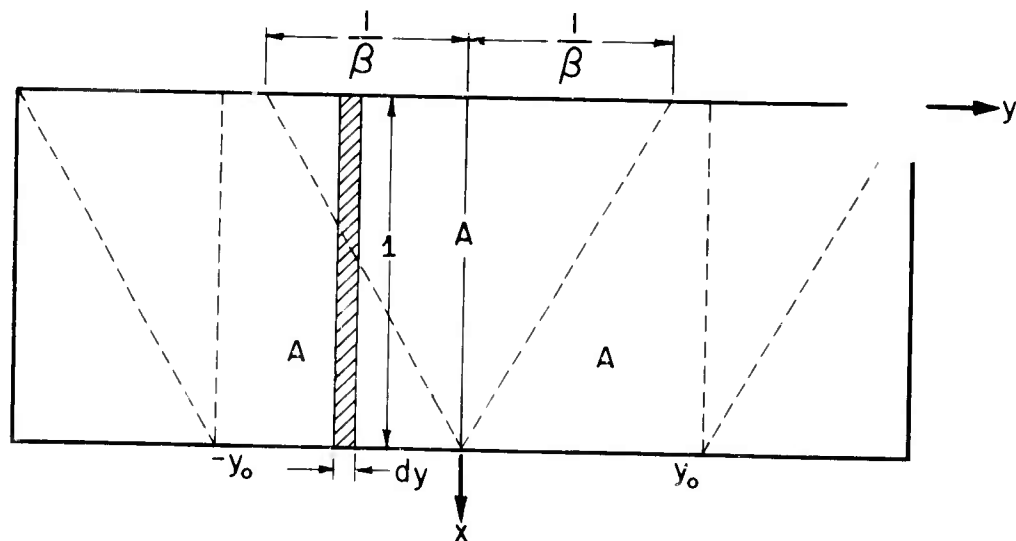


Fig. III.10 Notations for a Finite Rectangular Wing in Steady Flow with Spanwise Variation in Downwash

attention is focused on the portion A of the planform which is purely supersonic and uninfluenced by the wing tip. Of interest are the downwash distributions

CONFIDENTIAL

$$w(y) = U(\beta y) \quad \text{and} \quad w(y) = U(\beta y)^2$$

for which one may easily prove that the steady-flow lifts per unit span for a strip dy in Region A ($-y_0 \leq y \leq y_0$) are exactly

$$\frac{\text{Lift/unit span}}{\left(\frac{2\rho U^2}{\beta}\right)} = -\beta y \quad \text{and} \quad \frac{\text{Lift/unit span}}{\left(\frac{2\rho U^2}{\beta}\right)} = -\left(\frac{1}{6} + \beta^2 y^2\right)$$

respectively. Furthermore, in the case of linear variation of downwash, the dimensionless pressure is constant along the chord and is equal to $-\beta y$. Using any of the numerical procedures, the resultant pressures and the lifts per unit span will be exact (this is not true when the wing has a swept leading edge). However, when the downwash distribution is parabolic, none of the numerical methods yields the correct results for the pressures along the chord, and hence the associated lift distribution will also deviate from the exact. As may be seen from Table III.4, these discrepancies can be alleviated by taking sufficient number of boxes along the chord.

$ \beta y $	$\frac{\text{Lift/unit span}}{\left(\frac{2\rho U^2}{\beta}\right)}$ 4 Chordwise Mach Boxes	$\frac{\text{Lift/unit span}}{\left(\frac{2\rho U^2}{\beta}\right)}$ 6 Chordwise Mach Boxes	$\frac{\text{Lift/unit span}}{\left(\frac{2\rho U^2}{\beta}\right)}$ Exact
0	-0.139,95	-0.151,57	-0.166,67
(1/6)	---	-0.179,34	-0.194,44
(1/4)	-0.202,45	---	-0.229,17
(1/3)	---	-0.262,68	-0.277,78
(1/2)	-0.389,95	-0.401,57	-0.416,67
(2/3)	---	-0.596,01	-0.611,11
(3/4)	-0.702,45	---	-0.729,17
(5/6)	---	-0.846,01	-0.861,11

Table III.4 Comparison of Lift Distribution According to the Mach-Box Scheme with the Exact for the Purely Supersonic Region of a Rectangular Wing in Steady Motion. (Downwash Varying Parabolically Across the Span)

CONFIDENTIAL

III.3 Adequacy of the Assumption of Average Constant Downwash Over Each Elementary Area: Unsteady Motion

In the previous section, it was shown that the square and Mach box grid systems yield the exact pressure distribution for a two-dimensional unswept wing in steady motion, regardless of the variation of downwash across the chord. In this section, the same problem will be studied in unsteady motion. It follows from Eq. (2) of Ref. 2 and Eq. (2.3) that the amplitude of pressure difference between the upper and lower surface at (x) of a two-dimensional straight oscillating wing is

$$\bar{p}(x) = 2\rho \left[i\omega + U \frac{\partial}{\partial x} \right] \left\{ -\frac{1}{\beta} \int_0^x \bar{w}(\xi) I(\xi, x) d\xi \right\} \quad \text{Eq. (3.5)}$$

where \bar{w} is the downwash amplitude, and

$$I(\xi, x) = e^{-i \frac{\omega}{U} (x-\xi) \frac{M^2}{\beta^2}} J_0 \left(\frac{\omega M}{U \beta^2} (x-\xi) \right) \quad \text{Eq. (3.6)}$$

and J_0 is the Bessel function of the first kind of order zero. If the chord $2b$ is taken as the reference length, Eq. (3.5) becomes

$$\bar{p} = \frac{2\rho U}{\beta} \left[-2ik - \frac{\partial}{\partial x} \right] \int_0^x \bar{w}(\xi) I(\xi, x) d\xi \quad \text{Eq. (3.7)}$$

Here (x, ξ) are dimensionless chordwise coordinates, k is the reduced frequency based on the semi-chord, $k = \omega b/U$, $\bar{\omega}$ is the modified frequency $\bar{\omega} = 2kM^2/\beta^2$ and

$$I(\xi, x) = e^{-i \bar{\omega} (x-\xi)} J_0 \left(\frac{\bar{\omega}}{M} (x-\xi) \right)$$

Letting $x - \xi = u$, one has for Eq. (3.7)

$$\begin{aligned} \bar{p} &= \frac{2\rho U}{\beta} \left[-2ik - \frac{\partial}{\partial x} \right] \int_0^x \bar{w}(x-u) e^{-i \bar{\omega} u} J_0 \left(\frac{\bar{\omega}}{M} u \right) du \\ &= \frac{2\rho U^2}{\beta} \left[-2ik \int_0^x \frac{\bar{w}(x-u)}{U} e^{-i \bar{\omega} u} J_0 \left(\frac{\bar{\omega}}{M} u \right) du - \int_0^x e^{-i \bar{\omega} u} J_0 \left(\frac{\bar{\omega}}{M} u \right) \frac{\partial}{\partial x} \left\{ \frac{\bar{w}(x-u)}{U} \right\} du \right. \\ &\quad \left. - \frac{\bar{w}(0)}{U} e^{-i \bar{\omega} x} J_0 \left(\frac{\bar{\omega}}{M} x \right) \right] \quad \text{Eq. (3.8)} \end{aligned}$$

CONFIDENTIAL

Three types of motion will be considered (z being the deflection at any point):

(1) $z_1 = 2b e^{i\omega t} \quad \therefore \bar{\omega}_1/\bar{U} = 2ik \quad (\text{vertical-translation oscillation})$

(2) $z_2 = 2bx e^{i\omega t} \quad \therefore \bar{\omega}_2/\bar{U} = (2ikx+1) \quad (\text{pitching about an axis at the leading edge})$

(3) $z_3 = 2bx^2 e^{i\omega t} \quad \therefore \bar{\omega}_3/\bar{U} = (2ikx^2+2x) \quad (\text{parabolic chordwise bending})$
Eqs. (3.9a-c)

For the first motion, one obtains from Eqs. (3.8) and (3.9a),

$$\begin{aligned} p_1' &\equiv \frac{\bar{P}_1}{(2b\bar{U}^2)} = -2ik \int_0^x 2ike^{-i\bar{\omega}u} J_0\left(\frac{\bar{\omega}}{M}u\right) du - 2ike^{-i\bar{\omega}x} J_0\left(\frac{\bar{\omega}}{M}x\right) \\ &= -2ik \left\{ 2ikx f_0(M, \bar{\omega}x) + e^{-i\bar{\omega}x} J_0\left(\frac{\bar{\omega}}{M}x\right) \right\} \end{aligned}$$

Eq. (3.10)

where $f_0(M, \bar{\omega}x)$ is the zero-th order of the well-known function

$$f_\lambda(M, \bar{\omega}x) = \frac{1}{x^{\lambda+1}} \int_0^x u^\lambda e^{-i\bar{\omega}u} J_0\left(\frac{\bar{\omega}}{M}u\right) du.$$

Eq. (3.11)

This function has been tabulated by Schwarz (Ref. 35) and amplified for high values of the frequency in Ref. 36. One may use Eq. (23) of Ref. 36 or the method of Ref. 37 (for low values of the frequency parameter $\bar{\omega}x$) to compute f_λ for other values of M . * Similarly, for the motions (2) and (3), one has

$$p_2' = -2ik \left[x f_0(M, \bar{\omega}x) \{ 2 + 2ikx \} - x^2 f_1(M, \bar{\omega}x) \{ 2ik \} \right] - e^{-i\bar{\omega}x} J_0\left(\frac{\bar{\omega}}{M}x\right)$$

$$\begin{aligned} p_3' &= x f_0(M, \bar{\omega}x) \{ 4k^2 x^2 - 8ikx - 2 \} + x^2 f_1(M, \bar{\omega}x) \{ -8k^2 x + 8ik \} \\ &\quad + x^3 f_2(M, \bar{\omega}x) \{ 4k^2 \} \end{aligned}$$

Eqs. (3.12a-b)

*An extensive set of tabulations for the f_λ -function is currently being prepared by the Bureau of Standards for NACA, and it will appear shortly as a Technical Note.

CONFIDENTIAL

CONFIDENTIAL

Specifically, if the downwash (\bar{w}/U) was unity rather than $2ik$, Eq. (3.10) would be

$$p' = - \left\{ 2ikx f_0(M, \bar{w}x) + e^{-i\bar{w}x} J_0\left(\frac{\bar{w}x}{M}\right) \right\} \quad \text{Eq. (3.13)}$$

Equation (3.13), applied in succession to the two triangular regions 102 and 403 of Fig. III.11, yields for the contribution of the strip A (for unit w/U) to the pressure at point 0

$$p'_A = - \left\{ 2ikx f_0(M, \bar{w}x) + e^{-i\bar{w}x} J_0\left(\frac{\bar{w}x}{M}\right) - 2ikx_1 f_0(M, \bar{w}x_1) - e^{-i\bar{w}x_1} J_0\left(\frac{\bar{w}x_1}{M}\right) \right\} \quad \text{Eq. (3.14)}$$

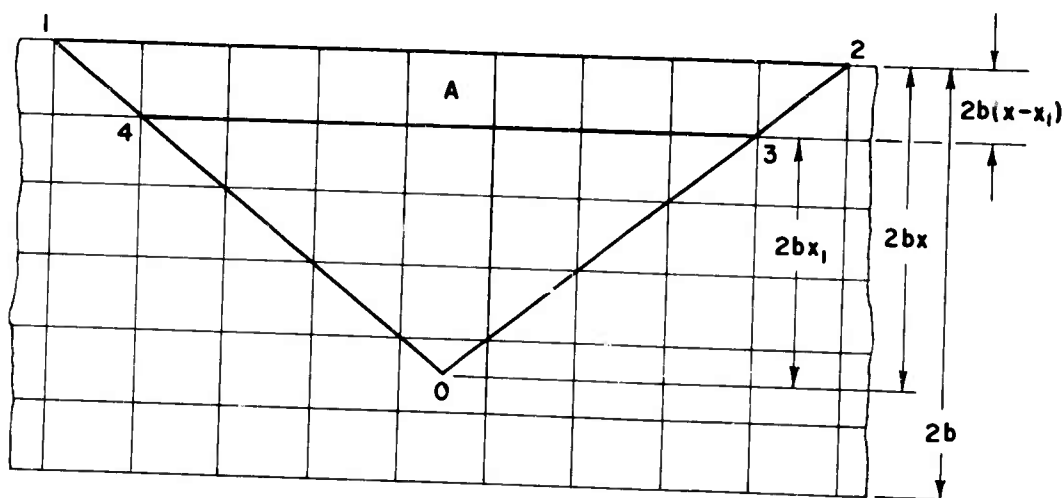


Fig. III.11 Illustrative Example: the Use of the Mach Grid System for a Two-Dimensional Wing with Variation of Downwash Across the Chord.

If the strip A is taken to be the row \bar{v} of the Mach box grid

CONFIDENTIAL

system, Eq. (3.14) represents exactly the sum of the AIC of all boxes in this row, provided the exact expressions, Eqs. (2.29), are employed:

$$p'_A = \sum_{\bar{\mu}=-\bar{v}}^{\bar{v}} (R_{\bar{v},\bar{\mu}} + iJ_{\bar{v},\bar{\mu}}) \equiv p'_{\bar{v}}$$

Eq. (3.15)

When the Mach boxes are used for the evaluation of the chordwise pressure distribution due to the motions (2) and (3), one gets for the total pressure at point 0

$$p' = \sum_{\bar{v}} \frac{\bar{w}_{\bar{v}}}{U} p'_{\bar{v}}$$

Eq. (3.16)

Here $\bar{w}_{\bar{v}}$ now represents the downwash at mid-chord of strip \bar{v} , so Eq. (3.16) is an approximation. As an example, let the parameters assume the values

$$k = 0.3, 0.99 \text{ and } M = 1.2$$

The lowest Mach number for which the linearized theory is expected to apply satisfactorily ($M \cong 1.2$) is taken in these computations since conclusions drawn for such critical cases are expected to apply at higher Mach numbers with an element of conservatism. The pressure distributions by the Mach-box numerical method are compared with the exact results in Figs. III.12 through III.17.

Several interesting conclusions may be drawn from these plots:

(1) At moderate frequencies (around $k = 0.3$), a few chordwise boxes yield satisfactory accuracy for the pressure distributions, and the precision improves as the number of boxes is increased. Also, for motion (3) the results are slightly poorer than those for motion (2).

(2) At higher frequencies (around $k = 0.99$), the pressure distributions using six boxes again are acceptable, but a lower number of boxes will yield very poor estimates (the latter are not shown on the plot for the sake of clarity). When the foregoing computation was made, it was felt that at this Mach number and reduced frequency, the governing parameter was the modified reduced frequency per box, i.e., $\bar{k}_1 = (\omega b_1/U)(M^2/\beta^2)$ and that

CONFIDENTIAL

— EXACT

○ SIX CHORDWISE MACH (or SQUARE) BOXES.
EXACT EXPRESSIONS FOR AICs

x THREE CHORDWISE MACH (or SQUARE) BOXES
EXACT EXPRESSIONS FOR AICs

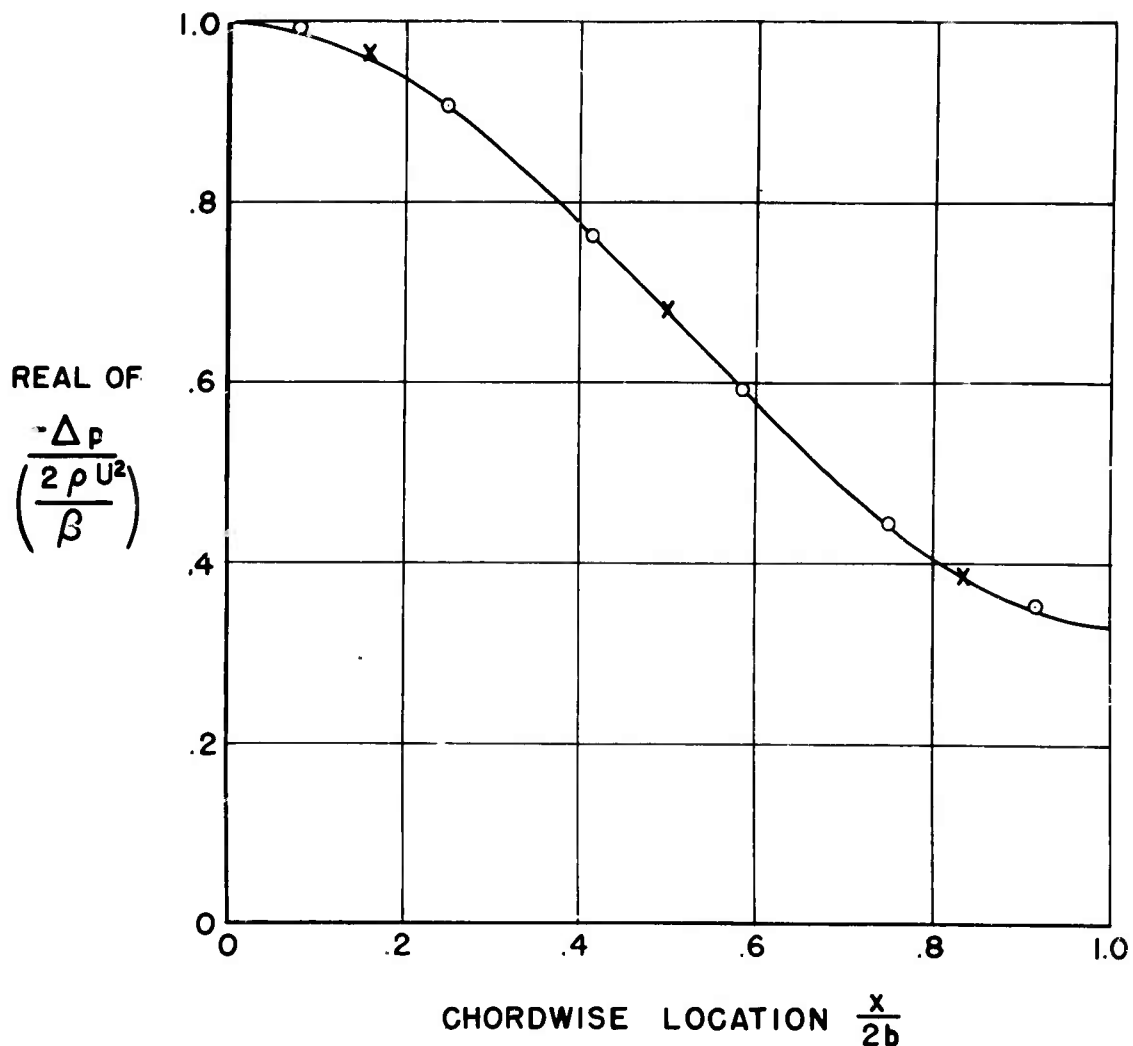


Fig. III.12 Real Part of Chordwise Pressure Distribution for a Two-Dimensional Unswept Wing.
(Motion: $z = 2bx e^{i\omega t}$, $k = 0.3$, $M = 1.2$)

CONFIDENTIAL

CONFIDENTIAL

- EXACT
- SIX CHORDWISE MACH (or SQUARE) BOXES.
EXACT EXPRESSIONS FOR AICs
- x THREE CHORDWISE MACH (or SQUARE) BOXES
EXACT EXPRESSIONS FOR AICs

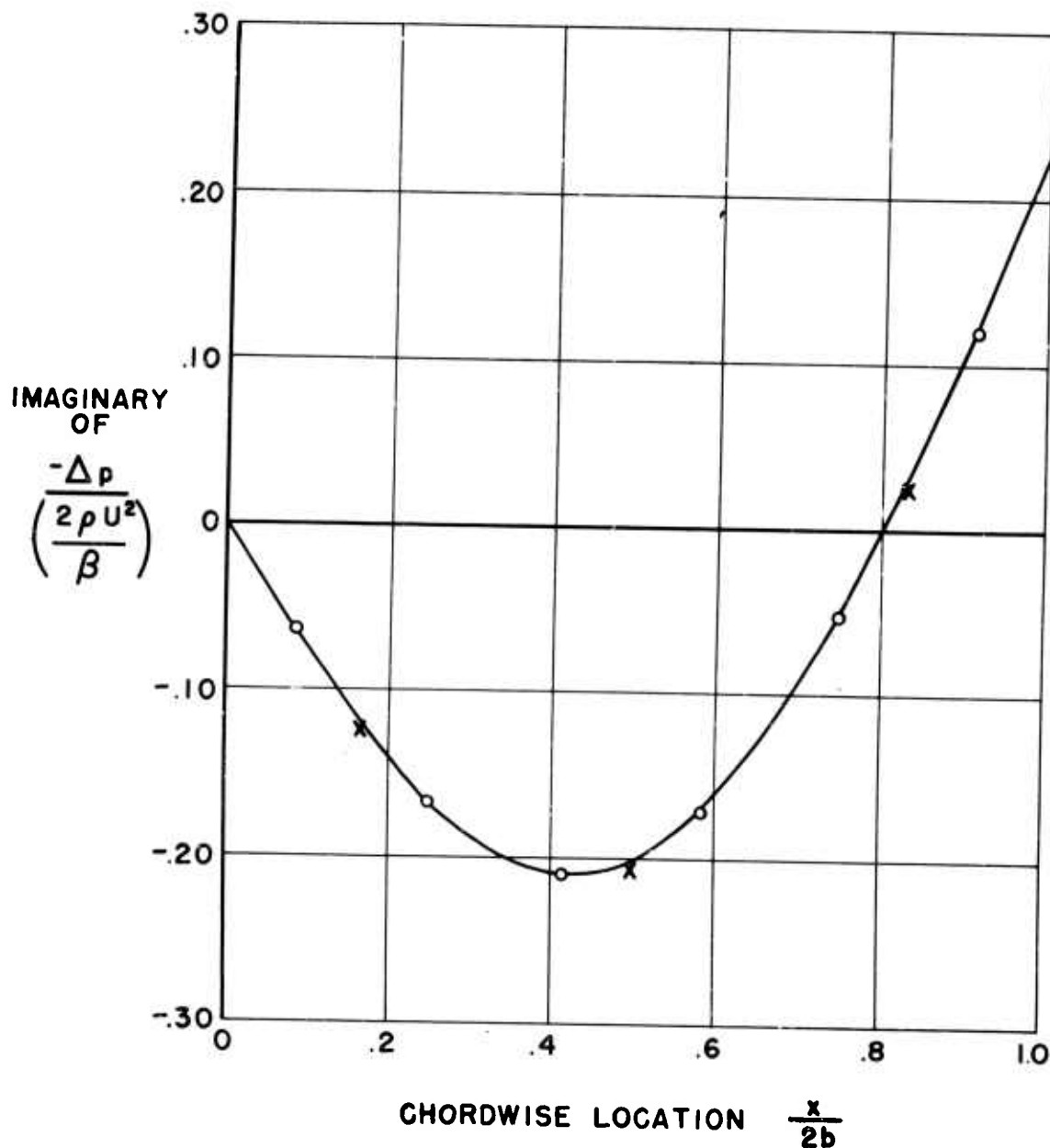


Fig. III.13 Imaginary Part of Chordwise Pressure Distribution for a Two-Dimensional Unswept Wing.
(Motion: $z = 2bx e^{i\omega t}$, $k = 0.3$, $M = 1.2$)

CONFIDENTIAL

— EXACT

○ SIX CHORDWISE MACH (or SQUARE) BOXES.
EXACT EXPRESSIONS FOR AICs

x THREE CHORDWISE MACH (or SQUARE) BOXES
EXACT EXPRESSIONS FOR AICs

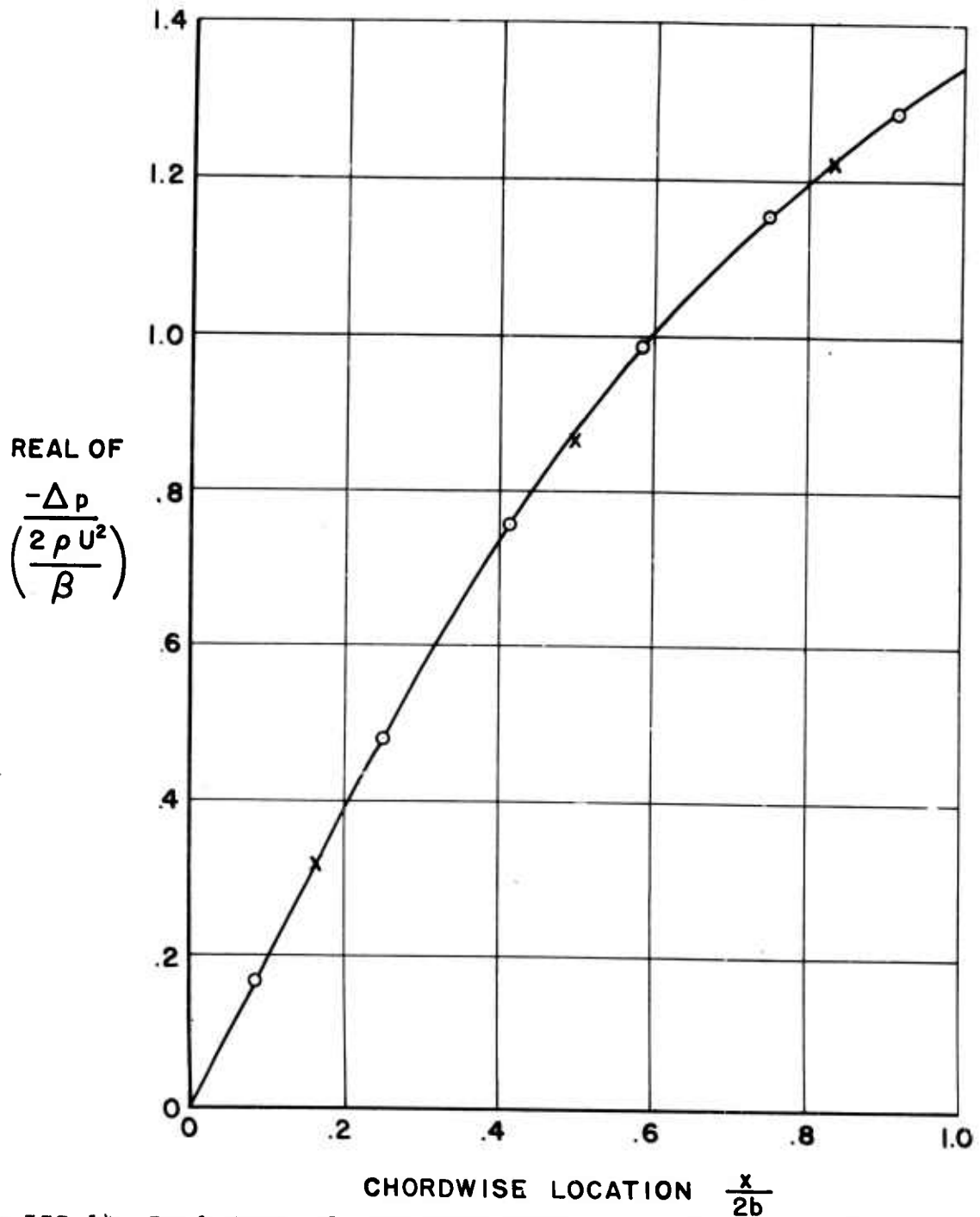


Fig.III.14. Real Part of Chordwise Pressure Distribution for a Two-Dimensional Unswept Wing. (Motion: $z = 2bx^2e^{i\omega t}$, $R=0.3$, $M=1.2$)

WADC TR 56-97, Part 1

-49-

CONFIDENTIAL

CONFIDENTIAL

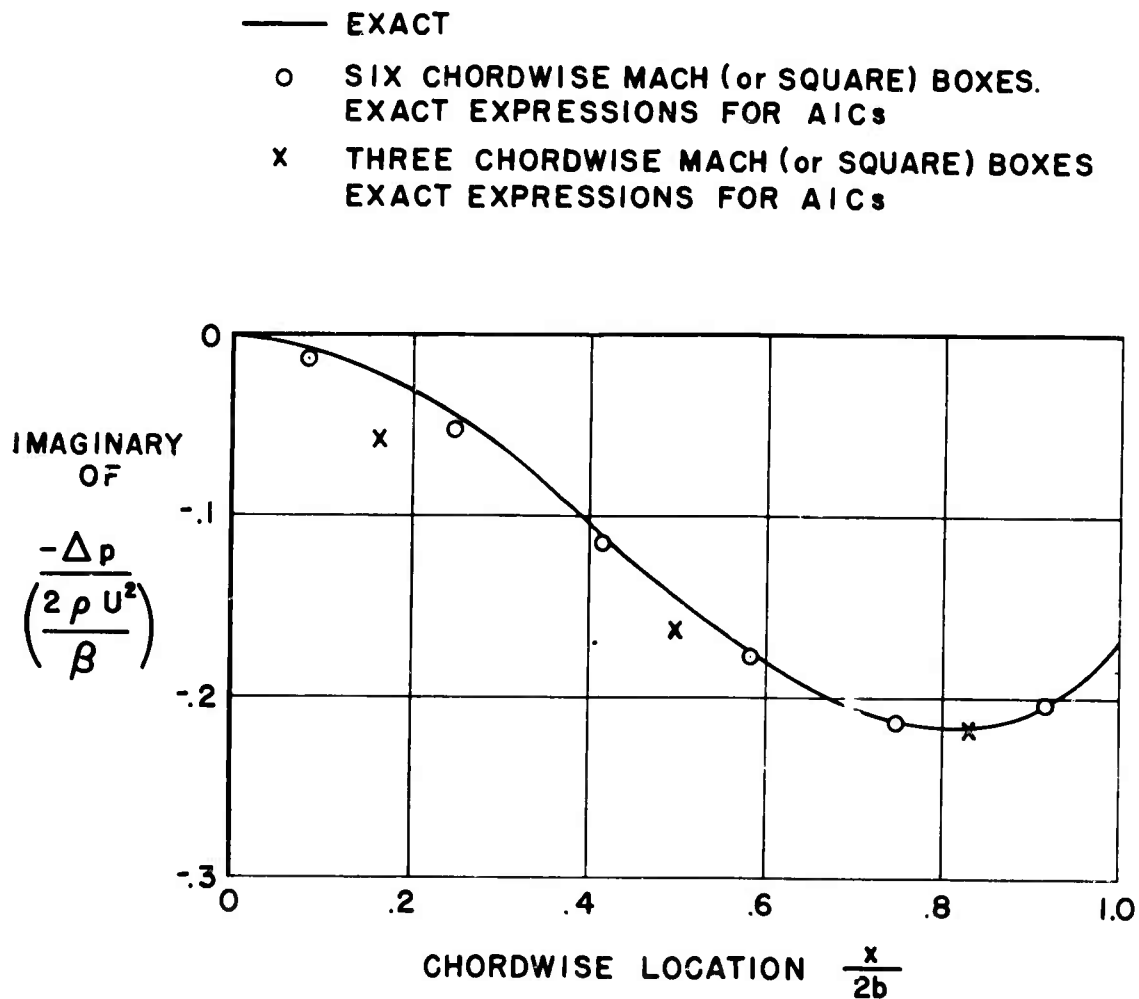


Fig. III.15. Imaginary Part of Chordwise Pressure Distribution for a Two-Dimensional Unswept Wing.
(Motion: $z = 2bx^2e^{i\omega t}$, $k=0.3$, $M=1.2$)

CONFIDENTIAL

CONFIDENTIAL

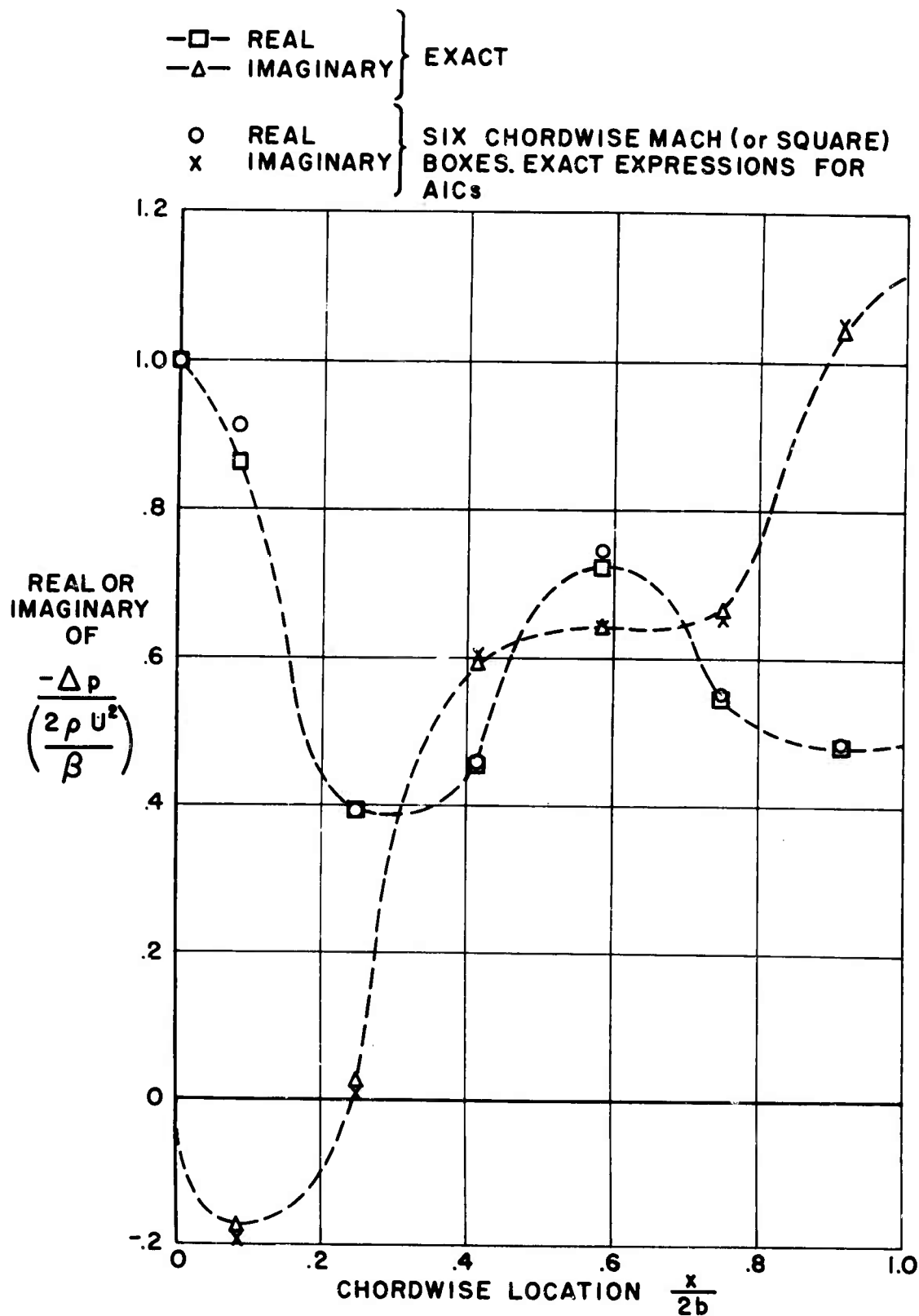


Fig. III.16 Chordwise Pressure Distribution for a Two-Dimensional Unswept Wing. (Motion: $z = 2bx e^{i\omega t}$, $k = 0.99$, $M = 1.2$)

CONFIDENTIAL

CONFIDENTIAL

- REAL
 -Δ- IMAGINARY
- } EXACT
- REAL
 x IMAGINARY
- } SIX CHORDWISE MACH (or SQUARE) BOXES.
 EXACT EXPRESSIONS FOR AICs.

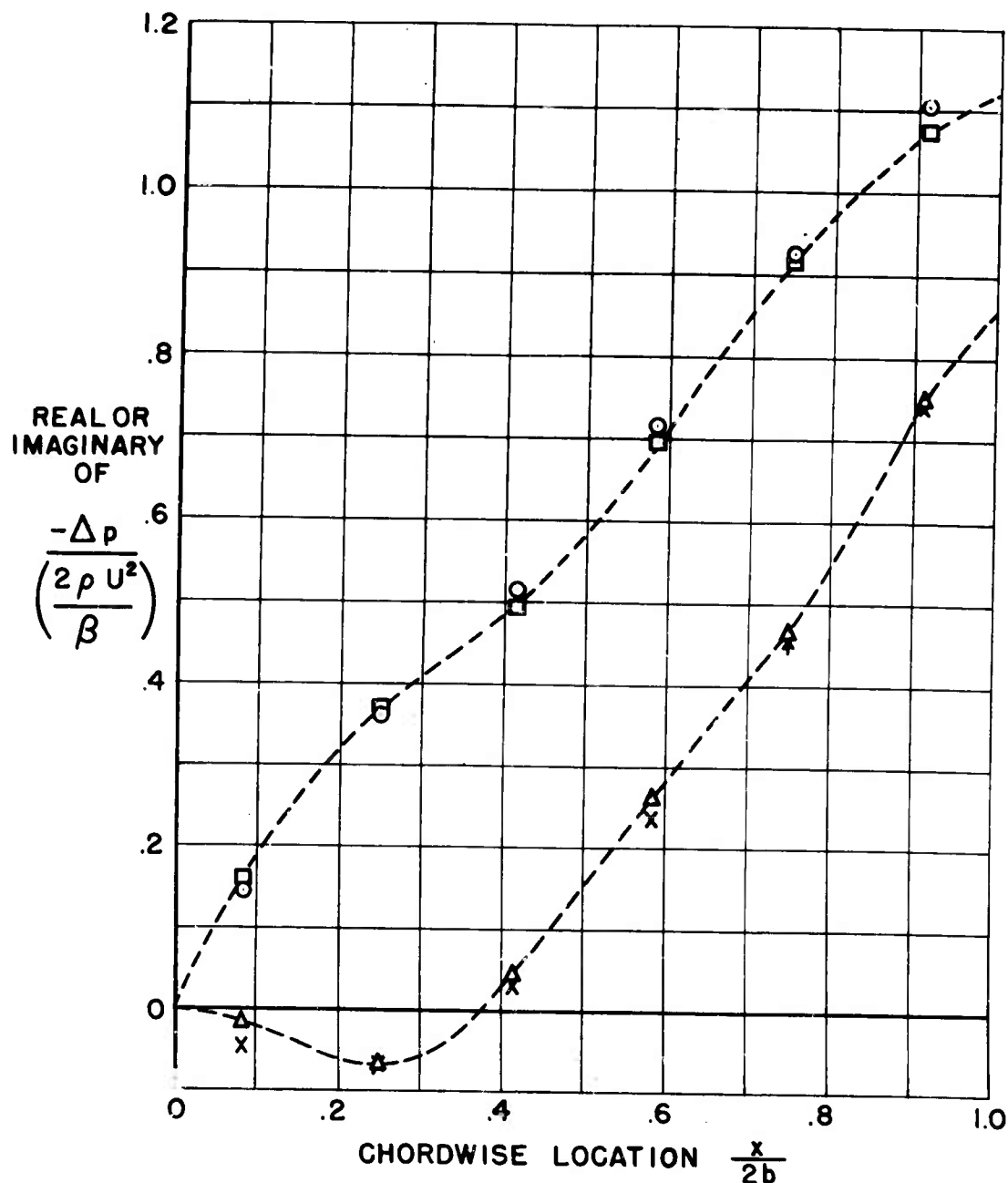


Fig. III.17 Chordwise Pressure Distribution for a Two-Dimensional Unswept Wing. (Motion: $z = 2\beta x^2 e^{i\omega t}$, $\beta = 0.99$, $M = 1.2$)

CONFIDENTIAL

CONFIDENTIAL

this quantity was too large at the higher value of k . Hence, calculations were carried out for the case $M=1.5$, $k=0.99$; but again the pressure distributions were accurate to about the same degree as those for $M=1.2$, $k=0.99$. It has therefore been concluded that the primary parameter is k , (which enters the formulas through the expression for downwash) rather than k . As k increases, it appears that the problem requires more and more chordwise boxes, regardless of the Mach number.

A more meaningful criterion for selecting the number of boxes is furnished by a comparison of the generalized forces calculated by any of the numerical schemes with their exact values. Using the rectangular rule for the chordwise integration when Mach boxes are employed, the lift and pitching moment about the leading edge per unit span were computed for three combinations of Mach number and reduced frequency. These are compared with the exact results in Tables III.5-III.7.

		2 Boxes	3 Boxes	6 Boxes	Exact
$\frac{L}{\left(\frac{2gU^2}{\beta}\right)^{2b}}$	k=0.3, M=1.2	-0.204,96 -0.352,521	-----	-0.190,31 -0.351,511	-0.188,46 -0.351,391
	k=0.99 M=1.2	-0.378,43 -0.645,691	-----	-0.075,59 -0.918,841	-0.064,91 -0.923,601
	k=0.99 M=1.5	-0.070,43 -1.221,551	-----	-0.046,62 -1.247,611	-0.044,08 -1.250,291
$\frac{M}{\left(\frac{2gU^2}{\beta}\right)^{2b^2}}$	k=0.3 M=1.2	-0.214,77 -0.264,561	-----	-0.202,87 -0.250,811	-0.200,73 -0.249,321
	k=0.99 M=1.2	-0.259,38 -0.741,941	-----	0.103,74 -0.837,671	0.107,31 -0.823,981
	k=0.99 M=1.5	0.181,12 -1.068,101	-----	0.171,80 -1.106,431	0.170,88 -1.110,701

Table III.5 Comparison of Lift and Moment About the Leading Edge per Unit Span, Computed Using Mach Boxes, with the Exact Values for a Two-Dimensional Unswept Wing Oscillating in the Motion $z = 2be^{i\omega t}$

CONFIDENTIAL

		2 Boxes	3 Boxes	6 Boxes	Exact
$\frac{L}{(\frac{2\beta U^2}{\beta})^{2\beta}}$	k=0.3 M=1.2	-0.685,24 +0.121,36i	-0.678,70 +0.102,55i	-0.674,72 +0.091,08i	-0.673,74 +0.087,37i
	k=0.99 M=1.2	-0.574,85 -0.083,60i	-----	-0.591,53 -0.461,83i	-0.583,42 -0.478,83i
	k=0.99 M=1.5	-1.029,47 -0.143,77i	-----	-0.762,62 -0.670,85i	-0.760,97 -0.672,67i
$\frac{M}{(\frac{2\beta U^2}{\beta})^{2\beta^2}}$	k=0.3 M=1.2	-0.564,26 +0.093,19i	-0.550,37 +0.069,38i	-0.542,43 +0.054,85i	-0.540,07 +0.047,93i
	k=0.99 M=1.2	-0.670,76 -0.224,40i	-----	-0.553,75 -0.689,45i	-0.544,40 -0.693,60i
	k=0.99 M=1.5	-1.085,55 -0.169,42i	-----	-0.711,45 -0.962,88i	-0.711,63 -0.967,25i

Table III.6 Comparison of Lift and Moment About the Leading Edge per Unit Span, Computed Using Mach Boxes, with the Exact Values for a Two-Dimensional Un-swept Wing Oscillating in the Motion $z = 2\beta x e^{i\omega t}$

		2 Boxes	3 Boxes	6 Boxes	Exact
$\frac{L}{(\frac{2\beta U^2}{\beta})^{2\beta}}$	k=0.3 M=1.2	-0.793,41 +0.171,56i	-0.801,59 +0.145,49i	-0.805,69 +0.129,75i	-0.807,42 +0.126,87i
	k=0.99 M=1.2	-0.455,29 +0.097,60i	-----	-0.628,78 -0.227,83i	-0.622,44 -0.264,05i
	k=0.99 M=1.5	-0.905,11 -0.514,61i	-----	-0.813,48 -0.370,17i	-0.810,32 -0.378,10i
$\frac{M}{(\frac{2\beta U^2}{\beta})^{2\beta^2}}$	k=0.3 M=1.2	-0.964,13 +0.196,40i	-1.002,53 +0.181,00i	-1.024,60 +0.171,11i	-1.036,06 +0.167,97i
	k=0.99 M=1.2	-0.606,44 +0.082,72i	-----	-0.814,23 -0.386,47i	-0.804,46 -0.429,82i
	k=0.99 M=1.5	-1.146,76 -0.796,56i	-----	-1.049,32 -0.580,76i	-1.050,65 -0.593,84i

Table III.7 Comparison of Lift and Moment About the Leading Edge per Unit Span, Computed Using Mach Boxes, with the Exact Values for a Two-Dimensional Un-swept Wing Oscillating in the Motion $z = 2\beta x^2 e^{i\omega t}$

CONFIDENTIAL

CONFIDENTIAL

The following points may be deduced:

- (1) At moderate $k's$ (around $k = 0.3$) and for all three motions where the pressure distributions are satisfactory, the approximate lifts and moments deviate somewhat from the exact, but improve markedly as the number of boxes is increased. This might be expected because more and more pressure points are available for the chordwise integration.
- (2) At higher $k's$ (around $k = 0.99$), and for all motions, at least six chordwise boxes are required for tolerable accuracy. For $M = 1.2$, the integrated lifts and moments are poorer than those for $M = 1.5$ at the same k . This fact is primarily due to an insufficient number of chordwise points for integration of the sinuous pressure distributions shown in Figs. III.16 and III.17. For $M = 1.5$ and $k = 0.99$, the pressure distributions are less sinuous; hence one obtains the better accuracy.

So far only three types of motion and the two lowest-order generalized forces have been considered. If higher-order generalized forces are required, which is often the case in flutter analysis, more than six chordwise boxes are needed. The same requirement must be imposed if motions more sinuous than (2) and (3) are considered. On the basis of assuming that the "half wave" of each such chordwise mode is adequately represented by a second-order polynomial, one may extrapolate and accept the number 6 as a minimum for chordwise boxes per half wave of any chordwise mode.

The case of the three-dimensional wing with all edges supersonic (e.g., the wide delta) represents only a slight extension of the case of the two-dimensional airfoil discussed above. Pines et al (Refs. 21-24) have demonstrated that such wings can be treated with satisfactory accuracy by the AIC methods. Two examples of this type, one involving steady motion and the other oscillations at a moderate reduced frequency, are presented in Section V. From examination of those calculations, in conjunction with the various two-dimensional cases given above, it has been concluded that a conservative rule for wings with all supersonic edges is that a minimum of eight boxes should be taken along the midspan chord. This minimum should be increased if the wavelength of the mode of chordwise deformation becomes too short.

The rule involves a slight upward revision of the requirement of six chordwise boxes recommended for purely two-dimensional cases. This modification is introduced to account for the possibility of added errors which may arise due to spanwise deformation of the finite wing, since these errors

CONFIDENTIAL

may be additive upon those due to chordwise deformation and already reduced to acceptable size by the six-box rule. Another consideration affecting the decision to recommend eight boxes is that the increment in computational labor caused by going from six to eight is not severe.

III.4 Comments on the Accuracy of the Approximate Formulas for the Aerodynamic Influence Coefficients.

The approximate formulas given in Section II for the square and Mach-box grid systems must be investigated for their precision at high values of k_1 . The most extreme case in the tabulations of Ref. 25 ($k_1 = 0.4$, $M = 1.2$) will be tested. For rows $\bar{v} = 0$ and 1, some caution was exercised in Ref. 25 for high values of k_1 ; a subdivision technique which splits the basic square area into 25 smaller squares was introduced to improve the accuracy. However, for rows $\bar{v} \geq 2$, no such step was taken, because it would entail a much lengthier set of calculations. One can determine the order of accuracy for $\bar{v} = 2$, $k_1 = 0.4$ and $M = 1.2$ by using a subdivision technique. For instance, if the large box $\bar{v} = 2$, $\bar{\mu} = 1$ (Fig. II.1) is taken and subdivided into twenty-five smaller boxes, one has

$$(\bar{R}_{2,1} + i\bar{I}_{2,1})_{k_1=0.4} = \sum_{\bar{v}'=0}^{12} \sum_{\bar{\mu}'=3}^7 (\bar{R}_{\bar{v}',\bar{\mu}'} + i\bar{I}_{\bar{v}',\bar{\mu}'})_{k_1=0.08} \quad \text{Eq. (3.17)}$$

Since tabulations at this Mach number are also available from Ref. 25 for $k_1 = 0.08$, this check can be carried out very simply. Table III.8 shows the comparison of the AIC's for $k_1 = 0.4$, $M = 1.2$, $\bar{v} = 2$ given in Ref. 25 with those calculated by Eq. (3.17).

It is seen that all entries in the table are appreciably different from those computed by the subdivision method. The latter set, being obtained from a finer grid, must necessarily be much closer to the exact values (this will be proved later). A similar calculation could not be carried out for all boxes ($\bar{v} = 3$), there being insufficient entries in the tables of Ref. 25. Although a direct comparison of the values in the first column of Table III.8 with the corresponding exact values would have been preferable, such an undertaking would have required the difficult task of evaluating the AIC's from the exact formulas for a square box.

CONFIDENTIAL

	From Ref. 25, $k_1 = 0.4$, $M = 1.2$	With Subdivision, Using Ref. 25, $k_1 = 0.08$, $M = 1.2$
$\bar{R}_{2,0} + i \bar{I}_{2,0}$	-0.091,77-0.004,24i	-0.099,30-0.003,14i
$\bar{R}_{2,1} + i \bar{I}_{2,1}$	-0.107,66-0.036,25i	-0.117,82-0.037,88i
$\bar{R}_{2,2} + i \bar{I}_{2,2}$	-0.210,49-0.262,81i	-0.236,11-0.258,86i
$\bar{R}_{2,3} + i \bar{I}_{2,3}$	-0.060,88+0.077,15i	-0.020,95+0.045,89i
$\bar{R}_{2,4} + i \bar{I}_{2,4}$	0.176,40-0.016,24i	0.153,12-0.011,67i

Table III.8 Aerodynamic Influence Coefficients in Row $\bar{v} = 2$ Calculated with and without Subdivision. ($k_1 = 0.4$, $M = 1.2$)

Rather than compare the accuracy for the individual boxes in a given row, one can more easily study the sum of the AIC in this row. As was pointed out in Section III.3, the exact sum of the contributions of all the boxes in a row is given by Eq. (3.14). Table III.9 shows this sum, computed in three different ways, and indicates significant deviations for rows $\bar{v} \geq 2$ at this value of k_1 and M . With subdivisions in row $\bar{v} = 2$, the accuracy improves markedly.

Additional calculations for lower values of k_1 at this Mach number have shown that, for the approximate formulas, the maximum tolerable value for k_1 is around 0.08 if one is to obtain adequate estimations of ρ_v' . At higher Mach numbers, k_1 can be increased somewhat, but in all cases the value of the modified reduced frequency should be lower than

CONFIDENTIAL

$$\bar{k}_1 = k_1 \frac{M^2}{\beta^2} \leq 0.3$$

Eq. (3.18)

\bar{v}	Ref. 25, $k_1=0.4, M=1.2$ $p'_v = \beta \sum_{\mu} (\bar{R}_{\bar{v},\mu} + i \bar{I}_{\bar{v},\mu})$	With Subdivisions (Table III.8) p'_v	Exact [Eq. (3.14)] p'_v
0	-0.794,33+0.382,33i	-----	-0.796,26+0.382,62i
1	+0.650,46-0.254,42i	-----	+0.651,92-0.251,39i
2	-0.329,69-0.318,75i	-0.360,07-0.350,35i	-0.364,61-0.352,96i
3	-0.021,63+0.312,31i	-----	+0.009,21+0.302,53i
4	0.116,31-0.307,01i	-----	0.131,36-0.265,07i

Table III.9 The Sum of the Aerodynamic Influence Coefficients
 p'_v in Rows $\bar{v}=0, \dots, 4$ for $k_1=0.4$,
 $M=1.2$, Calculated by Various Methods

It should be pointed out that the majority of the tables in Ref. 25 fall within the limitations of Eq. (3.18). This statement can also be made with regard to most actual cases of flutter, so that no reflection on the practical utility of these tables should be inferred. On the other hand, it is strongly recommended that exact expressions such as those in Section II.3b be used in the preparation of all future tabulations. If new

CONFIDENTIAL

CONFIDENTIAL

tables are to be based on the Mach-box scheme, no serious difficulty should be experienced in adapting the exact formulas to high-speed machine computation.

One further minor point should be made regarding the tables of Ref. 25. When the Mach number is less than 1.4, the entries are not complete in the sense that a full 20 boxes along the chord of a wing cannot be employed. Additional entries would be needed for integral values of $\bar{\mu}$ in the range $[(\bar{v}+2)/\beta] \geq \bar{\mu} \geq 19$, which cover two small but significant regions more than 19 boxes to the left and right of the "receiving point" but still between the forward Mach lines emanating from this point. Inasmuch as 20 boxes chordwise would probably never appear in an application, no inconvenience can be expected to result from this incompleteness.

CONFIDENTIAL

CONFIDENTIAL

SECTION IV

LOADING OF PLANFORMS WITH SUBSONIC EDGES

For finite but purely supersonic lifting surfaces (e.g., the wide delta wing), the pressures on the planform are not influenced by any area off the planform. However, when the planform has subsonic edges, there exist disturbed regions of the $x-y$ -plane adjacent to such edges which affect the pressure distribution on the whole or parts of the planform. Following Evvard's concept (Ref. 38) a fictitious, thin, impermeable "diaphragm" may be introduced in these regions. This diaphragm is assumed to coincide with a stream sheet, and therefore it cannot alter the flow, nor can it sustain a pressure difference at any point between its top and bottom surfaces. The combination of the planform and the diaphragm forms a new surface, which is purely supersonic and for which downwashes are known on the planform, while the pressure jump is zero over the remaining area. The problem is to find the strengths of sources and sinks (or equivalently the downwash distribution) which must be placed on the diaphragm to satisfy there the boundary condition of zero pressure. Once this is accomplished, the pressure distribution on the planform may then be determined as for a purely supersonic surface.

When a numerical approach such as the AIC method is to be used, satisfaction of the zero-pressure condition on the diaphragm region is necessarily limited to a finite number of points of this region. At other points the pressures will not in general be zero. There are two alternatives for minimizing the effects of this approximation. The first is to take a large number of boxes on the diaphragm. The second is to take fewer boxes but assume beforehand a downwash variation over each box which is specially adjusted to agree with the zero-pressure condition.

It is a major objective of this section to suggest possible methods for the proper treatment of subsonic edges. At first, the particularly simple problem of a subsonic edge parallel to the flow will be studied. Afterward subsonic leading and trailing edges will be discussed. In most instances, the illustrative examples consist of cases of steady flow. The main conclusions reached are expected to hold for unsteady motion, however, for reasons given from time to time in subsequent paragraphs.

CONFIDENTIAL

CONFIDENTIAL

IV.1 The Side-Edge Problem in Steady Flow

Consider a rectangular wing in steady flow at a constant angle of attack α (Fig. IV.1). The aspect ratio is sufficiently large that the Mach lines ab and cd intersect behind the trailing edge (this is not a necessary restriction on the method of approach). The exact dimensionless pressure difference at any point on the "mixed" region B_1 is given by Lighthill in Ref. 39 to be

$$\rho' \equiv \frac{\Delta p}{\left(\frac{2\rho U^2 \alpha}{\beta}\right)} = - \left[\frac{1}{\pi} \cos^{-1} \left(1 - \frac{2\beta y}{x} \right) \right]. \quad \text{Eq. (4.1)}$$

At any point in the purely supersonic region A , one has the Ackeret result

$$\rho' \equiv \frac{\Delta p}{\left(\frac{2\rho U^2 \alpha}{\beta}\right)} = -1 \quad \text{Eq. (4.2)}$$

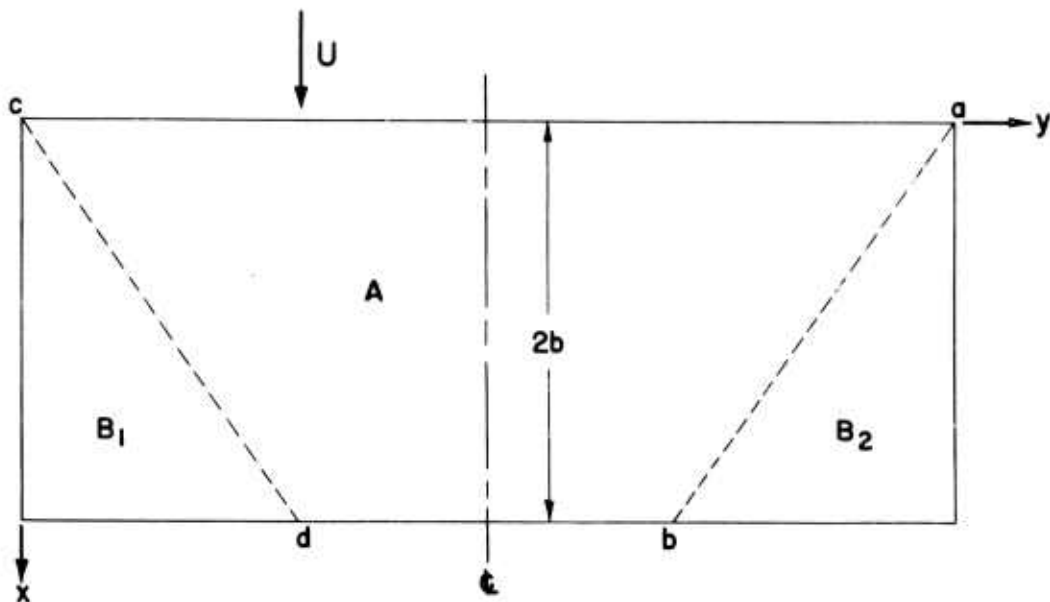


Fig. IV.1 Illustrative Example for the Treatment of a Side Edge

CONFIDENTIAL

Because of the manner in which $\beta = \sqrt{M^2 - 1}$ is employed to make Eqs. (4.1) and (4.2) dimensionless, β' is independent of Mach number, as are all the loadings calculated by approximate numerical methods in this subsection.

As a first example of approximate calculation of the loading of this wing by AIC methods, the characteristic grid system is chosen. Since there exists no chordwise variation in downwash, the most serious objection to the use of this system (see Section III) is eliminated. It also offers the advantage of being able to satisfy the zero-pressure condition at discrete points on the side edge, a fact which will become apparent as the procedure is illustrated. Four chordwise characteristic boxes are assumed, as shown in Fig. IV.2. The problem is

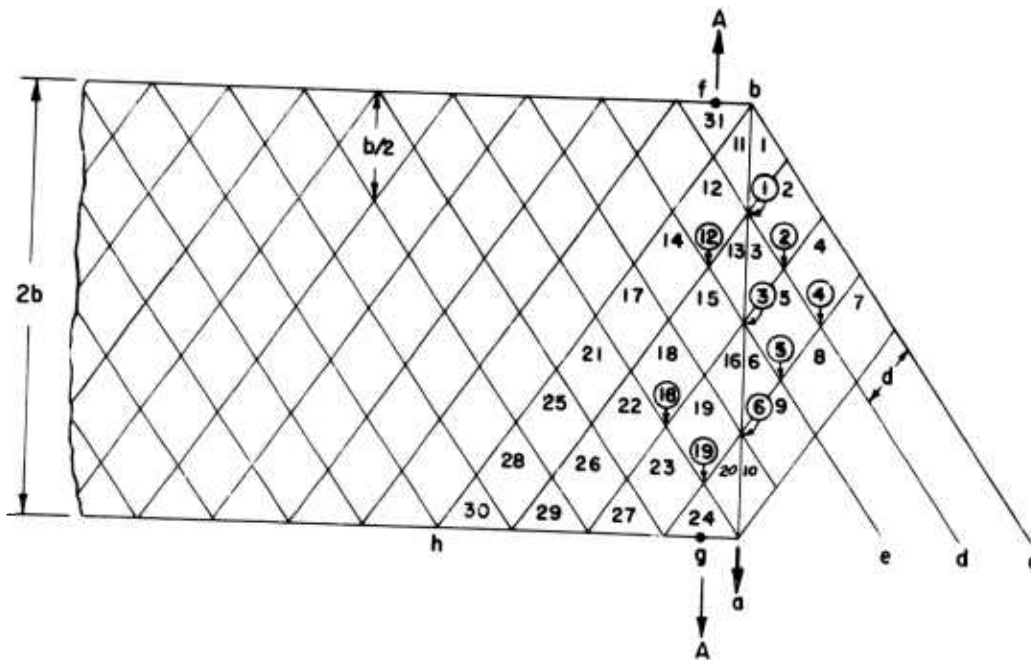


Fig. IV.2 Characteristic Grid System for a Rectangular Wing in Steady Motion at Constant Angle of Attack

solved in two different ways, based on the following two assumptions:

- (1) The diaphragm region is replaced by the rhombuses. Over each such rhombus, the disturbance (and hence the downwash) is assumed constant.

CONFIDENTIAL

- (2) The distribution of downwash on the diaphragm region is made singular at the side edge. This singular behavior is indicated by the exact linearized solution given by Lagerstrom (Ref. 40), and involves inverse proportionality to the square root of perpendicular distance off the edge.

Procedure 1:

At all points on the wing, the downwash is $U\alpha$. Denote the downwashes over boxes 1, ..., 6 in Fig. IV.2 by w_1, \dots, w_6 , respectively, and let p'_n be the pressure at the lowest corner of box n . The condition of zero pressure at point (1) yields the relation

$$U\alpha p'_1 = U\alpha (C_{0,0}^{(3)} + C_{0,1}^{(2)}) + w_1 C_{0,0}^{(3)} = 0 \quad \text{Eq. (4.3a)}$$

or

$$w_1 = - \frac{U\alpha}{C_{0,0}^{(3)}} (C_{0,0}^{(3)} + C_{0,1}^{(2)}) \quad \text{Eq. (4.3b)}$$

where the AIC's $C_{\nu,\mu}^{(i)}$ are those of Eqs. (2.48). The same condition for point (2) leads to

$$w_2 = - \frac{U\alpha}{C_{0,0}^{(1)}} \left(\frac{w_1}{U\alpha} C_{0,1}^{(3)} + C_{1,0}^{(3)} + C_{0,2}^{(2)} \right) \quad \text{Eq. (4.4)}$$

It can be seen that a sequential solution for the downwash strengths w_1, \dots, w_6 results from setting the pressures at (1), ..., (6) successively equal to zero. (Note that boxes 7-10 need not be considered, since they do not affect the pressures at the discrete points of interest.) Once these downwashes are determined, the pressure at any point n on the wing can be calculated by simple summation of the effects of all boxes in the forward Mach cone emanating from n . The values of p'_n are shown in Table IV.1 and compared with the exact according to Eq. (4.1). The accuracy obtainable is not regarded as satisfactory. As the number of boxes is increased, the results improve somewhat, but the convergence is rather slow. For instance, if eight boxes had been taken instead of four, $p'_{1/8}$ would have the value of $-0.273, 62$ ($p'_{1/8}$ with four boxes)

CONFIDENTIAL

instead of $-0.254,62$, as compared to the exact $-0.391,83$. As will be seen later, this convergence is more rapid when Mach or square boxes are employed. The reason for the discrepancies in the present calculation is that the assumption of constant downwash over each diaphragm box is not adequate, and a better representation of the variation over each such box is required.

	Procedure (1)	Procedure (2) Downwash Singularity Included	Exact [Eq. (4.1)]
P'_{12}	-0.254,62	-0.401,07	-0.391,83
P'_{15}	-0.171,97	-0.291,31	-0.295,17
P'_{19}	-0.135,03	-0.238,01	-0.246,75
P'_{14}	-0.377,99	-0.507,75	-0.5
P'_{18}	-0.273,62	-0.389,33	-0.391,83
P'_{23}	-0.221,55	-0.326,29	-0.333,33
P'_{17}	-0.454,83	-0.570,86	-0.564,09
P'_{22}	-0.334,10	-0.452,62	-0.454,37
P'_{21}	-0.508,67	-0.614,25	-0.608,17
P'_{26}	-0.396,95	-0.498,70	-0.5
P'_{25}	-0.549,12	-0.646,54	-0.640,98
P'_{28}	-0.580,96	-0.671,82	-0.666,67

Table IV.1 Dimensionless Pressures on the Mixed Region of a Rectangular Wing in Steady Supersonic Motion at a Constant Angle of Attack. Comparison Between Exact Results and Two Forms of the Characteristic Box Method

CONFIDENTIAL

Procedure 2:

It is known from Lagerstrom's exact solution (Ref. 40) that the downwash over the diaphragm region exhibits a square-root singularity as the side edge is approached from the outside and vanishes on the forward Mach line bc . The effect of this singularity can be approximately accounted for. In Cartesian coordinates, the receiving point is (x, y) while ξ, η are the running variables representing the influencing point (see Fig. IV.3). A characteristic coordinate system r, s with origin at (x, y) is defined such that the axes r and s are, respectively, the right and left forward Mach lines emanating from (x, y) .*

$$\begin{aligned} r &= \frac{M}{2\beta} [(x-\xi) - \beta(y-\eta)] \\ s &= \frac{M}{2\beta} [(x-\xi) + \beta(y-\eta)] \end{aligned} \quad \text{Eqs. (4.5a-b)}$$

If the receiving point (x, y) lies on the side edge where $r=s$, one may assume for the downwash distribution on the diaphragm region

$$w(r, s) = \frac{w_s}{\sqrt{d}} \frac{r_1 - r}{\sqrt{r-s}} \quad (r \geq s) \quad \text{Eq. (4.6)}$$

Equation (4.6) exhibits the proper singular behavior at the edge and vanishes on the Mach line bc ($r=r_1$). Here d is a typical length** and w_s is the "strength" of the downwash. If the receiving point is on the diaphragm region, Eq. (4.6) becomes

$$w(r, s) = \frac{w_s}{\sqrt{d}} \frac{r_1 - r}{\sqrt{r-(s-s_0)}} \quad (\text{Fig. IV.4a}) \quad \text{Eq. (4.7a)}$$

and if the receiving point is on the planform,

*Note that in this section the coordinates r, s are dimensional, in contrast to Section II.

**For convenience, this typical length d is taken in subsequent derivations to be the side of a rhombus or half the diagonal of a Mach box.

CONFIDENTIAL

$$w(r,s) = \frac{w_5}{\sqrt{d}} \frac{r_1 - r}{\sqrt{(r-r_0)-s}} \quad (\text{Fig. IV.4 b})$$

Eq. (4.7b)

where the notation is that of Figs. IV.4.

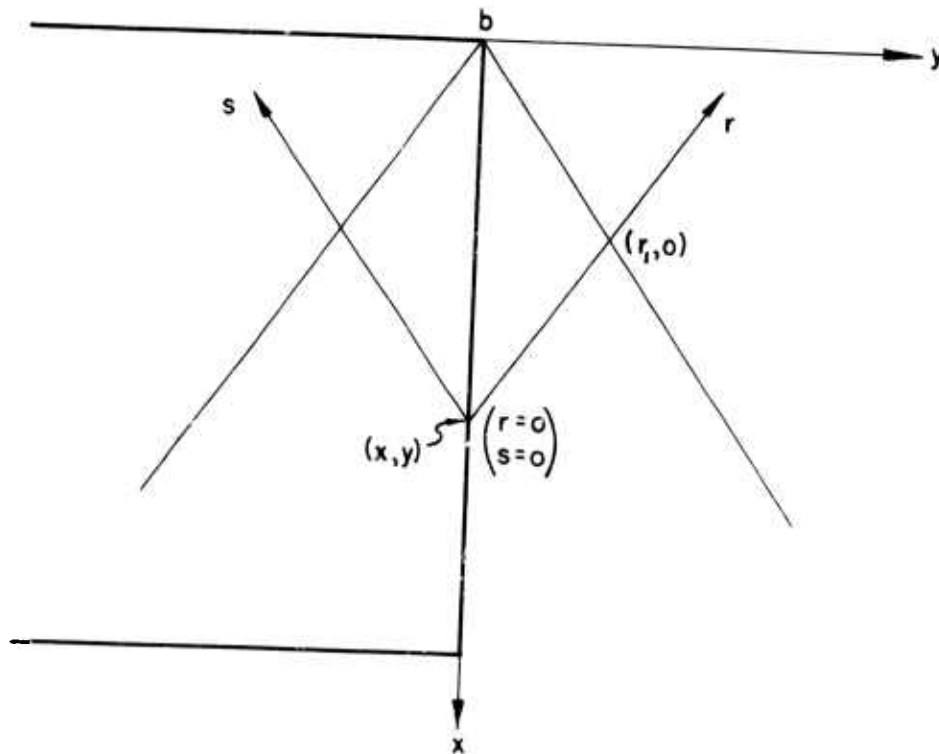


Fig. IV.3 Characteristic Coordinate System for the Treatment of the Side-Edge Downwash Singularity

CONFIDENTIAL

CONFIDENTIAL

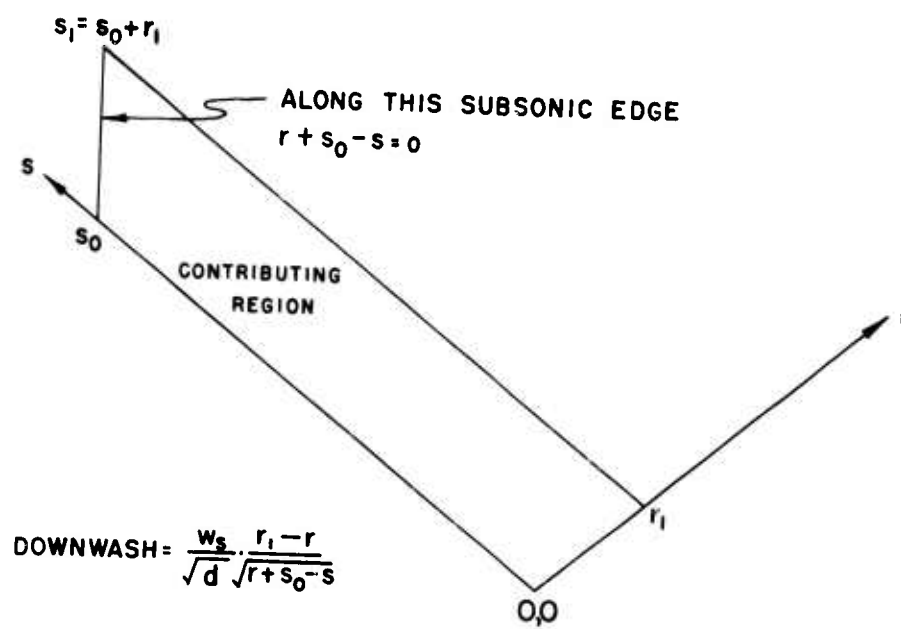


Fig. IV.4a

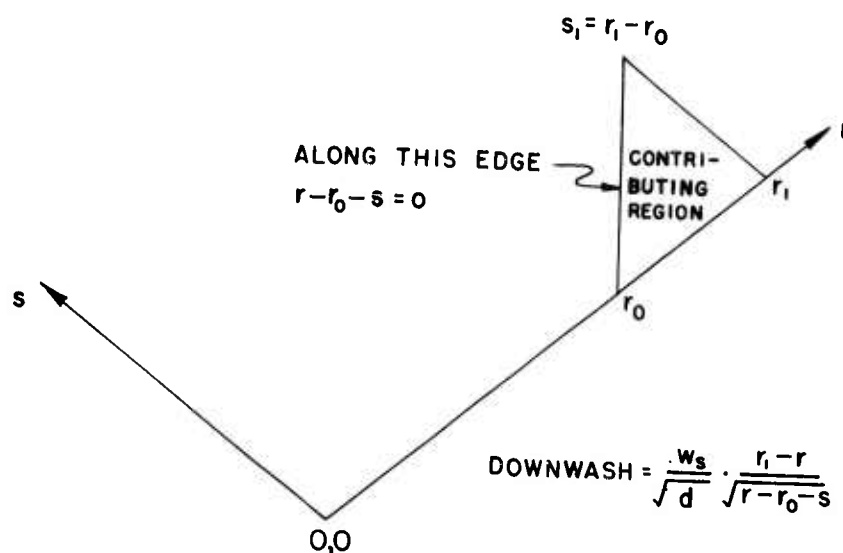


Fig. IV.4b

Figs. IV.4a-b. Singular Downwash Distribution Near a Side Edge

CONFIDENTIAL

CONFIDENTIAL

One can easily prove by direct substitution of Eqs. (4.7a-b) into the characteristic-coordinate form of Eq. (2.3) that the associated pressure influence coefficients are given by (for $\omega = 0$)

$$C^{(s)} = \frac{\Delta p}{\left(\frac{2\rho U \omega_5}{\beta}\right)} = -\sqrt{\frac{r_i}{a}} \equiv C_a^{(c)} \text{ for Fig. IV.4a}$$

$$= -\sqrt{\frac{r_i}{a}} + \sqrt{\frac{r_o}{a}} \equiv C_c^{(s)} \text{ for Fig. IV.4b.} \quad \text{Eqs. (4.8a-b)}$$

Returning to Fig. IV.2, the following downwash distributions are assumed:

- (1) A singular downwash distribution w_{51} over the region bounded by abc . Additional singular distributions w_{53} , w_{56} over the regions $a(1)d$ and $a(3)e$, respectively.
- (2) Additional constant downwashes w_2 , w_4 and w_5 over boxes 2, 4 and 5.

One obtains from the zero-pressure condition at points (1)-(6)

$$U\alpha p'_1 = U\alpha (C_{0,0}^{(3)} + C_{0,1}^{(2)}) + w_{51} C_a^{(s)} \left(\frac{r_i}{a} = 1\right) = 0$$

$$U\alpha p'_2 = U\alpha (C_{1,0}^{(3)} + C_{0,2}^{(2)}) + w_{51} C_a^{(s)} \left(\frac{r_i}{a} = 1\right) + w_2 C_{0,0}^{(1)} = 0$$

$$U\alpha p'_3 = U\alpha (C_{0,0}^{(3)} + C_{1,1}^{(3)} + C_{0,1}^{(1)} + C_{0,2}^{(1)} + C_{0,3}^{(2)} + C_{1,2}^{(2)})$$

$$+ w_{51} C_a^{(s)} \left(\frac{r_i}{a} = 2\right) + w_2 C_{1,0}^{(1)} + w_{53} C_a^{(s)} \left(\frac{r_i}{a} = 1\right)$$

$$\vdots$$

$$\vdots$$

$$\vdots$$

Eq. (4.9)

as in Procedure 1 a sequential solution yields the required values for the assumed downwashes. Incidentally, this sequential solution is equivalent to the inversion of a triangular matrix, as shown by Pines and Dugundji in Ref. 24, if the equations are cast in matrix form. Once $w_{51}, \dots, w_5, w_{56}$, are determined, the pressure at any point in the mixed wing region can be calculated. For instance,

CONFIDENTIAL

$$U\alpha p'_{12} = U\alpha (C_{0,0}^{(1)} + C_{0,1}^{(1)} + C_{0,2}^{(2)} + C_{1,1}^{(2)} + C_{0,1}^{(3)} + w_{s1} C_b^{(5)} (\frac{r_1}{d} = 2, \frac{r_0}{d} = 1)) \quad \text{Eq. (4.10)}$$

The pressures obtained in this manner are also shown in Table IV.1. A marked improvement is evidently achieved when the singularity of downwash is accounted for, even though the zero-pressure condition is satisfied at the same number of points on the diaphragm as in Procedure (1).

Next considered is the Mach grid system for the same wing, with six chordwise boxes. As may be seen from Fig. IV.5, two difficulties arise:

- (1) The pressures cannot be made identically zero at points on the side edge since the control points (centers of the nearest diaphragm boxes) lie off the wing;
- (2) if Procedure (1) above is to be followed, no disturbances can be assumed in the triangular regions \mathcal{D} unless additional tables for such regions are prepared.

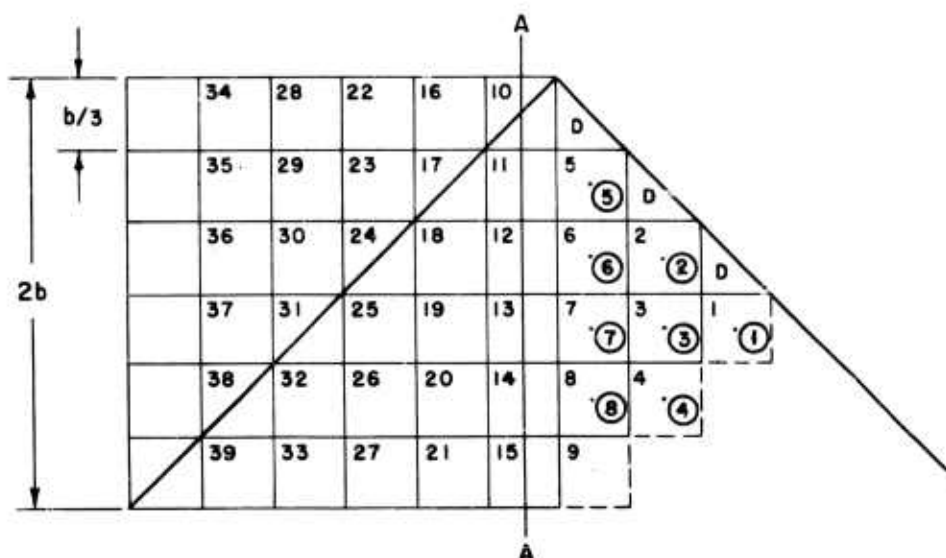


Fig. IV.5 Mach Grid System for a Rectangular Wing in Steady Motion at Constant Angle of Attack

CONFIDENTIAL

Table IV.2 presents the pressures at the centers of the boxes calculated according to Procedures (1) and (2) above.

	Procedure (1)	Procedure (2) Downwash Singularity Included	Exact [Eq. (4.1)]
P_{11}'	-0.608,17	-0.445,87	-0.391,83
P_{12}'	-0.410,57	-0.326,22	-0.295,17
P_{13}'	-0.352,90	-0.248,31	-0.246,75
P_{14}'	-0.300,01	-0.233,31	-0.216,35
P_{15}'	-0.274,05	-0.191,69	-0.194,98
P_{18}'	-0.704,83	-0.599,84	-0.564,09
P_{19}'	-0.525,33	-0.475,17	-0.454,37
P_{20}'	-0.460,54	-0.391,79	-0.391,83
P_{21}'	-0.401,99	-0.362,09	-0.349,80
P_{25}'	-0.753,25	-0.669,62	-0.640,98
P_{26}'	-0.590,81	-0.552,19	-0.535,44
P_{27}'	-0.525,88	-0.470,63	-0.471,02
P_{32}'	-0.783,65	-0.712,07	-0.687,49
P_{33}'	-0.634,79	-0.602,35	-0.587,93
P_{39}'	-0.805,02	-0.741,43	-0.719,56

Table IV.2 Dimensionless Pressures on the Mixed Region of a Rectangular Wing in Steady Supersonic Flow at a Constant Angle of Attack. Comparison between Exact Results and Calculations by Two Forms of the Mach Box Method

CONFIDENTIAL

As in the case of characteristic boxes, the pressures found without accounting for the singular downwash distribution are not satisfactory, whereas the inclusion of the singularity improves the accuracy. However, Procedure (2), which gives excellent results in conjunction with characteristic boxes, fails to yield a comparable accuracy with Mach boxes. This discrepancy can be attributed entirely to the fact that one has to satisfy the zero-pressure condition at points (5), (6), (7), (8), rather than at the side edge. If half Mach boxes had been used at the side edges with centers on that edge (i.e. if boxes were half boxes) the precision could have been improved. However, the latter arrangement is very inconvenient from the practical standpoint.

It should be pointed out that the values in Table IV.2 calculated by Procedure (1) exhibit a somewhat faster convergence, as more chordwise boxes are taken, than those found by the characteristic-box method.

By simple integrations of Eqs. (4.1) and (4.2), one obtains the following formulas for the dimensionless lift and pitching moment about the y -axis per unit span for the left half-span (See Fig. IV.1):

$$l(y) = \frac{\text{Lift/unit span}}{\left(\frac{2\rho U^2 \alpha}{\beta}\right) 2b} = -1, \quad y \geq \frac{2b}{\beta}$$

$$= -\frac{1}{\pi} \cos^{-1}\left(1 - \frac{2\beta y}{2b}\right) - \frac{2}{\pi} \sqrt{\frac{\beta y}{2b}} \sqrt{1 - \frac{\beta y}{2b}}, \quad \frac{2b}{\beta} \geq y \geq 0$$

$$m(y) = \frac{\text{Moment/unit span}}{\left(\frac{2\rho U^2 \alpha}{\beta}\right) 2b^2} = -1, \quad y \geq \frac{2b}{\beta}$$

$$= -\frac{1}{\pi} \cos^{-1}\left(1 - \frac{2\beta y}{2b}\right)$$

$$- \frac{2}{3\pi} \sqrt{\frac{\beta y}{2b}} \sqrt{1 - \frac{\beta y}{2b}} \left(1 + \frac{2\beta y}{2b}\right), \quad \frac{2b}{\beta} \geq y \geq 0$$

Eqs. (4.11a-d)

If any one of the box schemes is employed in the determination of the pressures, corresponding chordwise integrations must be carried out numerically since the pressures are given only at

CONFIDENTIAL

discrete points. In general, these approximate integrations introduce errors which can be quite significant, especially if only a few points are available in the ranges of the integrations. For instance, at Section A-A (Fig. IV.2) the trapezoidal rule yields ($p'_x = p'_{31} = -1$, $p'_9 \approx p'_{19}$)

$$2b \ell_{A-A} \approx \frac{b}{4}(-1) + \frac{b}{4}[-1 + 2p'_{12} + 2p'_{15} + p'_{19}] + \frac{b}{4}p'_{19}$$

$$2b^2 m_{A-A} \approx \frac{b}{4}(-1)\frac{b}{8} + \frac{b}{4}[-1]\frac{b}{4} + 2(p'_{12}\frac{3b}{4}) + 2(p'_{15}\frac{5b}{4}) + (p'_{19}\frac{7b}{4}) + \frac{b}{4}(p'_{19}\frac{15b}{8})$$

Eqs. (4.12a-b)

At Section A-A (Fig. IV.5) the rectangular rule yields ($p'_{10} = -1$)

$$2b \ell_{A-A} \approx \frac{b}{3}[-1 + p'_{11} + p'_{12} + p'_{13} + p'_{14} + p'_{15}]$$

$$2b^2 m_{A-A} \approx \frac{b}{3}[-1]\frac{b}{6} + (p'_{11}\frac{b}{2}) + (p'_{12}\frac{5b}{6}) + (p'_{13}\frac{7b}{6}) + (p'_{14}\frac{3b}{2}) + (p'_{15}\frac{11b}{6})$$

Eqs. (4.13a-b)

Even if the pressures are determined from the exact Eqs. (4.1)-(4.2), the lift and moment distributions given by Eqs. (4.12)-(4.13) do not check their exact counterparts. These numerical integrations can be improved appreciably if one accounts for the slope discontinuity in the pressure distribution across the Mach line bc (Fig. IV.2), which is known to exist from the analytical solution, Eq. (4.2). The effect of the infinite slope in the stream direction can be included as shown in Appendix C, Ref. 31, provided the fluctuations of the pressure as a function of x are not excessive. This qualification limits the refined integration technique of the above reference to cases where the leading edge is supersonic, because subsonic leading edges produce severe fluctuations in the chordwise pressure distribution as estimated by any numerical approach.

For the particular numerical example at hand, even better numerical integrations can be devised. For example, at Section A-A (Fig. IV.2), if one uses the trapezoidal rule for segment $f-(31)$, the refinement of Ref. 31 for the sharp drop in pressure in segment $(31)-(12)$, Simpson's rule for segment $(12)-(19)$ and the trapezoidal rule for segment $(19)-g$, one obtains satisfactory accuracy. This combined approximation yields

CONFIDENTIAL

$$2b\ell_{A-A} \approx \frac{b}{4}(-1) + \frac{b}{6}(-1+2p'_{12}) + \frac{b}{6}(p'_{12}+4p'_{15}+p'_{19}) + \frac{b}{4}p'_{19}$$

$$2b^2m_{A-A} \approx \frac{b}{4}(-1)\frac{b}{8} + \frac{b}{2}\left[(-1)\left(\frac{2b}{15}\right) + \left(p'_{12}\frac{11b}{30}\right)\right] + \frac{b}{6}\left[\left(p'_{12}\frac{3b}{4}\right) + 4\left(p'_{15}\frac{5b}{4}\right) + \left(p'_{19}\frac{7b}{4}\right)\right] + \frac{b}{4}\left(p'_{19}\frac{15b}{8}\right)$$

Eqs. (4.14a-b)

Typical applications show Eqs. (4.14a-b) definitely preferable to Eqs. (4.12)-(4.13), and the improved formulas also allow a more rational evaluation of the improvement obtained by accounting for the downwash singularity.

In Figs. IV.6-IV.7, the spanwise running lift and moment about the leading edge are presented. Comparisons between the exact curves and the curves obtained by the AIC method and Eqs. (4.14a-b) reveal that the inclusion of the downwash singularity improves the accuracy considerably. This is especially true of the characteristic grid system, which permits satisfaction of the zero-pressure condition on the side edges.

So far the analysis is carried in such a form that the Mach number does not appear explicitly. This is possible only for steady-state cases with no spanwise variation in downwash and for Mach or characteristic box systems, where the box sizes are directly related to the Mach number. By contrast, if one employs the square grid system, one must specify beforehand the Mach number. If $M \geq \sqrt{2}$, no particular difficulty is encountered in carrying out the solution, the steps being parallel to those for Procedure (1) just illustrated. When one attempts to include the downwash singularity (Procedure 2), the forward Mach lines emanating from the centers of planform boxes (control points) cut the diaphragm region in an irregular manner, making this refinement a practical impossibility. Furthermore, when $M < \sqrt{2}$, it will be shown that the square grid system cannot be used for planforms with subsonic edges.

Consider a rectangular wing at an angle of attack α in steady flow at $M = 1.2$. As shown in Fig. IV.8, a diaphragm box (1,a) is influenced by boxes (1,1) and (1,b). In turn, (1,b) is influenced by (1,a) and (1,c), and so on. Consequently, if the pressures are to be made zero at the centers of all boxes off the wing, an infinite number of boxes must

CONFIDENTIAL

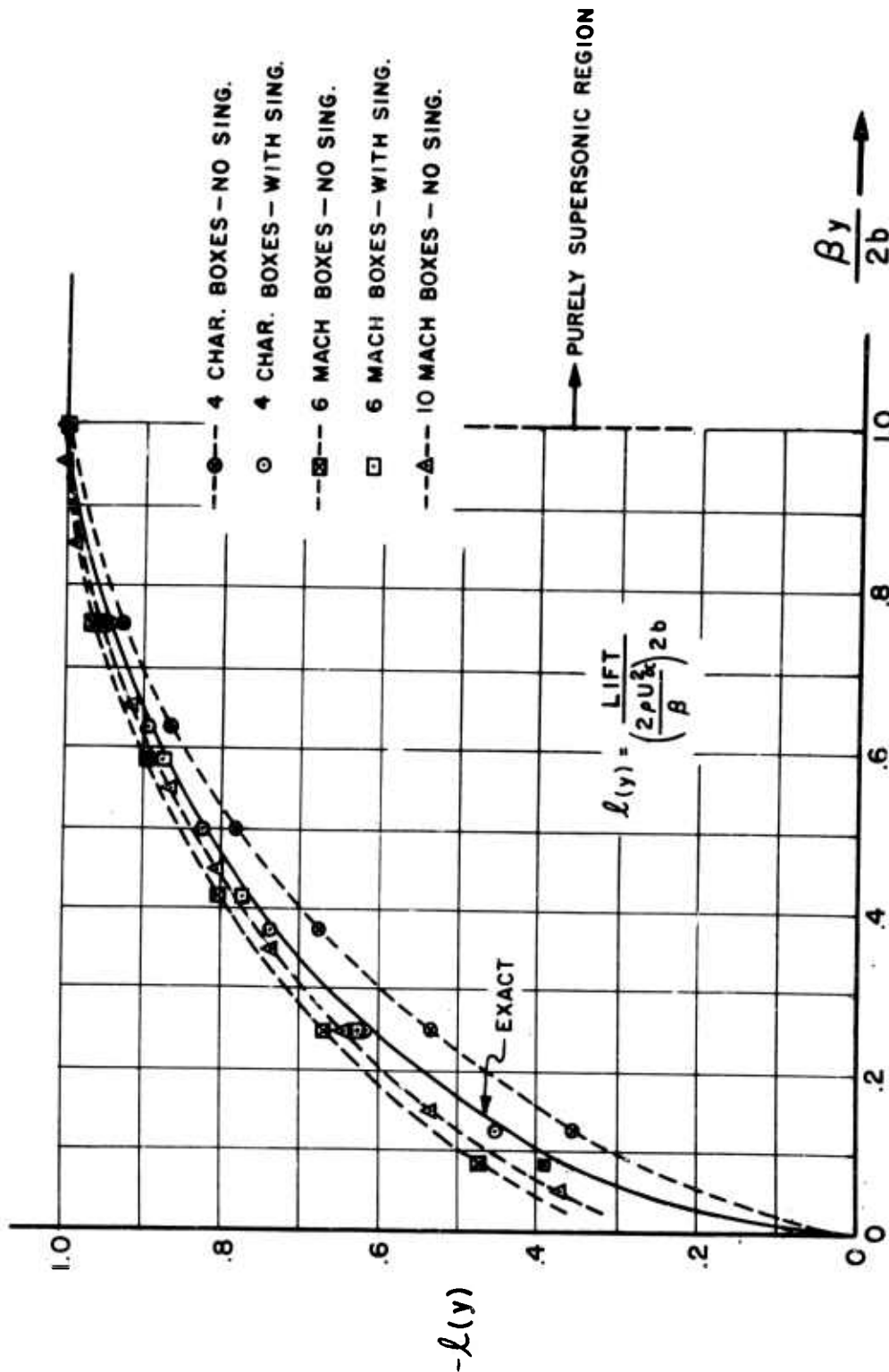


Fig. IV.6 Spanwise Lift Distribution on a Rectangular Wing in Steady Supersonic Flight at Constant Angle of Attack, as Calculated by the Methods Indicated on the Various Curves

CONFIDENTIAL

CONFIDENTIAL

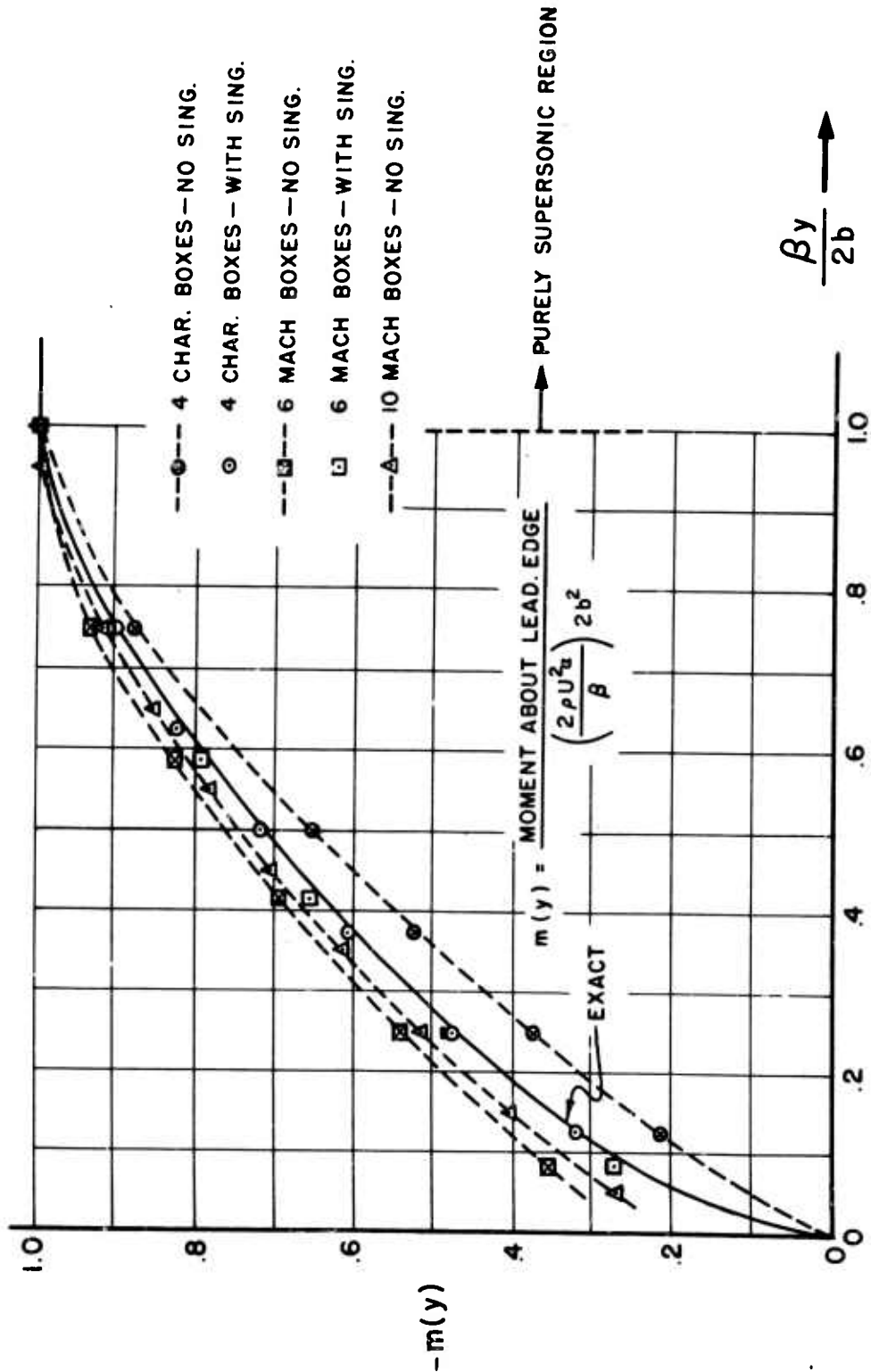


Fig. IV.7 Spanwise Moment Distribution on a Rectangular Wing in Steady Supersonic Flight at Constant Angle of Attack, as Calculated by the Methods Indicated on the Various Curves

CONFIDENTIAL

CONFIDENTIAL

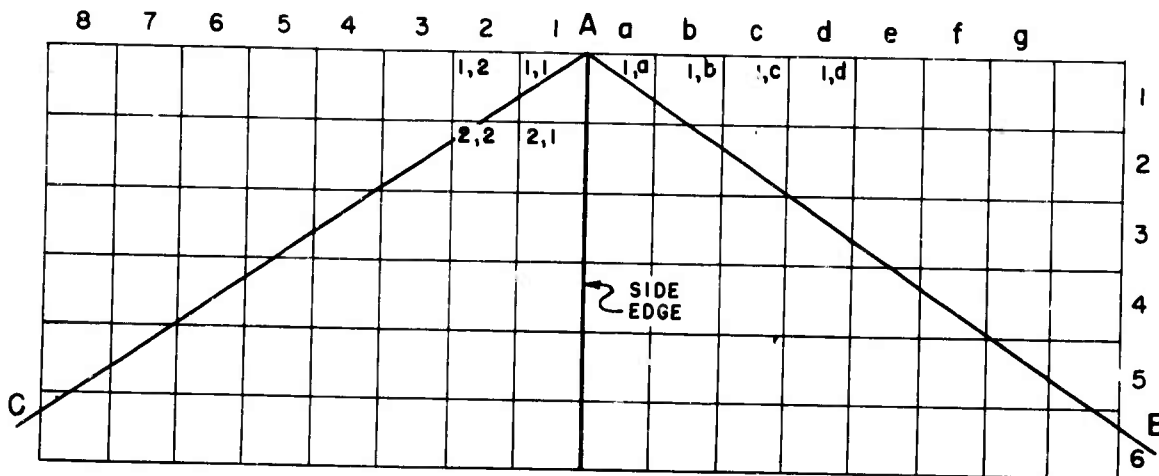


Fig. IV.8 Square Grid System for a Rectangular Wing in Steady Motion at Constant Angle of Attack. ($M = 1.2$)

be considered, and the downwashes on these boxes determined. In practice, the number of boxes must be limited, so that all boxes beyond some boundary line off the wing must be arbitrarily assumed to have zero downwash. As a start, let the following boxes and those which are further out have zero downwash

$$w_{1f}, w_{1c}, \dots, w_{2c}, \dots, w_{3e}, \dots = 0$$

The nonzero downwashes $w_{1a}, w_{2a}, w_{2b}, \dots$ etc. are then determined by the conditions of zero pressure at the centers of boxes

CONFIDENTIAL

CONFIDENTIAL

1a, 2a, 2b, etc., ... Here a sequential solution is not possible, since laterally adjacent boxes affect each other. The equations that yield the downwashes for the diaphragm boxes must be solved simultaneously. The resultant pressures at three points on the planform are computed to be

$$p'_{1,1} = -0.573,96, \quad p'_{2,2} = -0.573,96, \quad p'_{2,1} = -0.262,56,$$

as compared with the exact values

$$p'_{1,1} = -0.605,92, \quad p'_{2,2} = -0.605,92, \quad p'_{2,1} = -0.311,65.$$

During this computation the condition of zero pressure on boxes (1,t), (2,c), etc., is violated. In fact, a simple computation gives

$$p'_{1,t} = 0.419,45, \quad p'_{2,c} = 0.134,00$$

Next, one additional box is taken in each row, i.e.,

$$w_{1,t}, w_{2,c}, \dots, \neq 0.$$

The corresponding pressures at two points on the wing turn out to be

$$p'_{1,1} = -0.407,56, \quad p'_{2,2} = -0.407,56$$

If the foregoing process is continued, taking one additional box at a time in each row, the results can be shown to deviate more and more from the exact values. Therefore, the first trial, where only diaphragm boxes with centers inside the Mach line AB are considered, appears to give the best possible accuracy, even though the pressure conditions at (1,t), (2,c), etc., are violated.

A similar difficulty occurs for planforms with swept supersonic leading edges (c.f., points a and t, Fig. III.3 where $p' \neq 0$ according to the box scheme). While this violation of the zero-pressure condition is not serious for supersonic leading edges, as indicated by the results of Table III.3, it leads to much larger errors when there are subsonic edges. As can be seen from Table IV.3, the pressures for the first case treated above diverge more from the exact for boxes farther downstream and fluctuate violently.

CONFIDENTIAL

	Procedure (1) Using Square Boxes	Exact [Eq. (4.1)]
$P'_{1,1}$	-0.573,96	-0.605,94
$P'_{2,1}$	-0.262,56	-0.311,66
$P'_{2,2}$	-0.573,96	-0.605,94
$P'_{3,1}$	-0.310,63	-0.237,34
$P'_{3,2}$	-0.356,47	-0.288,28
$P'_{3,3}$	-0.644,50	-0.605,94
$P'_{3,4}$	-0.808,53	-0.827,89
$P'_{4,1}$	-2.410,91	-0.199,21
$P'_{5,2}$	-2.652,43	-0.311,66
$P'_{6,3}$	+0.098,80	-0.370,07

Table IV.3 Pressures on the Mixed Region of a Rectangular Wing in Steady Motion at a Constant Angle of Attack (Square Boxes, $M=1.2$)

IV.2 The Side-Edge Problem in Unsteady Flow

The foregoing illustrative examples have dealt with the relatively simple problem of steady flow. In unsteady motion, the general procedures just outlined are still valid. In addition to regular AIC tables, however, the use of Procedure (2) of Section IV.1 requires tabulation of aerodynamic influence coefficients associated with an unsteady singular downwash distribution near the side edge. Using Eq. (2.3) and the transformation of variables Eqs. (4.5a-b), one obtains for the pressure at the point ($r=0$, $s=0$) due to the downwash functions given by Eqs. (4.7a-b)

CONFIDENTIAL

$$\left(\frac{p'}{2\rho U \bar{u}_5}\right) = -\frac{i\omega}{U} \frac{4\beta r_i}{M} \sqrt{\frac{r_i}{d}} \left\{ \bar{I}_0 - \bar{I}_1 \right\} - 2\sqrt{\frac{r_i}{d}} \bar{I}_0$$

(origin on diaphragm)

$$\left(\frac{p'}{2\rho U \bar{u}_5}\right) = -\frac{i\omega}{U} \frac{4\beta r_i}{M} \sqrt{\frac{r_i}{d}} \left\{ \bar{P}_0 - \bar{P}_1 \right\} - 2\sqrt{\frac{r_i}{d}} \bar{P}_0$$

Eqs. (4.15a-b)

(origin on planform)

Here \bar{u}_5 is the amplitude of the singular downwash strength, now assumed to have simple harmonic time dependence, ω is the circular frequency of oscillation, and

$$\bar{I}_n = \frac{1}{4\pi r_i^{n+\frac{1}{2}}} \int_0^{r_i} \int_0^{s_0+r} \frac{r^n}{\sqrt{r-(s-s_0)}} \frac{1}{\sqrt{rs}} e^{-i\frac{\omega M}{U\beta}(s+r)} \cos\left(\frac{2\omega}{U\beta}\sqrt{sr}\right) ds dr,$$

$$\bar{P}_n = \frac{1}{4\pi r_i^{n+\frac{1}{2}}} \int_{r_0}^{r_i} \int_0^{r-r_0} \frac{r^n}{\sqrt{(r-r_0)-s}} \frac{1}{\sqrt{rs}} e^{-i\frac{\omega M}{U\beta}(s+r)} \cos\left(\frac{2\omega}{U\beta}\sqrt{sr}\right) ds dr, \quad (n=0,1).$$

Eqs. (4.16a-b)

The notation is that of Fig. IV.4.

By suitable changes of variables, the double integrals defining \bar{I}_n and \bar{P}_n can be reduced to the single integrated series

$$\begin{aligned} \bar{I}_n = \bar{I}_n(\epsilon, \sigma, M) = & e^{-i\epsilon\sigma} \int_0^1 z^{2n} e^{-3i\epsilon z^2} \left\{ \frac{1}{2} J_0\left(\frac{4\epsilon}{M} z \sqrt{z^2 + \sigma}\right) J_0[\epsilon(z^2 + \sigma)] \right. \\ & + \sum_{m=1}^{\infty} (-1)^m J_{4m}\left(\frac{4\epsilon}{M} z \sqrt{z^2 + \sigma}\right) J_{2m}[\epsilon(z^2 + \sigma)] \\ & \left. + i \sum_{m=0}^{\infty} (-1)^m J_{4m+2}\left(\frac{4\epsilon}{M} z \sqrt{z^2 + \sigma}\right) J_{2m+1}[\epsilon(z^2 + \sigma)] \right\} dz \end{aligned}$$

Eq. (4.17a)

CONFIDENTIAL

$$\begin{aligned} \bar{P}_n = \bar{P}_n(\epsilon, \bar{\sigma}, M) = e^{i\epsilon\bar{\sigma}} \int_{\sqrt{\bar{\sigma}}}^1 z^{2n} e^{-3i\epsilon z^2} \left\{ \frac{1}{2} J_0\left(\frac{4\epsilon}{M} z \sqrt{z^2 - \bar{\sigma}}\right) J_0[\epsilon(z^2 - \bar{\sigma})] \right. \\ \left. + \sum_{m=1}^{\infty} (-1)^m J_{4m}\left(\frac{4\epsilon}{M} z \sqrt{z^2 - \bar{\sigma}}\right) J_{2m}[\epsilon(z^2 - \bar{\sigma})] \right. \\ \left. + i \sum_{m=0}^{\infty} (-1)^m J_{4m+2}\left(\frac{4\epsilon}{M} z \sqrt{z^2 - \bar{\sigma}}\right) J_{2m+1}[\epsilon(z^2 - \bar{\sigma})] \right\} dz \end{aligned}$$

Eq. (4.17b)

where

$$\epsilon = \frac{r_1}{2} \frac{\omega M}{U\beta}$$

$$\sigma = \frac{s_0}{r_1}, \quad \bar{\sigma} = \frac{r_0}{r_1}$$

Since J_p is the Bessel function of the first kind and order p .

$$J_0(0) = 1, \quad J_p(0) = 0 \quad \text{when } p \neq 0$$

Eqs. (4.17a-b) in conjunction with Eqs. (4.15a-b) confirm the expressions previously given for steady flow [Eqs. (4.8a-b)]. The infinite series of products of Bessel functions in the integrands are rapidly convergent for the frequency and Mach number ranges of interest, so that only a few terms need be retained. The integrations indicated by Eqs. (4.17a-b) must be carried out numerically. In this connection, it is worth noting that the integrands are functions of z^2 only. Moreover, for the Mach and characteristic grid systems (the only ones which permit introducing the singularity effect), σ is an integer or a rational fraction, and $\bar{\sigma}$ is a rational fraction less than unity. A suggested method for the evaluation of these integrals is given in Appendix A.

As an example to demonstrate that the inclusion of the side-edge downwash singularity is feasible and results in fairly accurate airload distributions, calculations have been carried out for a rectangular wing in rigid body translational

CONFIDENTIAL

CONFIDENTIAL

oscillation. Since the downwash is constant everywhere, the characteristic system can be used without encountering the problems caused by w -variation over a box. This system is chosen since it permits the satisfaction of the zero pressure condition at points along the side edge. In Figs. IV.9-IV.10, the aerodynamic derivatives (Ref. 13)

$$L_1 + iL_2 = \frac{\text{Lift/unit span}}{-4\rho U^2 k^2 h_0}$$

$$M_1' + iM_2' = \frac{\text{Moment about leading edge/unit span}}{-4\rho U^2 k^2 h_0 b}$$

are presented. These were calculated using four characteristic boxes along the chord of the rectangular wing at $k = 0.3$ and $M = 1.2$. The singular downwash was included in the diaphragm region, and the chordwise integrations were carried out by formulas like Eqs. (4.14a-b) to minimize errors associated with this step. All the symbols have been previously defined except the amplitude h_0 of the oscillation. The constant downwash amplitude is

$$\bar{w} = i\omega h_0.$$

Also on the figures are shown corresponding results computed by the more exact methods of Nelson, Rainey and Watkins (Ref. 13), which may be regarded as a rough standard of comparison. For the present combination of Mach number and frequency the unsteadiness parameter for supersonic flow is

$$\bar{\omega} = \frac{2kM^2}{M^2 - 1} = 1.963,$$

a value about as large as is allowable under the frequency-expansion technique of Ref. 13. The figures indicate that the Ref. 13 method gives values of L_1 , L_2 , M_1' , and M_2' in the two-dimensional region which are a few per cent off from the corresponding exact values according to Garrick and Rubinow (Ref. 36). Therefore, small percentage differences between the two sets of curves in these figures are not too significant. With this fact in mind, the lift and moment distributions by the box scheme can be regarded as quite satisfactory.

CONFIDENTIAL

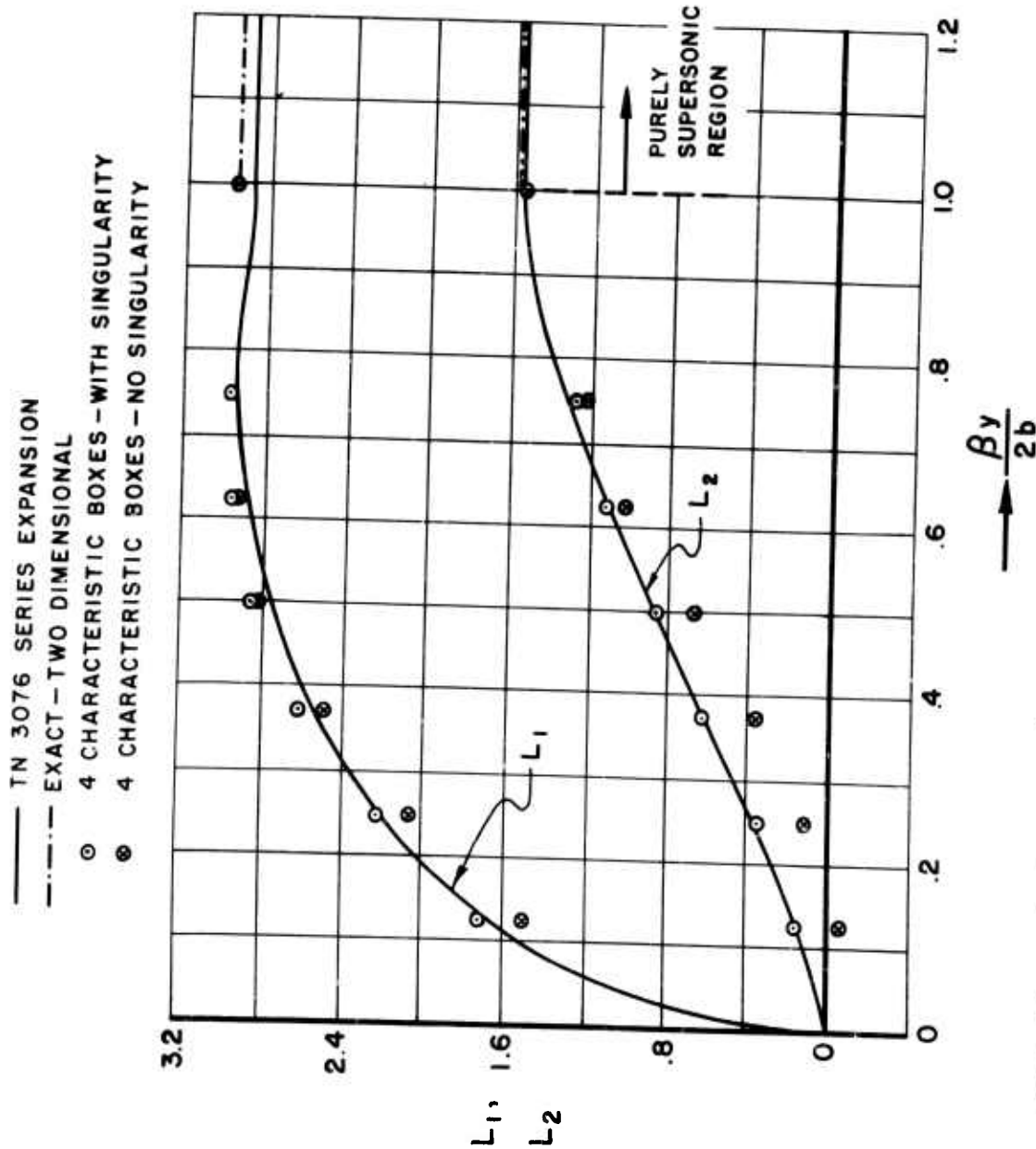


Fig. IV.9 Dimensionless Spanwise Lift Distribution on a Rectangular Wing in Translational Oscillation, as Calculated by the Methods Indicated on the Curves. ($A = 0.3$, $M = 1.2$)

CONFIDENTIAL

CONFIDENTIAL

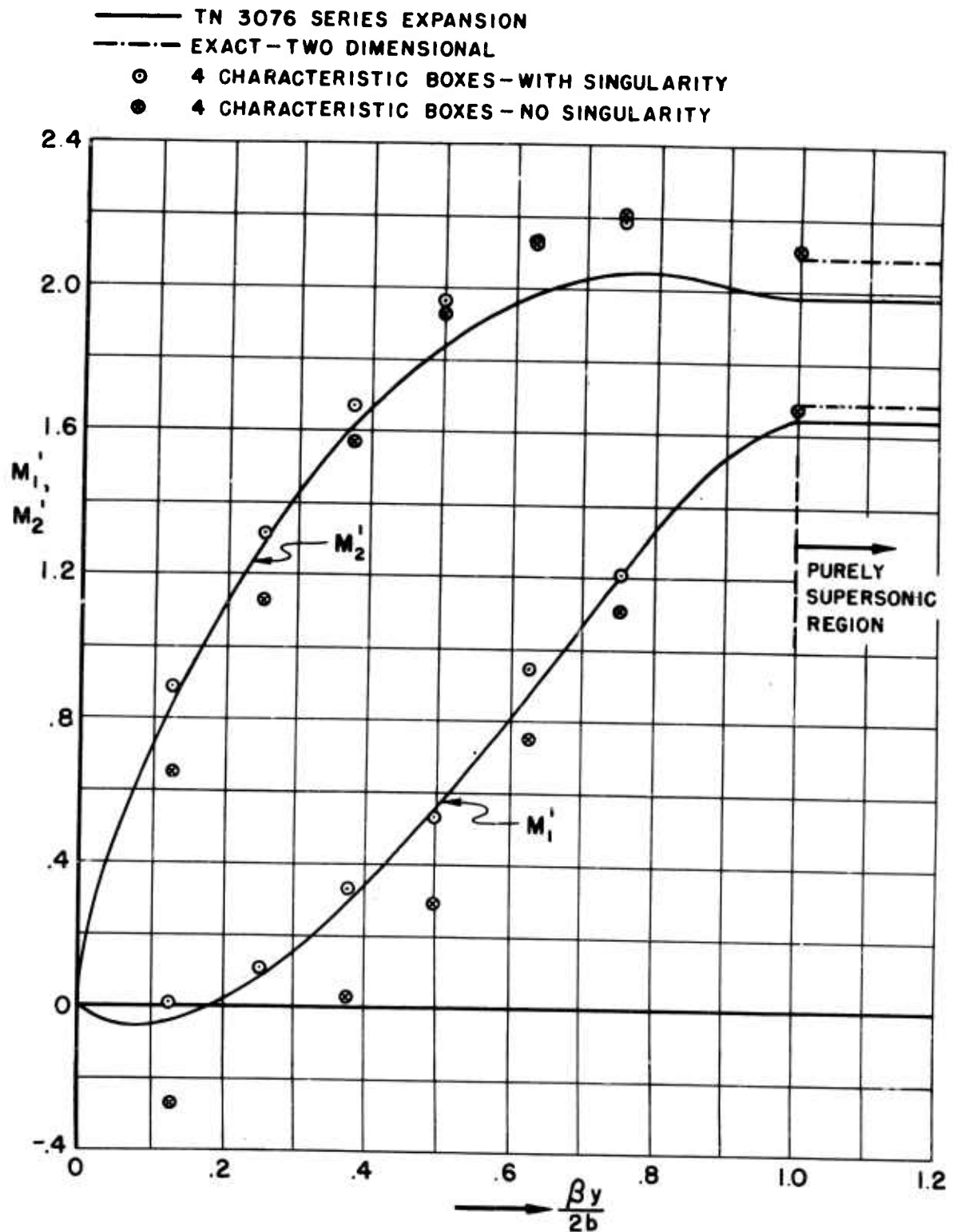


Fig. IV.10 Dimensionless Spanwise Moment Distribution on a Rectangular Wing in Translational Oscillation, as Calculated by the Methods Indicated on the Curves. ($k = 0.3$, $M = 1.2$)

WADC TR 56-97, Part 1

-83-

CONFIDENTIAL

CONFIDENTIAL

In the calculation above, only four chordwise boxes were used, yet accuracy sufficient for most purposes was obtained. By contrast, when the same number of boxes were used and the downwash singularity had not been accounted for, much poorer precision resulted.

Since individual pressures are not easily obtainable from the expressions of Ref. 13, the pressure was checked only at one point. For point 14, Fig. IV.2,

$$\begin{aligned} \frac{\Delta \bar{p}_{14}}{\left(\frac{2U}{\beta}\right) i \omega h_0} &= -0.307,60 + 0.116,41i && (\text{Ref. 13}) \\ &= -0.312,50 + 0.115,18i && (\text{Characteristic Boxes with Singularity in Downwash}). \end{aligned}$$

Although the technique of including the downwash singularity was shown to be feasible for unsteady flow, some question arises as to its practical value. In steady flow the AIC's associated with the singular distributions have such simple mathematical expressions [Eqs. (4.8a-b)] that Procedure (2) is no more difficult than Procedure (1). When the motion is unsteady, however, one must first tabulate the functions \bar{I}_n and \bar{P}_n [Eqs. (4.17a-b)], each of which depends on three variables. The scope of such a tabulation is not as great as it might seem at first glance for the following reasons:

- (1) Tables* need be prepared only for discrete values of σ and $\bar{\sigma}$. When a large number of chordwise boxes is taken, the ranges of σ and $\bar{\sigma}$ may become excessive. However, it will be shown below that the inclusion of the downwash singularity is no longer necessary when a great many boxes are used.
- (2) \bar{I}_n and \bar{P}_n are both smoothly varying functions of the frequency parameter ϵ . Therefore, it is not necessary to take a large number of ϵ -entries, because interpolation can be done accurately over large intervals.

Since tables are not as yet in existence, it is desirable to establish a lower limit on the number of chordwise boxes required near the side edge if Procedure (1) is to be employed. If Mach boxes (or square boxes for $M \geq \sqrt{2}$) are used, it can be shown (c.f., Figs. IV.6-IV.7) that the significant inaccuracies

*These tables are three-dimensional, whereas the tabulations for the usual AIC are four-dimensional.

CONFIDENTIAL

in the lift and moment distributions are confined to the first two or three stations near the side edge. The more boxes that are taken, the more these critical stations will be confined to a small portion of the total mixed region, and the lifts and moments will then be closer to their exact values. This is demonstrated by the points calculated by the ten-box analysis in Figs. IV.6-IV.7. There the total lifts and moments for the mixed region are expected to be sufficiently accurate. On the basis of this steady-state example, a minimum of ten chordwise boxes is believed to be required when using Procedure (1).

To substantiate this conclusion for unsteady motion, another numerical example has been carried out. The lift and moment distributions calculated with six and ten square boxes along the chord for a rectangular wing in rigid-body pitching oscillation about its mid-chord ($\theta=0.6$, $M=1.5$) are presented in Figs. IV.11-IV.12 and compared with corresponding three-dimensional values from Ref. 13 and two-dimensional values from Ref. 36. For this combination of Mach number and reduced frequency, the former can be regarded as a standard of reference.

It is seen that with ten square boxes, the AIC results are much improved over those obtained with six boxes. The total lifts and moments over the mixed region with ten boxes are acceptable, since the major discrepancies are confined to a limited area near the tip. If the contributions of the mixed regions to the airloads are small compared with those of the total wing, one might tolerate somewhat poorer accuracy in these regions and accept fewer than ten chordwise boxes. However, this can be done only for certain special planforms and motions. If the motion involves spanwise elastic deformations such that the deflections near the tip are large, which is often the case in flutter, the aerodynamic loads will be concentrated on the outboard sections. Maximum accuracy is then demanded in the mixed region, regardless of the aspect ratio. Therefore, the conservative and generally acceptable rule seems to be either to adopt at least ten boxes along the wing-tip chord or make special provisions to include the proper downwash singularity off this tip.

IV.3 The Subsonic Leading and Trailing Edge Problems

In the previous section a method was devised which included the effect of the downwash singularity at a side edge on the pressure distribution over a finite wing oscillating in supersonic flow. When a similar procedure is attempted for a

CONFIDENTIAL

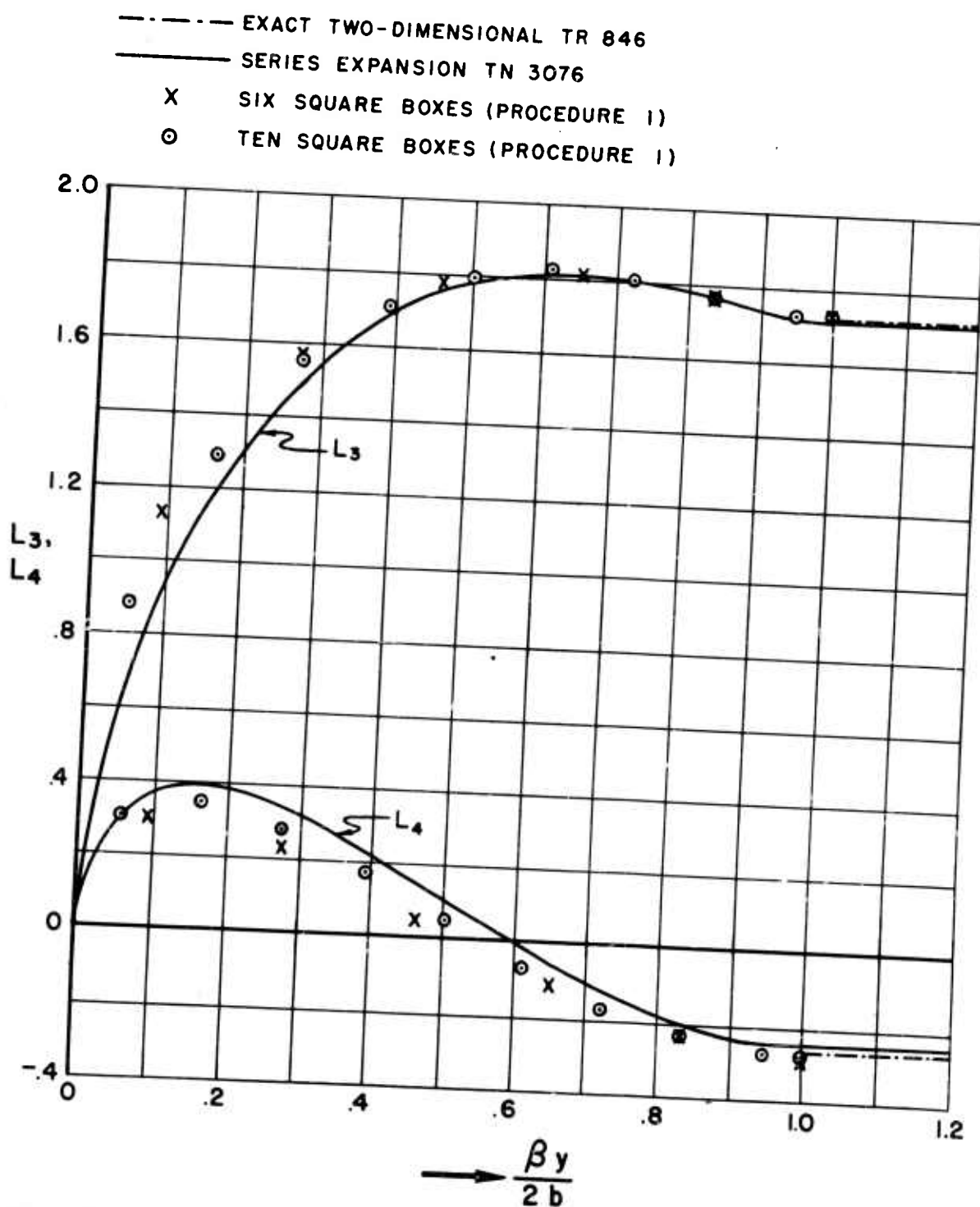


Fig. IV.11 Dimensionless Spanwise Lift Distribution on a Rectangular Wing in Pitching Oscillation About Its Mid-Chord Axis, as Calculated by the Indicated Methods. ($k=0.6, M=1.5$)

CONFIDENTIAL

CONFIDENTIAL

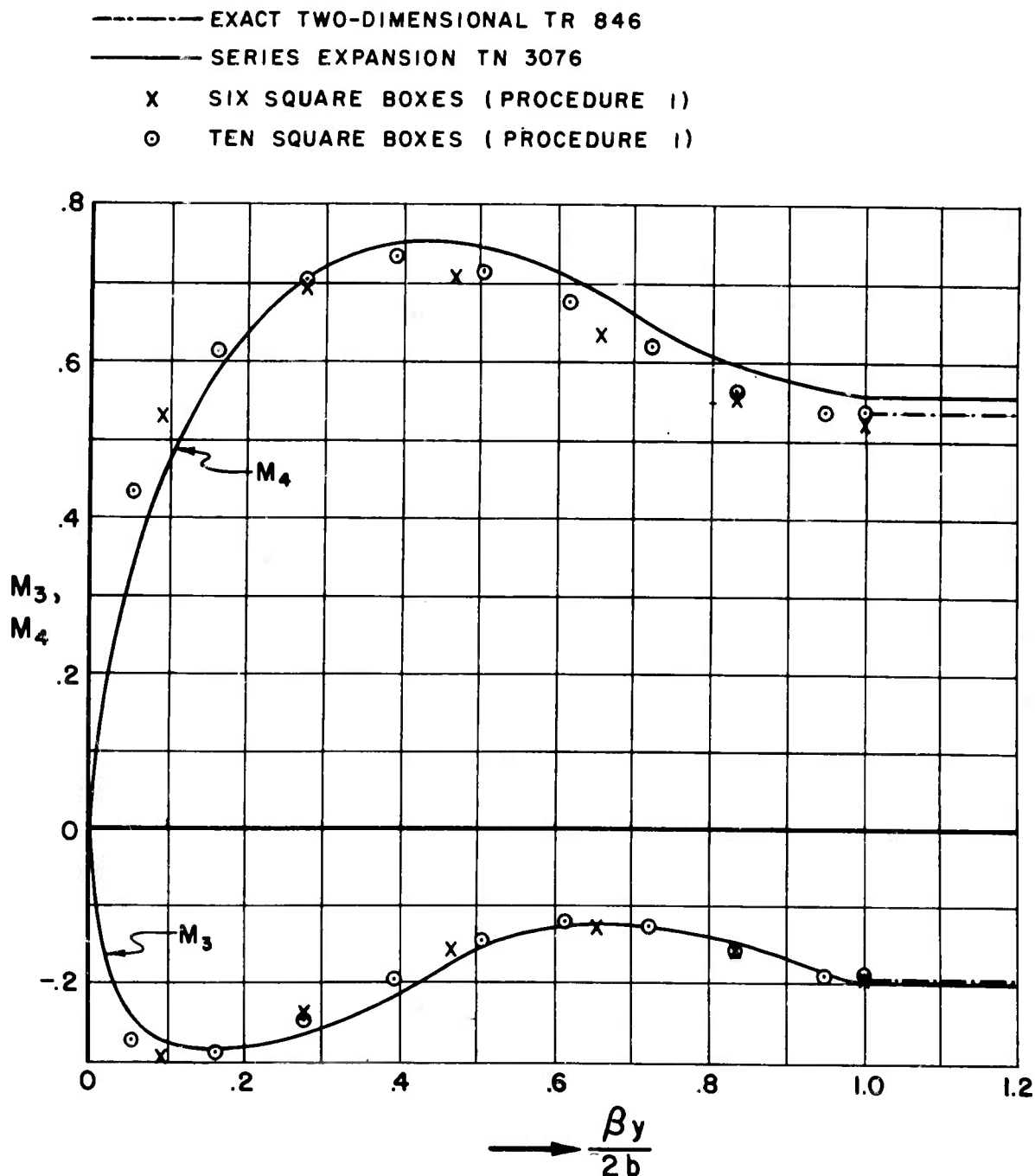


Fig. IV.12 Dimensionless Spanwise Distribution of Pitching Moment About the Mid-Chord of a Rectangular Wing in Pitching Oscillation About Its Mid-Chord Axis, as Calculated by the Indicated Methods. ($k=0.6$, $M=1.5$)

WADC TR 56-97, Part 1

-87-

CONFIDENTIAL

CONFIDENTIAL

subsonic edge which is not parallel to the flow, it leads to such complications that this approach is regarded as impractical if not impossible.

It was pointed out in Section III.1 that a swept leading edge must be represented by a broken line in order to avoid tabulating the AIC's for partial boxes. If this approximation is accepted, the question arises as to how one can represent singular downwash distributions near such edges. On the actual wing the axis of the singularity parallels the swept edge. To conform with the jagged edges in the box pattern, this axis must be adjusted so that it follows the step-like segments of the broken line. Practical difficulties are encountered, and there is no assurance that the distortion of the singular distribution will improve the results over what would be found by neglecting the singularity altogether.

Having established the unsuitability of the singularity scheme for subsonic edges other than side edges, the authors investigated another alternative, which consists of removing the singularity by analytical means and treating the remaining portion of the solution by the box method. This proved equally impractical. The downwash singularity at a point on the subsonic leading edge of a finite wing is determined by the motion of the portion of the wing inside the forward Mach lines emanating from this point. The influencing area may include a part of the trailing edge, if the latter is also subsonic. Hence, any analytical method for calculating this singularity in advance could be used just as well to find the entire load distribution and would supersede the AIC approach entirely.

The foregoing considerations led to the conclusion that, if AIC's are to be employed at all for wings of this type, they must be made to yield satisfactory accuracy without any special provisions of the type represented by Procedure (2) of the previous subsection.

As in the case of a side edge, it can be proved for other planforms that progressively increasing the number of boxes along the chord causes the results for the generalized forces to converge toward the exact values. To establish a lower limit on the number of boxes required to achieve satisfactory precision in the treatment of a subsonic leading edge problem, the following numerical example is first presented. A triangular or delta wing with sweep angle $\Lambda = \cot^{-1} 0.64$ is considered. The flow is at $M = \sqrt{2}$ ($\beta = 1$) and the wing is in steady motion at constant angle of attack α ($k = 0$, $w = U\alpha$). For this case, the exact theoretical airloads can be derived from the expressions for the velocity potential given by Watkins and Berman (Ref. 20).

CONFIDENTIAL

CONFIDENTIAL

$$\frac{\Delta p}{(2\rho U_\infty^2)} = -\frac{\cot \Lambda}{E(\sqrt{1-\cot^2 \Lambda}, \frac{\pi}{2})} \frac{1}{\sqrt{1-\left(\frac{y}{x \cot \Lambda}\right)^2}}$$

$$l(y) = \frac{\text{Lift/unit span}}{(2\rho U_\infty^2) 2b} = -\frac{\cot \Lambda}{E(\sqrt{1-\cot^2 \Lambda}, \frac{\pi}{2})} \sqrt{1-\left(\frac{y}{2b \cot \Lambda}\right)^2}$$

$$m(y) = \frac{\text{Moment/unit span}}{(2\rho U_\infty^2)(2b^2)} = -\frac{\cot \Lambda}{E(\sqrt{1-\cot^2 \Lambda}, \frac{\pi}{2})} \cdot$$

$$\cdot \left\{ \sqrt{1-\left(\frac{y}{2b \cot \Lambda}\right)^2} + \left(\frac{y}{2b \cot \Lambda}\right)^2 \cosh^{-1} \frac{2b \cot \Lambda}{y} \right\}$$

Eqs. (4.18a-c)

Here E is the complete elliptic integral of the second kind, the coordinates x, y are those of Fig. IV.13, and the pitching moment is about the y -axis; $\cot \Lambda / E = 0.490, 94$. By spanwise integrations of Eqs. (4.18a-c), one obtains for the dimensionless total lift and total moment

$$L = \frac{\text{Lift}}{(2\rho U_\infty^2)(2b^2)} = -\frac{\pi \cot^2 \Lambda}{E} = -0.987, 09$$

Eqs. (4.19a-b)

$$M = \frac{\text{Moment}}{(2\rho U_\infty^2)(2b^3)} = -\frac{4}{3} \frac{\pi \cot^2 \Lambda}{E} = -1.316, 11$$

The figure illustrates the pattern of Mach boxes adopted for the AIC calculation. At this particular Mach number, incidentally, Mach and square boxes are identical.

In each box of Fig. IV.13 two values for the pressure are given, the upper being that calculated by the box scheme and the lower from the exact formula [Eq. (4.18a)]. It is seen that the individual pressures given by the numerical method

CONFIDENTIAL

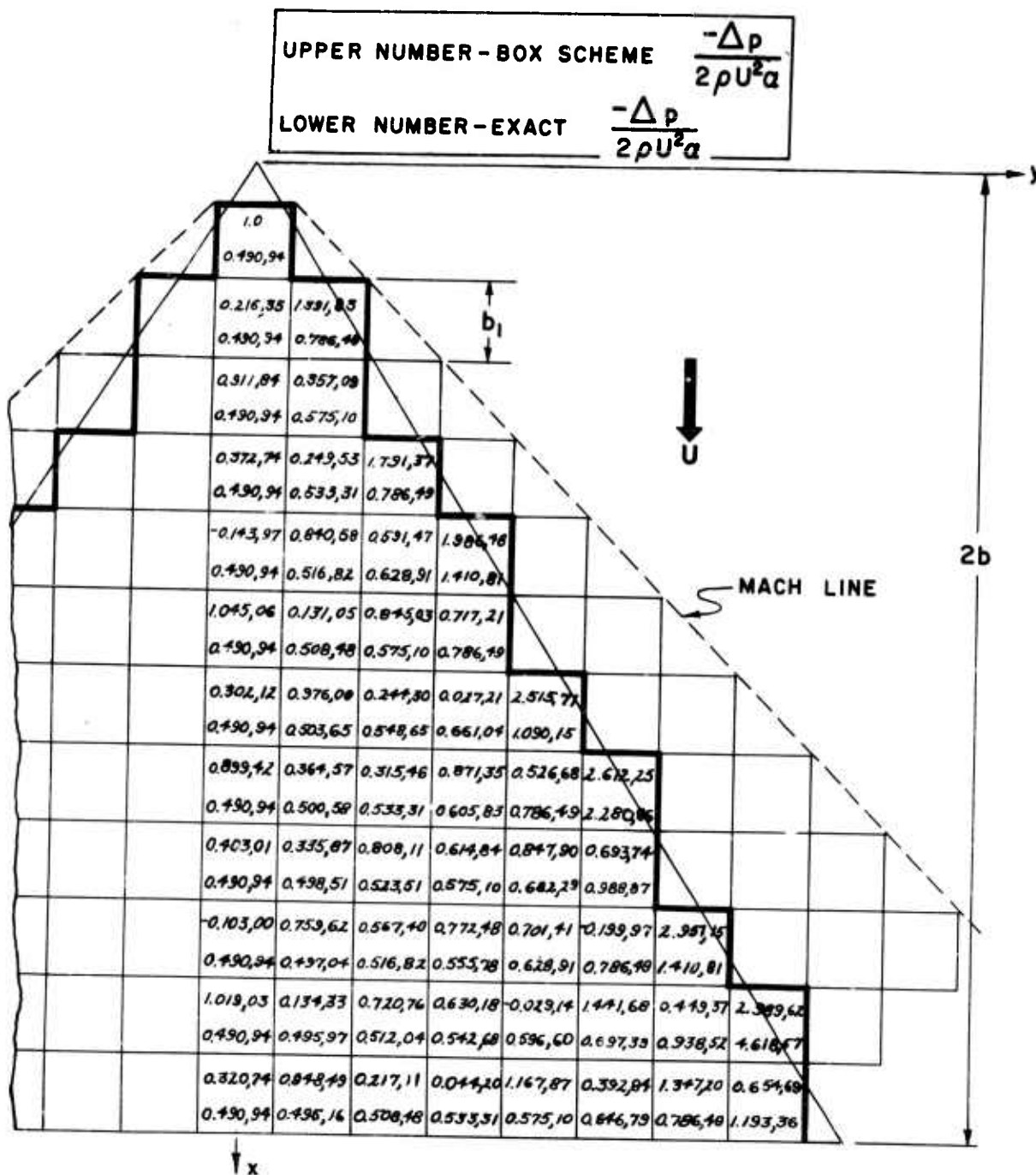


Fig. IV.13 Dimensionless Pressure Distribution on a Triangular Wing at Constant Angle of Attack.
($k=0$, $\cot \Lambda = 0.64$, $M = \sqrt{2}$)

CONFIDENTIAL

CONFIDENTIAL

fluctuate considerably in the stream direction. A similar phenomenon was observed in connection with a swept supersonic edge (see Section III.1), although there it was much less severe. Despite these fluctuations, the spanwise lift and moment distributions follow the trends of the exact curves (Figs. IV.14-15) rather well. There is marked improvement when one goes to twelve chordwise boxes at midspan in place of six. The results for the lift appear somewhat better than those for the moment.

Spanwise integrations to obtain total lift and total moment seem once more to average out the deviations, so that better accuracies are achieved for these resultant airloads than for the spanwise distributions. Table IV.4 shows the behavior of the calculated values for these two generalized forces as one takes more and more chordwise boxes.* The following points can be made regarding the rate of convergence toward the exact results:

- (1) The convergence is not uniform but proceeds in cycles. It happens in this example that the error increases gradually and then suddenly jumps to a smaller value, this phenomenon repeating each time the number of boxes is increased by three. The only rational way of estimating convergence is to examine the maximum deviations of successive cycles.
- (2) The convergence based on successive cycles is slow. Therefore, many more than twelve boxes would have to be taken to achieve a significant reduction of the 8-10 % errors characteristic of the lower portion of Table IV.4.
- (3) Practical considerations of manageable computations rule out any increase far beyond twelve boxes, since the labor grows at least in proportion to the square of this number. It is therefore tentatively concluded that twelve boxes along the midspan chord affords an acceptable compromise between accuracy and computational labor. Two additional examples of triangular wings with subsonic leading edges in unsteady motion are presented in Section V. It is seen

*In all these cases, the box sizes are adjusted so that the sum of the areas of the complete boxes which replace the planform is exactly equal to the area of the wing. Since the chordwise pressures fluctuate, the rectangular rule has been used for all numerical integrations.

CONFIDENTIAL

CONFIDENTIAL

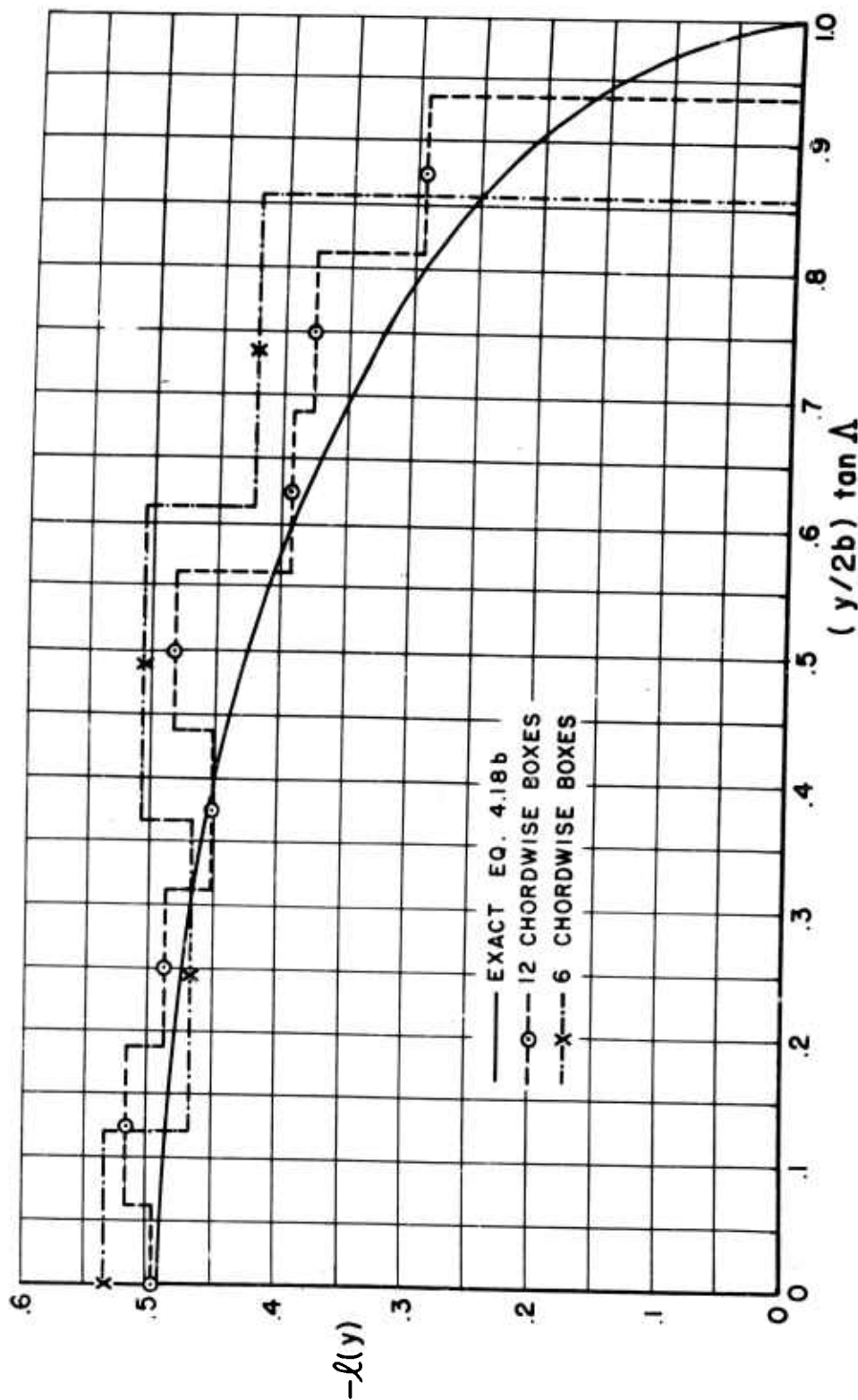


Fig. IV.14 Spanwise Lift Distribution on a Triangular Wing at Constant Angle of Attack as Calculated by the Methods Indicated on the Curves.
($\alpha = 0$, $\cot \Delta = 0.64$, $M = \sqrt{2}$)

CONFIDENTIAL

CONFIDENTIAL

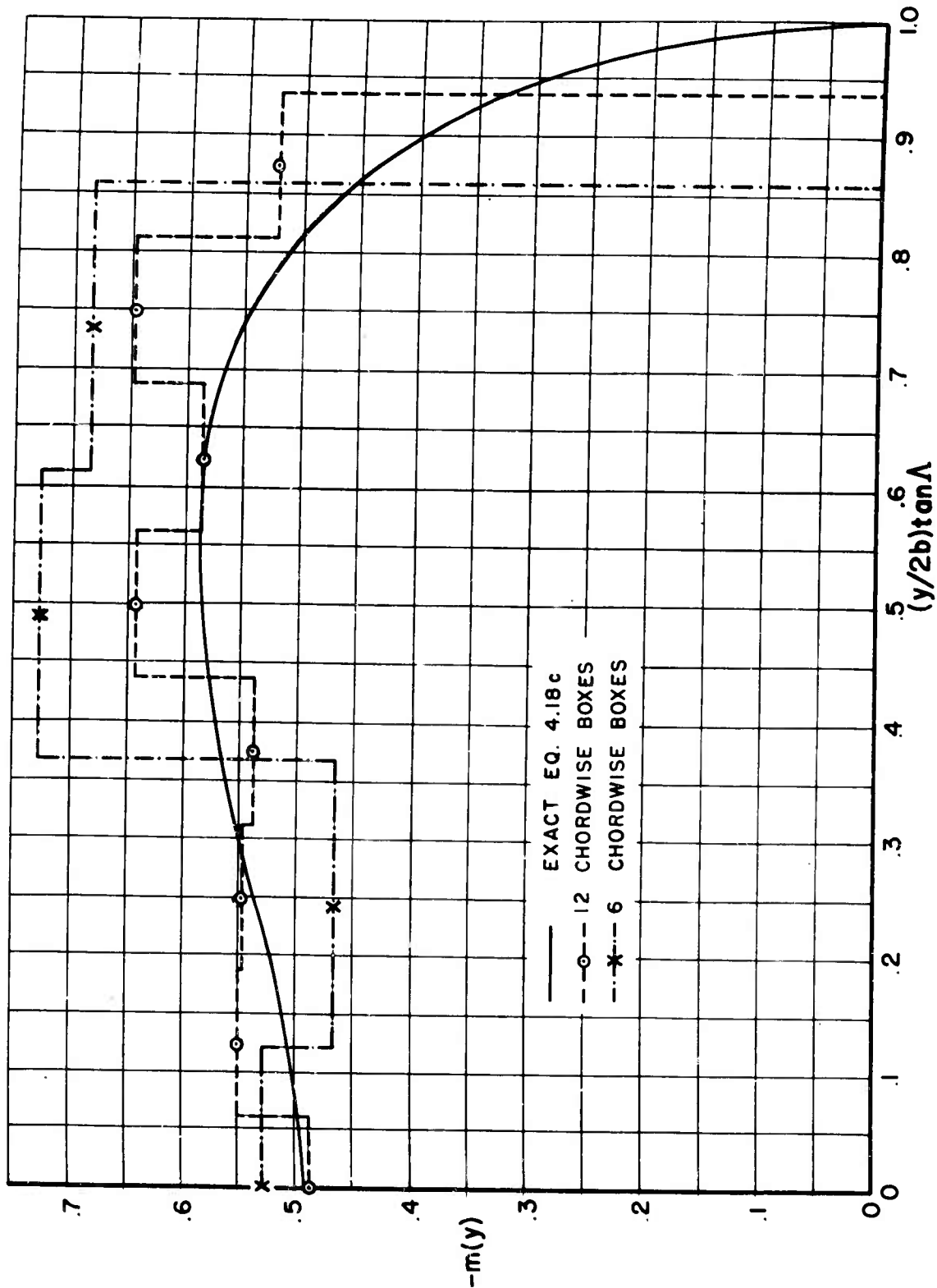


Fig. IV.15 Spanwise Pitching Moment Distribution on a Triangular Wing at Constant Angle of Attack as Calculated by the Methods Indicated on the Curves.
($k=0$, $\cot \Lambda = 0.64$, $M = \sqrt{2}$)

CONFIDENTIAL

CONFIDENTIAL

Number of Chordwise Boxes at the Midspan Station	L	M
1	-1.28	-1.536
2	-1.28	-1.792
3	-1.028,75	-1.193,55
4	-1.075,26	-1.378,69
5	-1.130,02	-1.540,59
6	-1.043,96	-1.345,13
7	-1.061,81	-1.399,60
8	-1.093,96	-1.483,04
9	-1.040,12	-1.365,48
10	-1.048,12	-1.389,83
11	-1.069,35	-1.443,09
12	-1.035,23	-1.369,79
Exact [Eqs. (4.19a-b)]	-0.987,09	-1.316,11

Table IV.4. Total Lifts and Moments on a Triangular Wing at Constant Angle of Attack in Steady Flow, Calculated by the AIC Method with an Increasing Number of Chordwise Boxes. ($\cot A = 0.64$, $M = \sqrt{2}$)

CONFIDENTIAL

CONFIDENTIAL

there that six or eight boxes along the midspan chord, which proved sufficient for purely supersonic planforms, are inadequate when subsonic edges are present. If large-scale digital facilities are available and costs do not have to be held down, the requirement of higher accuracy in particular cases may increase the tentative minimum by a substantial amount. The experience of the authors to date, however, does not permit any quantitative estimation of the probable error associated with any given number of boxes.

Originally it was believed that one could alleviate the errors in calculations like the foregoing (wings with supersonic trailing edges and subsonic leading edges) by making use of the reverse-flow theorem. After reversing the flow, it is a case of dealing with a planform with subsonic trailing edges and supersonic leading edges, and thus eliminating regions of pressure singularity. It will be demonstrated that this artifice is unsuccessful. The identities implied by the reverse-flow theorem (Ref. 17) for the total lift and total moment on a wing at constant angle of attack in steady flow can be written

$$\begin{aligned} L &= \iint_{\underline{S}} p_1 \cdot 1 \, dx \, dy = \iint_{\underline{S}} p_2 \cdot \alpha \, dx \, dy \\ M &= 2b \iint_{\underline{S}} p_1 \cdot \left(\frac{x}{2b}\right) \, dx \, dy = 2b \iint_{\underline{S}} p_3 \alpha \, dx \, dy \end{aligned} \quad \text{Eqs. (4.20a-b)}$$

Here \underline{S} and \underline{S} are the regions of integration over the planform in forward and reversed flows, respectively; p_1 is the pressure due to a downwash α in forward flow, p_2 is due to a downwash $1 \cdot U$ and p_3 is due to a downwash $(x/2b) \cdot U$ in reverse flow. If the assumption of constant downwash over each diaphragm box near a subsonic trailing edge were less critical than the same assumption near a subsonic leading edge, then the reverse-flow approach would improve the accuracies of the total generalized forces. However, if one considers the triangular wing and solves the same problem in forward and reversed flows, one obtains identical results.* This indicates that, as far as *It is not obvious that the two configurations should yield the same results, even though Eqs. (4.20a-b) are exact expressions from linearized theory, since solutions by the box scheme for both flow directions are approximations.

CONFIDENTIAL

the generalized force estimations by the AIC method are concerned, the inherent errors introduced in the treatment of subsonic trailing edges are just as large as those from subsonic leading edges.

If one admits that a minimum of eight boxes along the root-chord is required for purely supersonic planforms and twelve boxes for planforms with subsonic leading edges, it is reasonable to extrapolate and set a minimum of sixteen such boxes for planforms with both subsonic leading and trailing edges. No calculations on examples of this sort have yet been made.

CONFIDENTIAL

CONFIDENTIAL

SECTION V

SUPPLEMENTARY NUMERICAL EXAMPLES

Certain additional examples of the application of the AIC method to oscillating delta wings are included in this section. Three of the cases involve the use of square boxes at $M=1.5$; the fourth illustrates the Mach-box scheme at $M=1.2$, which is regarded as just about the lower practical limit of linearized supersonic theory. These examples were worked out in the course of investigating various difficulties associated with numerical methods, and for the sake of clarity were left out from previous Sections. The reader will recognize from accompanying discussion, however, that each result tends to substantiate one or more of the conclusions and rules stated in foregoing sections.

V.1 Purely Supersonic Planforms

Case 1: The spanwise lift and pitching moment distributions are given in Figs. V.1-V.2 for a triangular wing with leading edge swept back forty-five degrees flying steadily at $M=1.5$ and constant angle of attack. Three, six and eight square boxes were employed in the computations. All these airload distributions are remarkably close to the exact ones, which also appear on the figures. One obtains even more accurate estimates for the total lift and total pitching moment because of the averaging effect of the spanwise integrations. Although in this particular case few boxes yield excellent results, the same cannot be said for other purely supersonic planforms undergoing elastic deformations at high frequencies, as shown in Section III.

Case 2: The same wing as Case (1) is considered to perform parabolic bending oscillations at $R=0.51$, this motion being described by $z = \bar{r}_0 (y/2b)^2 e^{i\omega t}$, where \bar{r}_0 is the tip amplitude. With eight chordwise boxes at the root, one obtains excellent estimates for the total lift and pitching moment about the apex, as shown by the following comparison with the corresponding quantities from the exact theory of Ref. (17):

CONFIDENTIAL

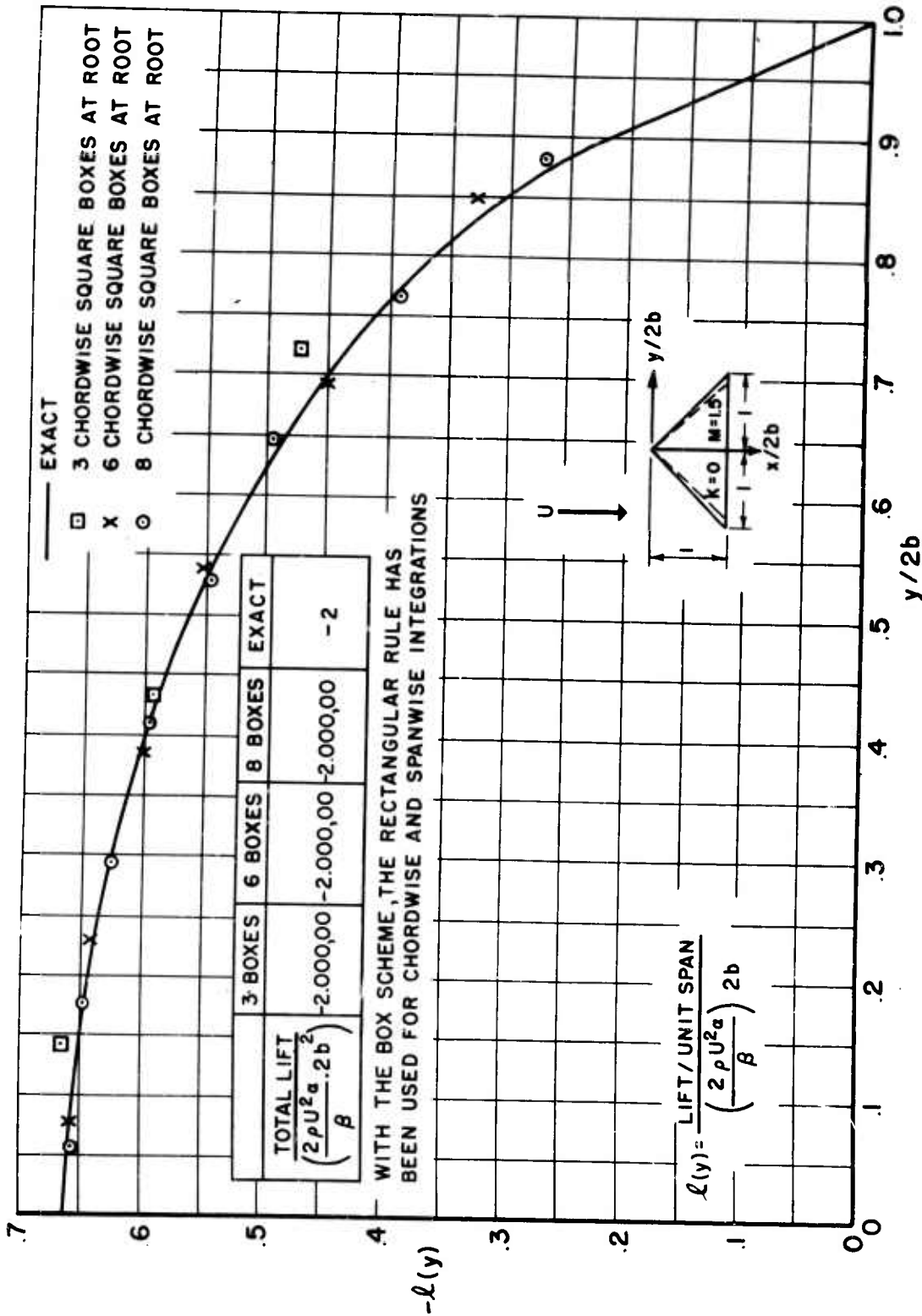


Fig. V.1 Spanwise Lift Distribution for a Triangular Wing at Constant Angle of Attack in Steady Flow. ($\Delta = 45^\circ$, $M = 1.5$)

CONFIDENTIAL

CONFIDENTIAL

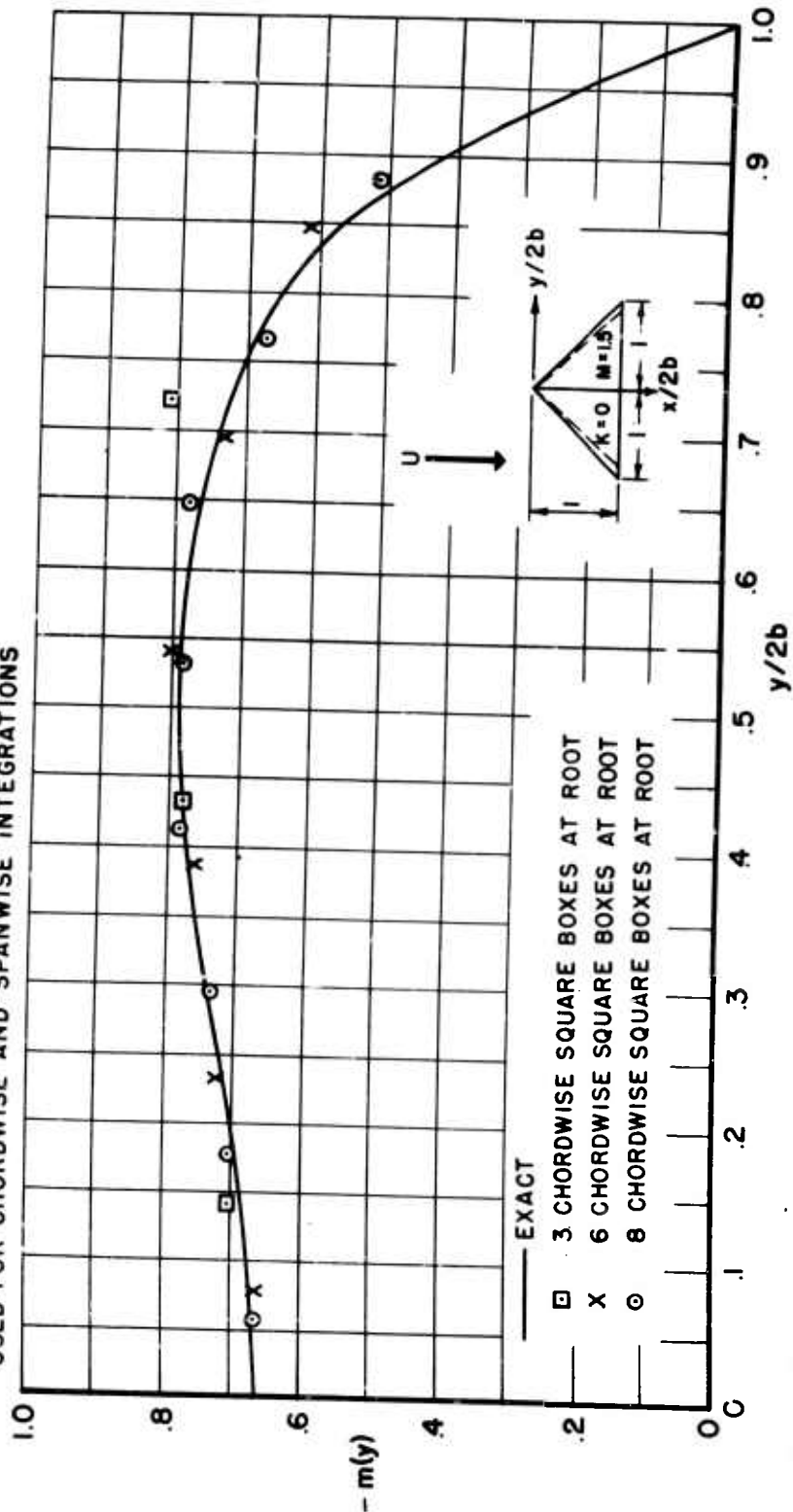
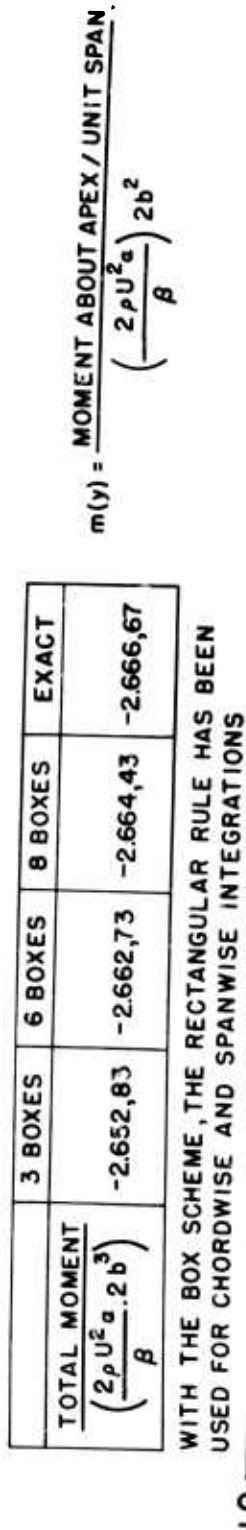


Fig. V.2 Spanwise Distribution of Pitching Moment About an Axis Through the Apex of a Triangular Wing at Constant Angle of Attack in Steady Flow. ($\alpha = 45^\circ$, $M = 1.5$)

CONFIDENTIAL

CONFIDENTIAL

$$\frac{\text{Total Lift}}{\left(\frac{25U^2}{\beta}\right) 2b \bar{h}_0} = -0.023,09 - 0.158,831 \quad \text{Exact}$$

$$= -0.023,21 - 0.158,911 \quad \text{Box Method}$$

$$\frac{\text{Total Moment}}{\left(\frac{25U^2}{\beta}\right) 2b^2 \bar{h}_0} = -0.038,06 - 0.252,951 \quad \text{Exact}$$

$$= -0.038,17 - 0.251,201 \quad \text{Box Method}$$

Both of the foregoing cases may be said to add further substantiation to the qualitative rule that eight boxes should be taken along the midspan chord of a wing with supersonic edges.

V.2 Planforms with Subsonic Edges

Case 3: Spanwise lift and pitching moment distributions are given in Figs. V.3-V.6 for a triangular wing with leading edge swept back sixty degrees performing rigid-body translation and pitching oscillations about the root mid-chord axis at $\alpha = 0.2$ and $M = 1.5$. Eight square boxes were employed along the midspan chordline. It is evident that appreciable discrepancies exist between the airloads from the AIC scheme and the more exact results of Ref. 20, especially for the moment distributions. Although the total lifts and moments turn out to be somewhat better because of the averaging effects of the spanwise integrations, one cannot obtain the same order of accuracy as with a purely supersonic planform overlaid with the same number of boxes. Experience has indicated that taking twelve boxes rather than eight along the midspan chord yields sufficient increase in precision to warrant the additional computational labor. This improvement may be expected to become even more significant for planforms undergoing elastic deformations. Further enlarging the number of boxes beyond twelve does not seem to be justifiable, however.

CONFIDENTIAL

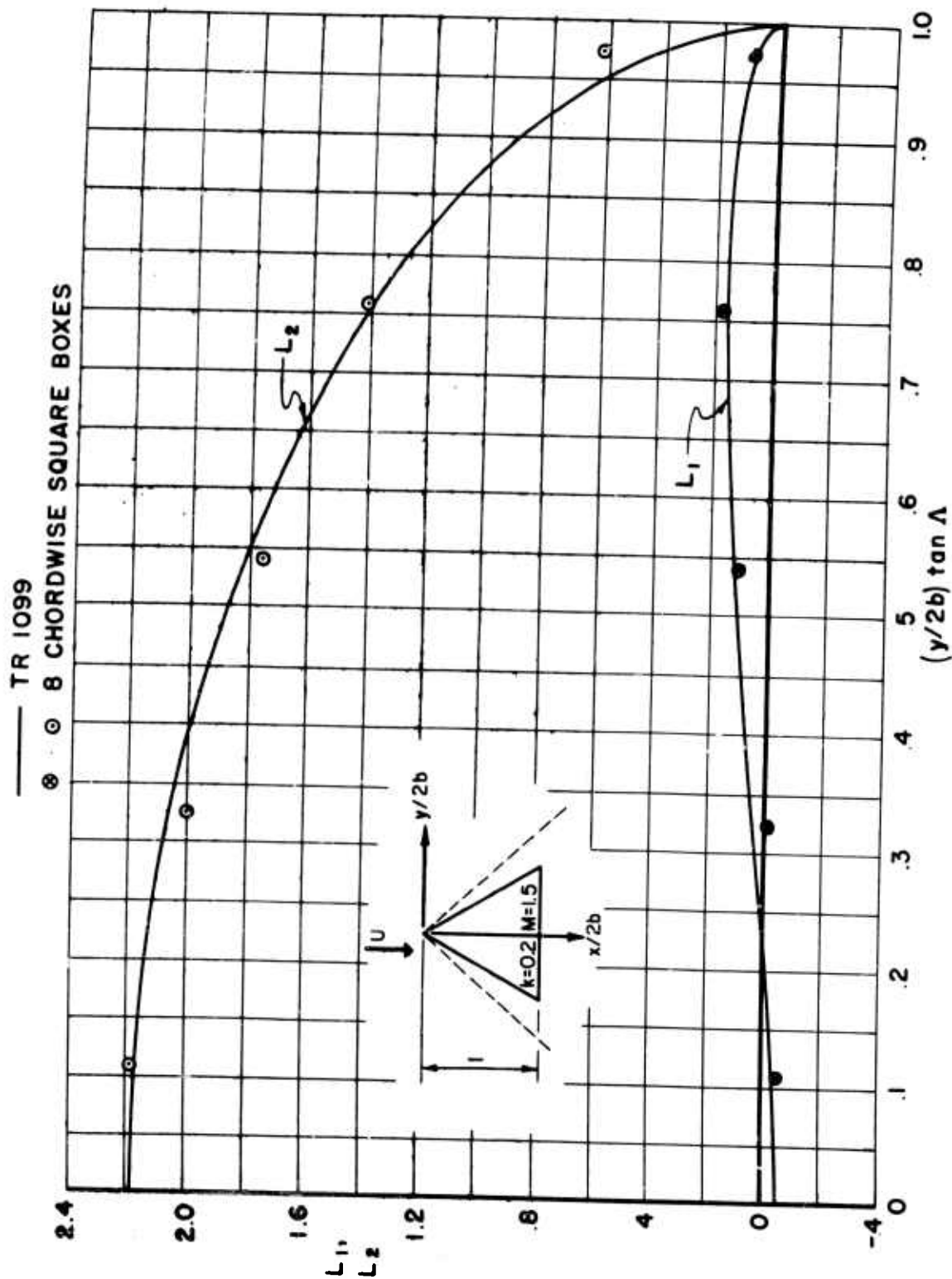


Fig. V.3 Spanwise Lift Distribution for a Triangular Wing in Uniform Translational Motion. ($k=0.2$, $\Lambda=60^\circ$, $M=1.5$)

CONFIDENTIAL

CONFIDENTIAL

TR 1099

8 CHORDWISE SQUARE BOXES

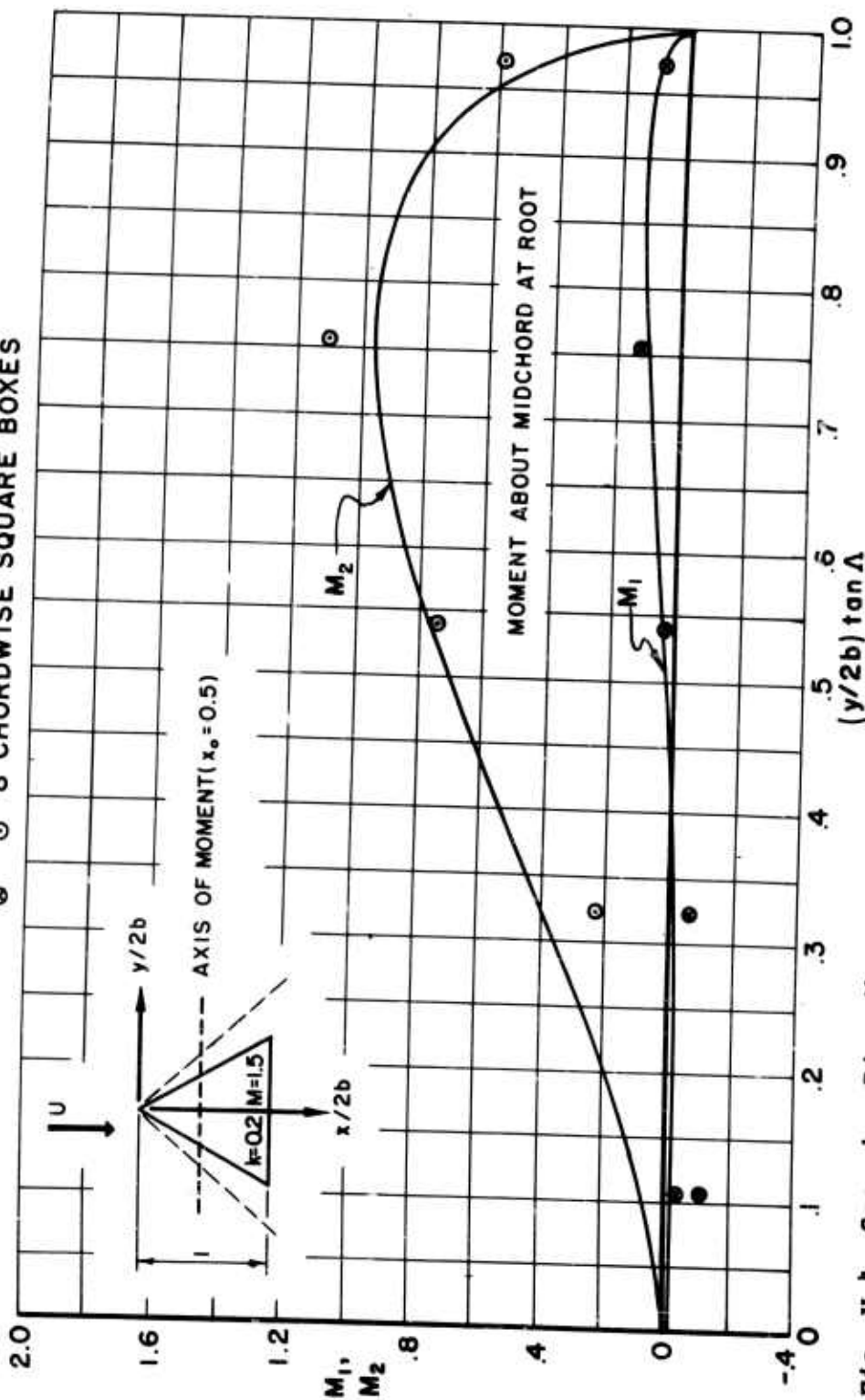


Fig. V.4 Spanwise Distribution of Pitching Moment About an Axis Through the Root Mid-Chord of a Triangular Wing in Uniform Translational Motion. ($k=0.2$, $\Delta=60^\circ$, $M=1.5$)

CONFIDENTIAL

CONFIDENTIAL

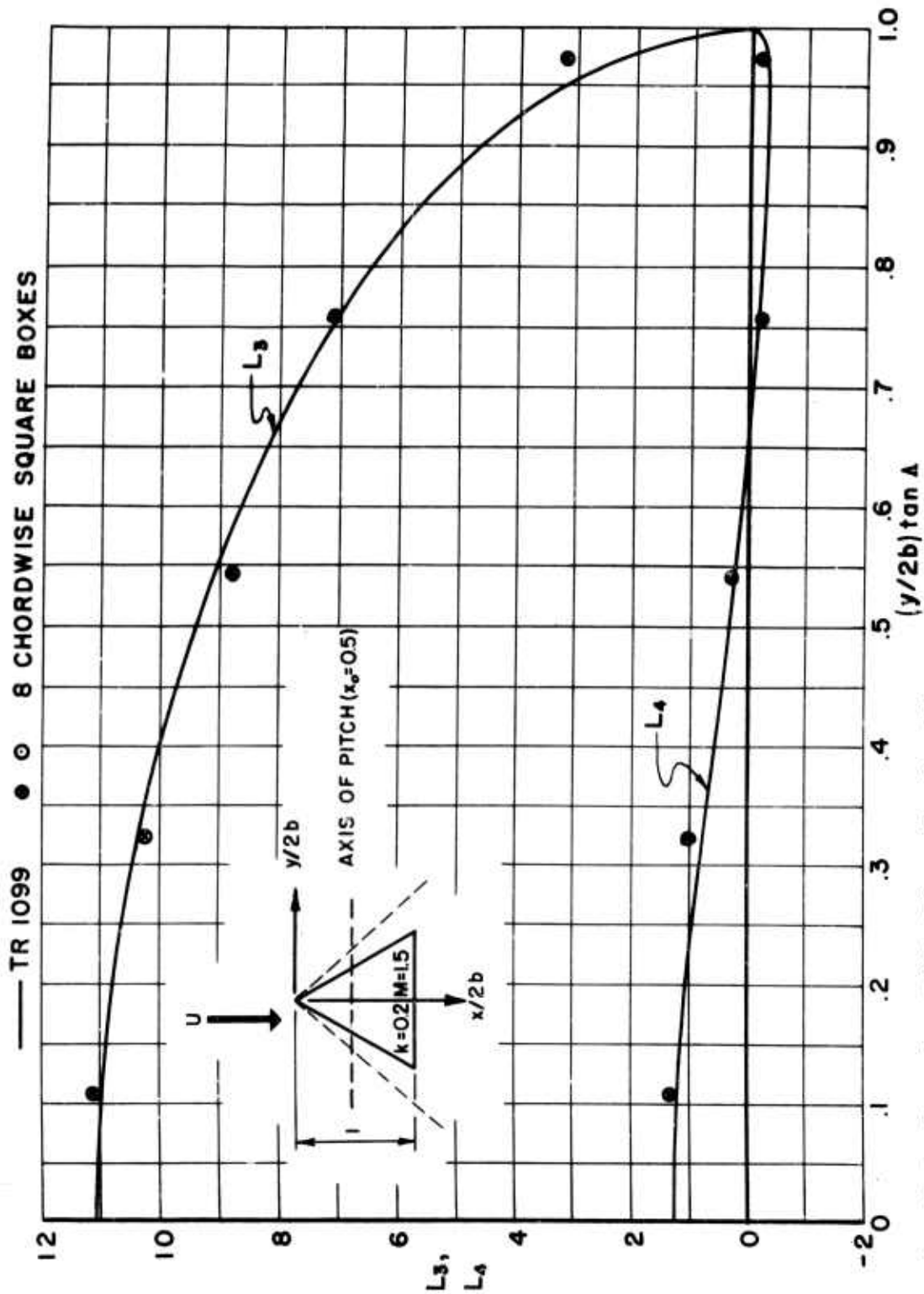


Fig. V.5 Spanwise Lift Distribution for a Triangular Wing in Uniform Pitching Motion About an Axis Through the Root Mid-Chord. ($k=0.2$, $\Delta=60^\circ$, $M=1.5$)

CONFIDENTIAL

CONFIDENTIAL

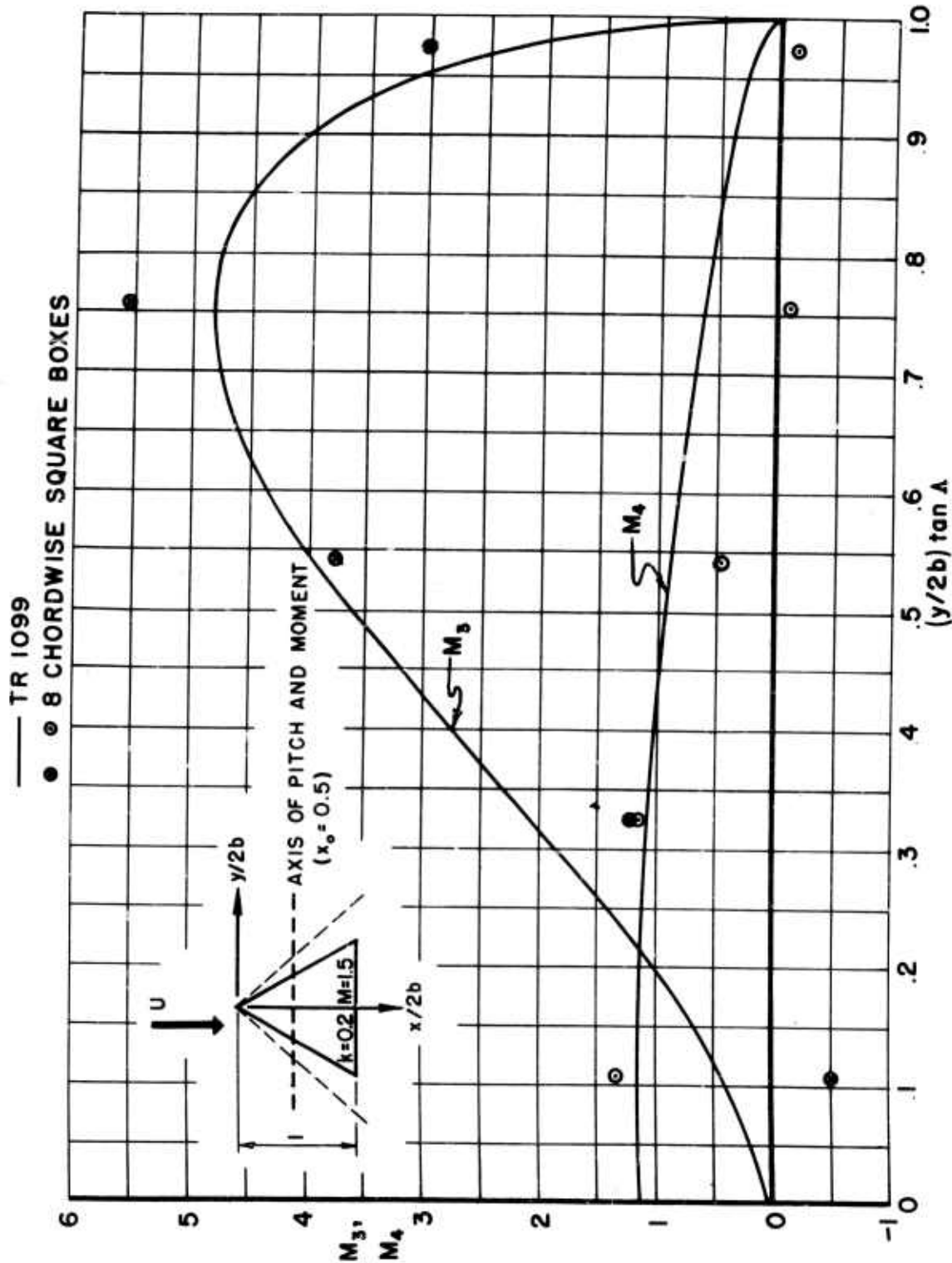


Fig. V.6 Spanwise Pitching Moment Distribution for a Triangular Wing in Uniform Pitching Motion About an Axis Through the Root Mid-Chord. ($k=0.2, \Delta=60^\circ, M=1.5$)

CONFIDENTIAL

CONFIDENTIAL

Case 4: The spanwise lift and moment distributions are given in Figs. V.7-V.8 for a triangular wing with leading edge swept back forty-five degrees, at $\delta = 0.1$, and $M = 1.2$, executing a spanwise parabolic bending oscillation. Six chordwise Mach boxes were employed in the calculation. The accuracies obtained for these airload distributions are seen to be rather poor. As in the previous case, one must apparently resort to the order of twelve chordwise boxes at the root if one is to get reasonable approximations for the airloads.

CONFIDENTIAL

CONFIDENTIAL

— TN 3009

• 6 CHORDWISE MACH BOXES

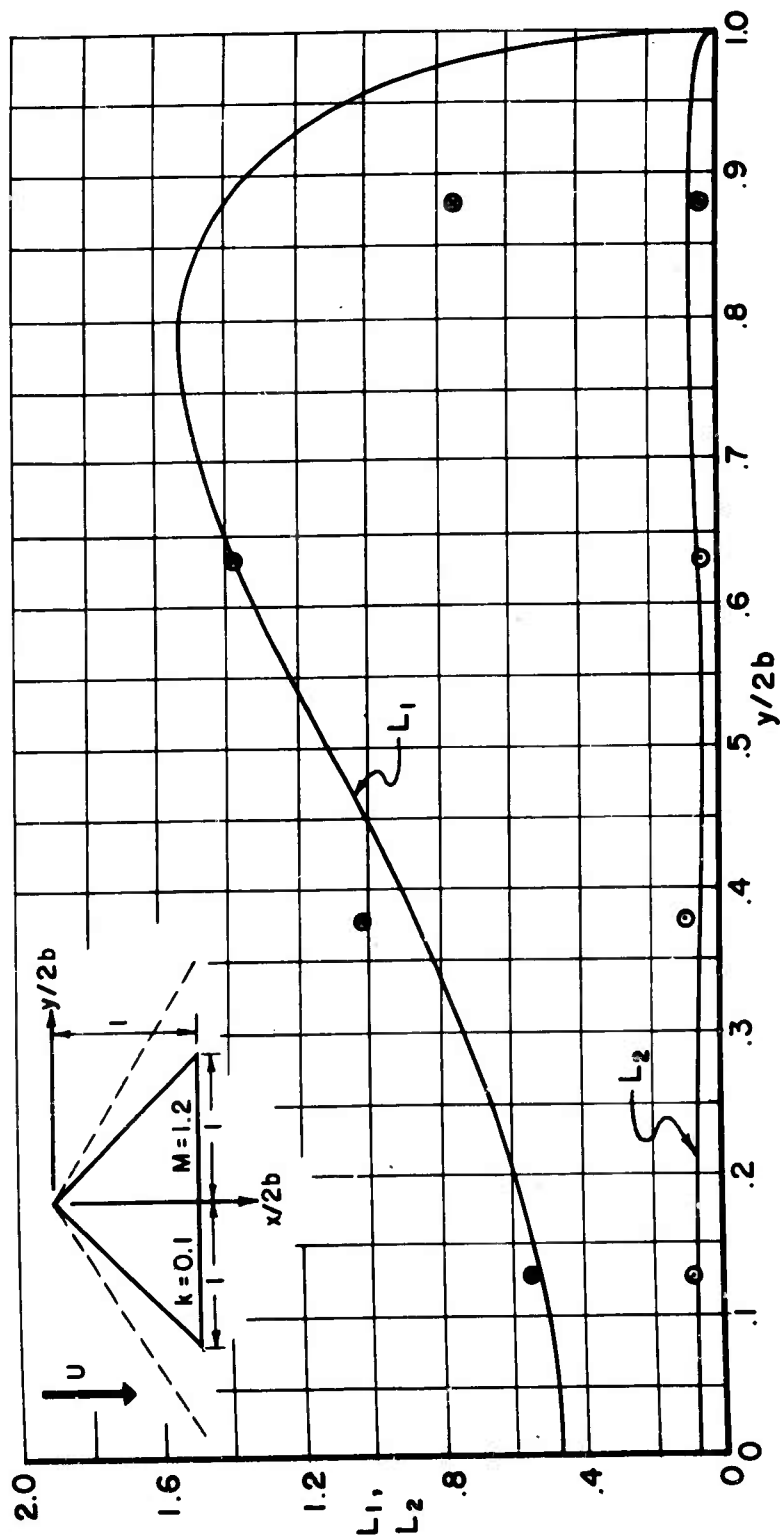


Fig. V.7 Spanwise Lift Distribution for a Triangular Wing in Parabolic Translational Motion. ($k=0.1$, $M=1.2$)

CONFIDENTIAL

CONFIDENTIAL

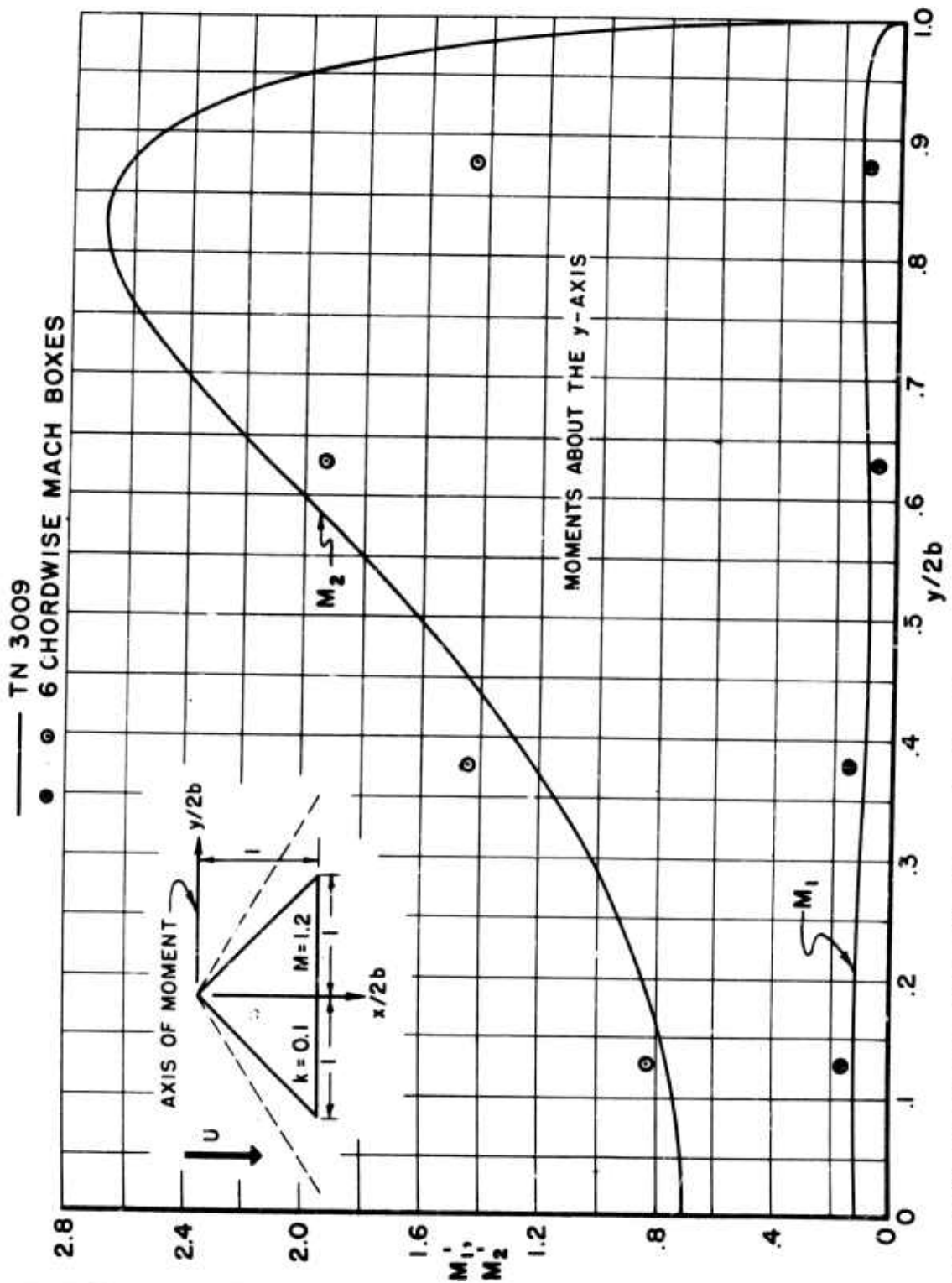


Fig. V.8 Spanwise Distribution of Pitching Moment About an Axis Through the Apex of a Triangular Wing in Parabolic Translational Motion. ($k=0.1$, $\lambda=45^\circ$, $M=1.2$)

CONFIDENTIAL

CONFIDENTIAL

SECTION VI

ALTERNATIVE NUMERICAL APPROACHES

The numerical method which forms the principal topic of the present report is based on the concept of the direct aerodynamic pressure influence coefficient, which gives pressure at a point due to an influencing elementary area with a prescribed downwash. Two other types of influence coefficients have been proposed and were studied to some extent by M.I.T.:

- (1) The inverse pressure influence coefficient, which gives the downwash at a point due to a prescribed pressure distribution over an influencing elementary area. This has the very desirable feature that it avoids consideration of the diaphragm region, where the pressure is everywhere zero, in cases of wings with subsonic edges. It forms the basis of numerical methods in unsteady, three-dimensional subsonic flow (Refs. 28, 41), where the direct AIC cannot readily be calculated.
- (2) The lift influence coefficient, which represents the total lift acting on an elementary area due to a prescribed downwash over another elementary area. This coefficient has been found to lead to complications (e.g., two additional integrations must be performed) and affords no special advantage over the originally proposed AIC. Therefore, for the sake of brevity, numerical investigations based on this type of influence coefficient are not reported here.

It will now be demonstrated that the inverse pressure coefficient, which seems quite promising at first, can be used with no difficulty for steady-state analyses. For unsteady motion, however, the required tabulations become so complex as to render this method quite impractical.

VI.1 The Inverse Pressure Influence Coefficient

In a recent publication Voss and the present authors (Ref. 28) outline a procedure for determining the airloads on an oscillating elastic wing in subsonic flow at low values of the frequency by the method of the inverse pressure influence

CONFIDENTIAL

CONFIDENTIAL

coefficients. It consists of obtaining expressions for the downwash at specified points on the wing in terms of the pressures at the same set of points. Since downwashes are the quantities usually known in advance, the resulting sets of simultaneous equations must be solved for the unknown pressures. In the subsonic range this indirect process is necessary because, for the general case, no simple expression exists that yields the pressure in terms of the downwash (i.e., no simple inversion of the integral equation has been found). In supersonic flow, however, the usual form of the integral equation gives the pressure directly in terms of a surface integral of the weighted downwash [as in Eq. (2.3)].

$$\bar{p} = \iint_S \bar{w}(\xi, \eta) F(x-\xi, y-\eta) d\xi d\eta \quad \text{Eq. (6.1)}$$

where F is the appropriate kernel. Equation (6.1) can be inverted to yield an expression which represents the downwash in terms of a surface integral of the weighted pressure distribution,

$$\bar{w} = \iint_S \bar{p}(\xi, \eta) K(x-\xi, y-\eta) d\xi d\eta \quad \text{Eq. (6.2)}$$

where K is the so-called "inverse" kernel.

One advantage of the latter form is that the diaphragm representation of disturbed areas near subsonic edges need not be considered, since in such regions the pressures are identically zero. Moreover, there is no need to introduce singular downwashes at subsonic edges.

From the most general form of the inverse kernel, derived by Watkins and Berman as given by Eq. (16b), Ref. 42, one has for the steady case

$$K(x-\xi, y-\eta) = \frac{1}{2\beta U} \frac{\partial}{\partial(x-\xi)} \bar{U}(x-\xi-\beta|y-\eta|) \sqrt{(x-\xi)^2 - \beta^2(y-\eta)^2} \quad \text{Eq. (6.3)}$$

where \bar{U} is the step function

CONFIDENTIAL

$$\begin{aligned}\bar{U}(x) &= 1 & x > 0 \\ &= 0 & x \leq 0\end{aligned}$$

Eq. (6.4)

If the inverse pressure influence coefficient P is defined as the downwash at a point due to a unit constant pressure over an influencing box, then in the Mach grid system (Fig. II.3) the relation corresponding to Eq. (2.14) for the "direct case" is

$$w_{n,m} = \frac{\beta}{2\pi U} \sum_{v,\mu} \bar{P}_{v,\mu} P_{\bar{v},\bar{\mu}} \quad \text{Eq. (6.5)}$$

Using Eqs. (6.2)-(6.3), one can derive the following expressions for these coefficients:

$$P_{0,0} = -1 \quad \bar{v} = \bar{\mu} = 0$$

$$P_{\bar{v},\bar{v}} = \frac{1}{\pi} \left\{ \sqrt{\left(\frac{2\bar{v}+1}{2\bar{v}-1}\right)^2 - 1} - \cos^{-1} \frac{2\bar{v}-1}{2\bar{v}+1} \right\} \quad \bar{v} = \bar{\mu} > 0$$

$$\begin{aligned}P_{\bar{v},\bar{\mu}} &= \frac{1}{\pi} \left\{ \frac{1}{2\bar{\mu}+1} \left[\sqrt{(2\bar{v}-1)^2 - (2\bar{\mu}+1)^2} - \sqrt{(2\bar{v}+1)^2 - (2\bar{\mu}+1)^2} \right] \right. \\ &\quad \left. - \frac{1}{2\bar{\mu}-1} \left[\sqrt{(2\bar{v}-1)^2 - (2\bar{\mu}-1)^2} - \sqrt{(2\bar{v}+1)^2 - (2\bar{\mu}-1)^2} \right] \right. \\ &\quad \left. + \left(\cos^{-1} \frac{2\bar{\mu}+1}{2\bar{v}+1} + \cos^{-1} \frac{2\bar{\mu}-1}{2\bar{v}-1} \right) - \left(\cos^{-1} \frac{2\bar{\mu}+1}{2\bar{v}-1} + \cos^{-1} \frac{2\bar{\mu}-1}{2\bar{v}+1} \right) \right\}\end{aligned}$$

$$\bar{v} > \bar{\mu} \geq 0$$

Eqs. (6.6a-c)

CONFIDENTIAL

A partial list of numerical values of $P_{\bar{v}, \mu}$ is given in Table VI.1. It is significant that this table covers all values of the Mach number, since this parameter does not appear directly in Eqs. (6.6).

$\bar{v} \backslash \mu$	0	1	2	3	4	5
0	-1					
1	-1.016,98	0.508,49				
2	-1.230,00	0.485,75	0.129,25			
3	-1.254,91	0.444,66	0.117,67	0.065,13		
4	-1.263,09	0.435,10	0.097,68	0.057,88	0.040,89	
5	-1.266,79	0.431,07	0.092,27	0.045,53	0.035,82	0.028,70

Table VI.1 A Short Table for Inverse Pressure Influence Coefficients in the Mach Grid System.
Steady State ($R=0$)

Regardless of which box scheme is to be followed, it is most efficient to assume a constant pressure over each box. This step limits the tabulations to a single type of inverse pressure influence coefficient. One must carefully examine the adequacy of this assumption, especially near subsonic leading edges where the pressures have singular behavior. For this purpose two numerical examples, which were considered in connection with previous studies, have been recomputed using Mach boxes and inverse coefficients:

- (1) A rectangular wing in steady flow at a constant angle of attack α .

CONFIDENTIAL

(2) A triangular wing, with leading edge sweep

$\Lambda = \cot^{-1} 0.64$, in steady flow at a constant angle of attack α .

a. The Rectangular Wing

The pressure distribution on the mixed region of this wing is presented in Fig. VI.1. A comparison between these values and those from Table IV.2 reveals that the inverse-coefficient approach yields better accuracy for the pressures at the box centers than the direct method which omits the effect of the side-edge singularity. However, the accuracy is poorer than the direct method including the refinement for the edge. The discrepancies between the results of the new method and their exact counterparts can be solely attributed to the approximation that the pressure over each box is constant and equal to its value at the center; this is most critical for a box adjacent to the side edge, where the slope of the pressure is singular. One might be able to get improved precision by accounting in an approximate fashion for the known variation of pressure over side-edge boxes. Such a step would require (as in the case of the refinement in the direct case) developing and tabulating an extra set of influence coefficients.

b. The Triangular Wing

The pressure distribution on this wing is presented in Fig. VI.2. A comparison between these values and the corresponding ones from Fig. IV.13 reveals that the chordwise pressure fluctuations are even more severe than those encountered with the direct method. The dimensionless total lift and total moment are

$$L = -1.006,67, \quad M = -1.290,99$$

These quantities are closer to the exact values of $-0.987,09$ and $-1.316,11$, respectively, than the corresponding estimates by the direct method using six chordwise boxes. The latter are $-1.043,96$ and $-1.345,13$ from Table IV.4.

It has been demonstrated so far that the inverse approach offers a satisfactory alternative way for estimating steady-state airload distributions. From the examples shown above it appears that one may often expect to obtain better accuracy than from the direct pressure influence coefficients without refinements. However, the new method has a serious disadvantage when extended to wings in unsteady motion. The

CONFIDENTIAL

CONFIDENTIAL

VALUES OF $\frac{-\Delta p}{\left(\frac{2\rho U^2 a}{\beta}\right)}$

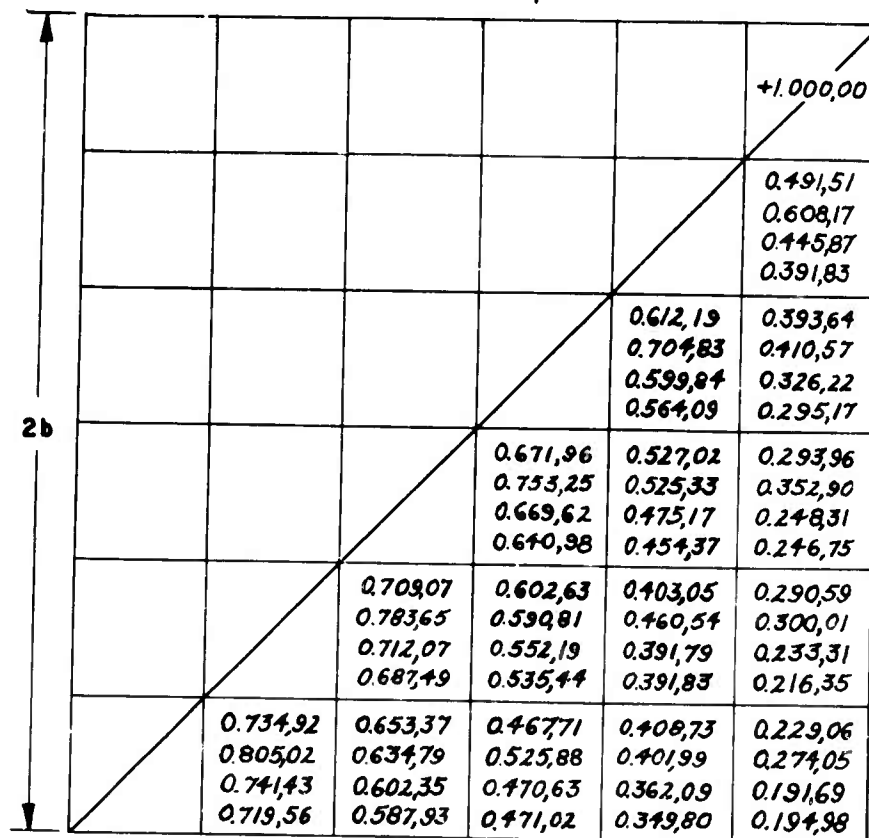


Fig. VI.1 Dimensionless Pressures on the Mixed Region of a Rectangular Wing in Steady Supersonic Motion at a Constant Angle of Attack. Comparison Between Exact Results and Three Forms of the Mach Box Method

[Values given are for the centers of boxes in the following order: (1) Inverse pressure method, (2) Direct method without downwash singularity, (3) Direct method with downwash singularity, (4) Exact.]

CONFIDENTIAL

CONFIDENTIAL

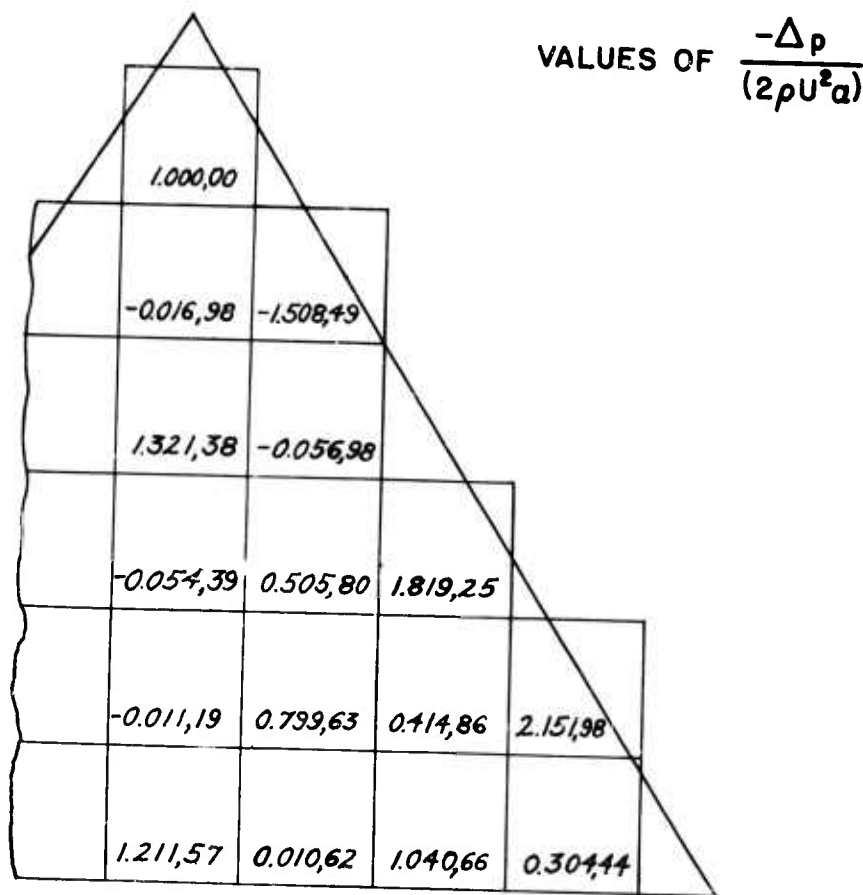


Fig. VI.2 Pressure Distributions on a Triangular Wing in Steady Supersonic Flow at a Constant Angle of Attack with the Inverse Pressure Coefficient Method.
($\alpha = 0$, $\cot \Lambda = 0.64$, $M = \sqrt{2}$)

CONFIDENTIAL

CONFIDENTIAL

form of the inverse kernel K is much more complicated than that of its counterpart F , rendering the task of evaluating the inverse pressure influence coefficients a difficult one. The downwash $\bar{w}_A(x, y)$ at a point (x, y) due to a unit constant pressure on an elementary area A inside the forward Mach cone from (x, y) can be written in dimensionless notation [cf. Eq. (16b) of Ref. 42]:

$$\begin{aligned} \bar{w}_A(x, y) = & \frac{1}{2\pi\eta} \int_A \frac{1}{(y-\eta)^2} \left\{ e^{-i \frac{kM^2}{\beta^2}(x-\xi)} \left(\frac{\beta^2}{Mk} \frac{\partial}{\partial(x-\xi)} + \frac{i}{M} \right) \sqrt{U(x-\xi - \beta|y-\eta|)} \right. \\ & \cdot \left. \sin \left(\frac{Mk}{\beta^2} \sqrt{(x-\xi)^2 - \beta^2(y-\eta)^2} \right) \right\} + \\ & + \frac{k}{M} e^{-ik(x-\xi)} \int_{\beta|y-\eta|}^{x-\xi} e^{-i \frac{k\lambda}{\beta^2}} \bar{U}(\lambda - \beta|y-\eta|) \sin \left(\frac{Mk}{\beta^2} \sqrt{\lambda^2 - \beta^2(y-\eta)^2} \right) d\lambda \int \eta d\eta \end{aligned}$$

Eq. (6.7)

Compared to the expression for the direct influence coefficient [Eq. (2.4)], the evaluation of the inverse coefficient \bar{w}_A according to Eq. (6.7) calls for an additional integration over the variable λ . Also, extreme caution must be exercised in carrying out the η -integration, since the integrand is highly singular at $\eta = y$. Although Eq. (6.7) can be integrated in closed form when $k=0$ to yield the influence coefficients Eqs. (6.6a-c), it is a difficult task to evaluate $\bar{w}_A(x, y)$

when $k \neq 0$. Even for low frequencies, when K can be approximated by a finite power series in k (cf. Ref. 42), one still is faced with the double integrations with respect to ξ, η which require lengthy sets of computations. Further research is recommended before any systematic tabulation of inverse coefficients is undertaken.

VI.2 The Lift Influence Coefficient

The lift influence coefficient is defined as the total lift over an elementary area due to a unit constant downwash over another elementary area. Consider two such areas to be the full boxes A, B , respectively in the Mach system as shown in Fig. VI.3.

CONFIDENTIAL

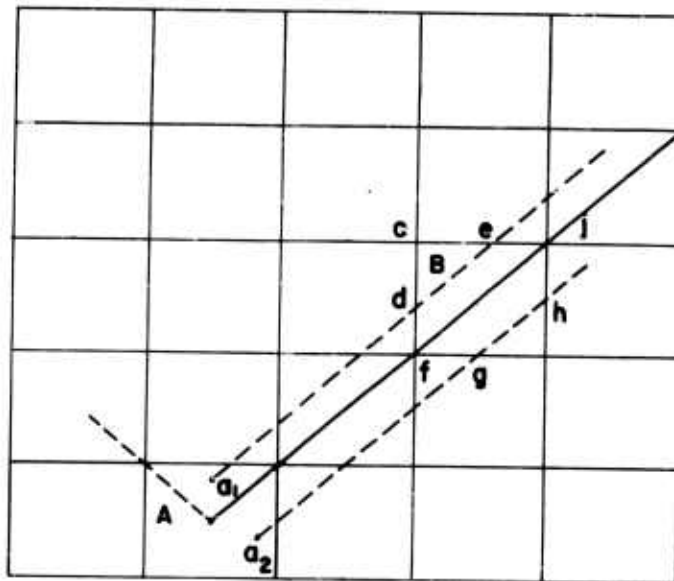


Fig. VI.3 The Use of Mach System in Connection with the Lift Influence Coefficient.

In order to evaluate the total lift over A due to B , one must first find the pressure distribution over A . For the point a_1 , the influencing area is the triangle cde , and for the point a_2 , the quadrilateral $gfcjh$. Since the evaluation of the lift influence coefficient requires a double integration over A , it is desirable to find the pressures at all points of A in closed form. Although this is possible for the steady-state case, the same cannot be said when $k \neq 0$. Furthermore this method was found to have no particular advantage over the original approach with the possible exception of "smoothing out" the chordwise and spanwise fluctuations of the airloads and allowing the specification of zero lift over each diaphragm box rather than zero pressure at the center of each such box. Since the usefulness of this approach is limited to the steady-state case, and even there the additional complications far outweigh its slight advantages, this approach was not pursued further.

CONFIDENTIAL

CONFIDENTIAL

BIBLIOGRAPHY

1. V. Borbely, S., Aerodynamic Forces on a Harmonically Oscillating Wing at Supersonic Velocity (2-Dimensional Case). R.T.P. Translation No. 2019, British Ministry of Aircraft Production. (From Z.f.a. M.M., Bd. 22, Heft 4, August 1942, pp. 190-205).
2. Garrick, I.E. and Rubinow, S.I. Theoretical Study of Air Forces on an Oscillating or Steady Thin Wing in a Supersonic Main Stream. NACA Report 872, 1947.
3. Miles, J.W. The Oscillating Rectangular Airfoil at Supersonic Speeds. U.S. Naval Ordnance Laboratory Report NAVORD 1170, Inyokern, California, July 1949.
4. Miles, J.W. A General Solution for the Rectangular Airfoil in Supersonic Flow. Quarterly of Applied Mathematics, Vol. XI, No. 1, April 1953, pp. 1-8.
5. Miles, J.W. A Note on Subsonic Edges in Unsteady Supersonic Flow. Quarterly of Applied Mathematics, Vol. XI, No. 3, October 1953, pp. 363-367.
6. Goodman, T.R. The Quarter-Infinite Wing Oscillating at Supersonic Speeds. Cornell Aeronautical Laboratory Report 36, 1951.
7. Stewartson, K., On the Linearized Potential Theory of Unsteady Supersonic Motion. Quarterly Journal of Mechanics and Applied Mathematics, Vol. III, 1950, pp. 182-199.
8. Rott, N., On the Unsteady Motion of a Rectangular Airfoil Wing in Supersonic Flow. Reader's Forum, Journal of the Aeronautical Sciences, Vol. 18, No. 11, November 1951, pp. 775-776.
9. Stewart, H.J. and Li, T.Y. Source-Superposition Method of Solution of a Periodically Oscillating Wing at Supersonic Speeds. Quarterly of Applied Mathematics, Vol. IX, No. 1, April 1951, pp. 31-45.
10. Chang, C.C. The Aerodynamic Behavior of a Harmonically Oscillating Finite Sweptback Wing in Supersonic Flow. NACA T.N. 2467, October 1951.

CONFIDENTIAL

CONFIDENTIAL

11. Li, T.Y. and Stewart, H.J., On an Integral Equation in the Supersonic Oscillating Wing Theory. Reader's Forum, Journal of the Aeronautical Sciences, Vol. 20, No. 10, October 1953, pp. 724-726.
12. Watkins, C.E., Effect of Aspect Ratio on the Air Forces and Moments of Harmonically Oscillating Thin Rectangular Wings in Supersonic Potential Flow. NACA Report 1028, 1951.
13. Nelson, H.G., Rainey, R.A. and Watkins, C.E., Lift and Moment Coefficients Expanded to the Seventh Power of Frequency for Oscillating Rectangular Wings in Supersonic Flow and Applied to a Specific Flutter Problem. NACA T.N. 3076, April 1954.
14. Miles, J.W., On Harmonic Motion of Wide Delta Airfoils at Supersonic Speeds. U.S. Naval Ordnance Laboratory Report NAVORD 1234, Inyokern, California, June 1950.
15. Froehlich, J.E., Nonstationary Motion of Purely Supersonic Wings. Journal of the Aeronautical Sciences, Vol. 18, No. 5, May 1951, pp. 298-310.
16. Nelson, H.C., Lift and Moment on Oscillating Triangular and Related Wings with Supersonic Edges. NACA T.N. 2494, September, 1951.
17. Walsh, J., Zartarian, G. and Voss, H.M., Generalized Aerodynamic Forces on the Delta Wing with Supersonic Leading Edges. Journal of the Aeronautical Sciences, Vol. 21, No. 11, November 1954, pp. 739-748.
18. Haskind, M.D. and Falkovich, S.V., Vibration of a Wing of Finite Span in Supersonic Flow. NACA T.M. 1257, 1950.
19. Watkins, C.E. and Berman, J.H., Air Forces and Moments on Triangular and Related Wings with Subsonic Leading Edges Oscillating in Supersonic Potential Flow. NACA Report 1099, 1952.
20. Watkins, C.E. and Berman, J.H., Velocity Potential and Air Forces Associated with a Triangular Wing in Supersonic Flow, with Subsonic Leading Edges, and Deforming Harmonically According to a General Quadratic Equation. NACA T.N. 3009, September 1953.
21. Pines, S., Liban, E., Neuringer, J. and Rabinowitz, S., Flutter Analysis of an Elastic Wing with Supersonic Edges. Republic Aviation Corporation Report E-SAF-1, April 1953.

CONFIDENTIAL

CONFIDENTIAL

22. Pines, S. and Dugundji, J., Aerodynamic Flutter Derivatives of a Flexible Wing with Supersonic Edges, Aircraft Industries Association Report Number ARTC-7, February 1954.
23. Pines, S. and Dugundji, J., Application of Aerodynamic Flutter Derivatives to Flexible Wings with Supersonic and Subsonic Edges. Republic Aviation Corporation Report E-SAF-2, April 1954.
24. Pines, S. and Dugundji, J. and Neuringer, J., Aerodynamic Flutter Derivatives for a Flexible Wing with Supersonic and Subsonic Edges. Journal of the Aeronautical Sciences, Vol. 22, No. 10, October 1955.
25. Harvard Computation Laboratory, Staff of, Tables of Oscillatory Supersonic Aerodynamic Influence Coefficients (AF Problem 101). Progress Report No. 39, Design and Operation of Digital Computing Machinery, Contract AF33(616)-2717, May 1955. (To be published as WADC Technical Report 54-113.)
26. Li, T., Aerodynamic Influence Coefficients for an Oscillating Finite Thin Wing, Part I. Chance Vought Aircraft, Inc. Report, June 1954.
27. Li, T., Tip Effect of an Oscillating Finite Thin Wing in Supersonic Flow. Chance Vought Aircraft, Inc. Report. (Not dated)
28. Voss, H.M., Zartarian, G. and Hsu, P.T., Application of Numerical Integration Techniques to the Low-Aspect-Ratio Flutter Problem in Subsonic and Supersonic Flows. M.I.T. Aeroelastic and Structures Research Laboratory Technical Report 52-3, Contract NOa(s) 53-564-c for Bureau of Aeronautics, USN, October 1954.
29. Brandstatter, J. and Mortzschky, H., A Method for Calculating the Potential on a Tapered Oscillating Wing in Supersonic Flow. Lockheed Aircraft Corporation Report MAM 245, April 1954.
30. Mortzschky, H. and Brandstatter, J., Calculation of the Potential on a Tapered Wing Oscillating in a Supersonic Flow Field. Lockheed Aircraft Corporation Report MAM 246, October 1954.
31. Zartarian, G., Theoretical Studies on the Prediction of Unsteady Supersonic Airloads on Elastic Wings. Part 2, Rules for Application of Oscillatory Supersonic Aerodynamic Influence Coefficients. WADC Technical Report 56-97, Part 2, February 1955. (Confidential - Title Unclassified).

CONFIDENTIAL

CONFIDENTIAL

32. Watson, G.N., A Treatise on the Theory of Bessel Functions. Second Edition, The Macmillan Company, New York, 1945.
33. National Bureau of Standards, Tables of Chebyshev Polynomials $S_n(x)$ and $C_n(x)$. Applied Mathematics Series 9, United States Government Printing Office, Washington, 1952.
34. Turner, R. and Downey, A.F., A Tabulation of the Fresnel Integrals. Cruft Laboratory, Harvard University, ONR Contract N5 ori-76 Task Order No. 1 NR-078-011, Technical Report 173, March 15, 1953.
35. Schwarz, L., Untersuchung einiger mit den Zylinderfunktionen nullter Ordnung verwandter Funktionen. Luft-fahrt-forschung Bd. 20, Lfg. 12, February 8, 1944, pp. 341-372.
36. Garrick, I.E. and Rubinow, S.I., Flutter and Oscillating Air-Force Calculations for an Airfoil in a Two-Dimensional Supersonic Flow. NACA Report 846, 1946.
37. Zartarian, G. and Voss, H.M., On the Evaluation of the Function $f_1(M, \bar{w})$. Reader's Forum, Journal of the Aeronautical Sciences, Vol. 20, No. 11, November 1953, pp. 781-782.
38. Evvard, J.C., Distribution of Wave Drag and Lift in the Vicinity of Wing Tips at Supersonic Speed. NACA Technical Note 1382, July 1947.
39. Lighthill, M.J., The Supersonic Theory of Wings of Finite Span, R and M 2001, October 1944.
40. Lagerstrom, P.A., Linearized Supersonic Theory of Conical Wings. NACA Technical Note 1685, January 1950.
41. Watkins, C.E., Runyan, H.L. and Woolston, D.S., On the Kernel Function of the Integral Equation Relating the Lift and Downwash Distributions of Oscillating Finite Wings in Subsonic Flow. NACA Technical Note 3131, January 1954.
42. Watkins, C.E. and Berman, J.H., On the Kernel Function of the Integral Equation Relating the Lift and Downwash Distributions of Oscillating Finite Wings in Supersonic Flow. NACA Technical Note 3438, February 1955.
43. Whittaker, E., Robinson, G., The Calculus of Observations, Fourth Edition, D. Van Nostrand Company Inc., New York 1948.
44. Miles, J.W., Unsteady Supersonic Flow. Monograph prepared for Air Research and Development Command under Contract AF18(600)-432, 1955.

CONFIDENTIAL

CONFIDENTIAL

APPENDIX A

EVALUATION OF THE FUNCTIONS \bar{I}_n AND \bar{P}_n

It was pointed out in Section IV that two additional functions must be tabulated in connection with the procedure for including the effect of the downwash singularity near a side edge. These are the \bar{I}_n - and \bar{P}_n -functions, defined by Eqs. (4.17a-b). The integrations required must be carried out numerically, and the recommended integration technique is the modified Gauss quadrature (Ref. 43), which appears to give satisfactory accuracy with a minimum of computational labor.

A.1 Numerical Integration Formula

Since the integrand in \bar{I}_n is a function of z^2 only, it represents an integral of the type

$$\int_0^1 f(z^2) dz = \int_0^1 f(y) \frac{1}{2\sqrt{y}} dy \quad \text{Eq. (A.1)}$$

Applying the general technique of Ref. 43 to Eq. (A.1), it can be shown that the numerical integration formula

$$\int_0^1 f(y) \frac{1}{2\sqrt{y}} dy = \sum_{j=1}^N H_j f(y_j) = \sum_{j=1}^N H_j f(z_j^2) \quad \text{Eq. (A.2)}$$

is exact, provided $f(y)$ is a polynomial of order $(2N-1)$ or less in y and the stations y_j are properly chosen. The H_j 's are associated weighting factors. The values of y_j are the roots of the equation

$$2\sqrt{y} \frac{d^N}{dy^N} \left(\frac{1}{2\sqrt{y}} y^N (1-y)^N \right) = 0 \quad \text{Eq. (A.3)}$$

For example, if $N=5$, these roots turn out to be

$$y_1 = 0.022, 163, 567$$

$$y_4 = 0.748, 334, 658$$

$$y_2 = 0.187, 831, 574$$

$$y_5 = 0.948, 493, 910$$

$$y_3 = 0.461, 597, 344$$

CONFIDENTIAL

The weighting factors H_j can then be obtained from the following set of simultaneous equations, which are derived by successively applying Eq. (A.2) to the functions $f(y)=1, y, y^2, y^3, \dots, y^{N-1}$:

$$\begin{aligned} H_1 + H_2 + H_3 + H_4 + \dots + H_N &= 1 \\ y_1 H_1 + y_2 H_2 + y_3 H_3 + y_4 H_4 + \dots + y_N H_N &= \frac{1}{3} \\ y_1^2 H_1 + y_2^2 H_2 + y_3^2 H_3 + y_4^2 H_4 + \dots + y_N^2 H_N &= \frac{1}{5} \\ &\vdots \\ y_1^{N-1} H_1 + y_2^{N-1} H_2 + y_3^{N-1} H_3 + y_4^{N-1} H_4 + \dots + y_N^{N-1} H_N &= \frac{1}{2N-1} \end{aligned}$$

Eqs. (A.4)

For $N=5$, one has

$$\begin{aligned} H_1 &= 0.295,524,215 & H_4 &= 0.149,451,361 \\ H_2 &= 0.269,266,739 & H_5 &= 0.066,671,338 \\ H_3 &= 0.219,086,348 \end{aligned}$$

Let $F_n(z^2)$ denote the integrand of the \bar{I}_n -integral. If a finite power series of order $(2N-1)$ in z^2 which takes the same values as $F_n(z^2)$ at the points $y_j = z_1^2, z_2^2, z_3^2, \dots$, approximates adequately the integrand over the range of integration, then one has from Eqs. (4.17a) and (A.2)

$$\bar{I}_n \cong e^{-i\epsilon\sigma} \sum_{j=1}^N H_j F_n(z_j^2) \quad \text{Eq. (A.4)}$$

where ϵ, σ are those defined following Eqs. (4.17a-b).

The number of integration points N that must be taken to ensure a given degree of accuracy depends on the sinuousness of the integrand over the range of integration. The integrand will become more and more sinuous as ϵ, σ are increased. Therefore, for a given Mach number M , the most

CONFIDENTIAL

critical case will be when the frequency is maximum. Let the maximum reduced frequency at which this method is to be applied be denoted by k_{max} . In the process of calculating the aerodynamic influence coefficients for a wing at k_{max} , one need consider only the ϵ -range for \bar{I}_n [Eq. (4.17a)]

$$0 < \epsilon \leq \frac{k_{max}}{2} \frac{M^2}{\beta^2} \equiv \epsilon_{max}$$

For different boxes in the diaphragm region, both ϵ and σ vary. However, it can be easily inferred from the locations of diaphragm boxes in Fig. IV.5 that

$$\sigma \leq \frac{\epsilon_{max}}{\epsilon} - 1$$

Therefore for a given ϵ in the tables, the only entries required are those for which

$$0 \leq \sigma \leq \frac{\epsilon_{max}}{\epsilon} - 1$$

If the Mach box system is used, and at most nine boxes are taken along the side edge (beyond this number of boxes, the inclusion of the downwash singularity is probably unnecessary, as stated in Section IV), this limitation yields $\sigma \leq 7$.* Therefore the tabulations would have to cover the ranges

$$\epsilon \leq \epsilon_{max}, \quad 0 \leq \sigma \leq \frac{\epsilon_{max}}{\epsilon} - 1, \quad 0 \leq \sigma \leq 7.$$

With these ranges established, it has been found that a five-point integration will suffice for all ϵ 's and σ 's for which $\epsilon_{max} \leq 1.6$.

When evaluating the function \bar{P}_n , the situation is somewhat different because the limits of integration are $\sqrt{\sigma}$ and 1 rather than 0 and 1. A numerical integration formula similar to Eq. (A.2) can be devised when the lower limit is some constant other than zero. However, the formula will be dependent on this lower limit. Since one must tabulate the coefficients \bar{P}_n for several values of σ , an equal number of integration formulas would be necessary. To by-pass this complication, the following alternative is suggested. Let

$G_n(z^2)$ denote the integrand of the \bar{P}_n -integral (Eq. 4.17b)

*It should be remembered that σ can have only discrete values when a box system is used; e.g., for nine Mach boxes, $\sigma = 1, 3, 5, 7, \frac{1}{2}, \frac{3}{2}, \dots, \frac{7}{2}, \frac{1}{3}, \frac{5}{3}, \dots$.

CONFIDENTIAL

$$\begin{aligned}\bar{P}_n &= e^{i\epsilon\bar{\sigma}} \int_{\sqrt{\bar{\sigma}}}^1 G_n(z^2) dz \\ &= e^{i\epsilon\bar{\sigma}} \left\{ \int_0^1 G_n(z^2) dz - \int_0^{\sqrt{\bar{\sigma}}} G_n(z^2) dz \right\}\end{aligned}$$

Eq. (A.5)

For $z^2 < \bar{\sigma}$, the arguments of the Bessel functions in Eq. (4.17b) become imaginary. Instead of taking the true values of G_n for $z^2 < \bar{\sigma}$, consider

$$\begin{aligned}\bar{G}_n(z^2) &= z^{2n} e^{-3i\epsilon z^2} \left\{ \frac{1}{2} J_0(\quad) J_0(\quad) + i \sum_1^{\infty} (\quad) + i \sum_0^{\infty} (\quad) \right\}; z^2 \gg \bar{\sigma} \\ &= z^{2n} e^{-3i\epsilon z^2} \left\{ \frac{1}{2} \right\}; z^2 \leq \bar{\sigma}\end{aligned}$$

Eq. (A.6)

The function $\bar{G}_n(z^2)$ is continuous across $z^2 = \bar{\sigma}$, and has also at least a continuous first derivative. Therefore $\bar{G}_n(z^2)$ is sufficiently smooth to be approximated by a finite polynomial in z^2 . Equation (A.5) then reduces to (since $G_n(z^2) = \bar{G}_n(z^2)$ for $z^2 \gg \bar{\sigma}$)

$$\begin{aligned}\bar{P}_n &= e^{i\epsilon\bar{\sigma}} \left\{ \int_0^1 \bar{G}_n(z^2) dz - \int_0^{\sqrt{\bar{\sigma}}} \bar{G}_n(z^2) dz \right\} \\ &= e^{i\epsilon\bar{\sigma}} \left\{ \int_0^1 \bar{G}_n(z^2) dz - \frac{\bar{\sigma}^{n+\frac{1}{2}}}{2} \int_0^1 z^{2n} e^{-3i\epsilon\bar{\sigma}z^2} dz \right\}\end{aligned}$$

Eq. (A.6)

Now both integrals have the limits 0 and 1; therefore, applying Eq. (A.2) to Eq. (A.6) yields

$$\bar{P}_n = e^{i\epsilon\bar{\sigma}} \sum_1^N H_j \left\{ \bar{G}_n(z_j^2) - \frac{\bar{\sigma}^{n+\frac{1}{2}}}{2} (z_j^2)^n e^{-3i\epsilon\bar{\sigma}z_j^2} \right\} \quad \text{Eq. (A.7)}$$

CONFIDENTIAL

CONFIDENTIAL

The number of integration points N that must be taken to ensure adequate numerical integration depends on the values of ϵ and $\bar{\sigma}$. By a method similar to that for \bar{I}_n , one can prove that tables of the \bar{P}_n have to cover the ranges

$$\epsilon \leq \epsilon_{max}, \quad 2 - \frac{\epsilon_{max}}{\epsilon} \leq \bar{\sigma}, \quad 0 \leq \bar{\sigma} \leq \frac{15}{16}.$$

Once more, nine is the maximum number of boxes to be taken along the side edge. n_{max} for this case is

$$\epsilon_{max} = k_{max} \frac{M^2}{\beta^2}.$$

It has been found that for the necessary tables, a five-point integration for $\epsilon \leq 1.6$, and a nine-point integration for $1.6 \leq \epsilon \leq 3.2$ will suffice, for all $\bar{\sigma}$'s, provided $\epsilon_{max} \leq 3.2$.

CONFIDENTIAL